A VARIABLE STRUCTURE SPACE VOLTAGE VECTOR CONTROLLED SWITCHED RELUCTANCE FLUX VECTOR DRIVE

Tzu-Shien Chuang

Thesis submitted for the examination of degree of Doctor of Philosophy

Department of Engineering
University of Warwick

Coventry CV4 7AL

August 1997

TABLE OF CONTENTS

ACKNOWLEDGMENTS

This thesis has made significant contributions to variable speed industrial drives. Its success should be due to Dr. Charles Pollock for his enthusiastic supervision and the guidance in the switched reluctance motor, and its associated Power Electronics. I also would like to express my gratitude to all the members in the Power Electronics and Drive Research Group of Warwick University for their help in times of need. Special thanks go to my wife and daughter for their continuous support and encouragement when I was frustrated.

ABSTRACT

Through simulation and experimental investigation this thesis shows that (i) the switched reluctance motor is not different from any other motor in energy conversion theory but the difference is only in the structure and the operating characteristics; (ii) under high loads or high speeds the relative phase angle of the current with respect to the rotor pole must be advanced; (iii) the kinetic energy in the motor can be quickly returned to the d.c. link source or be transferred to other phase windings by the regenerative operation.

A synchronous singly-excited control scheme is introduced to the switched reluctance motor. By this technology, a conventional current chopper can be used but the operating phase angle of the excited phase current must be limited. This approach makes the traditional switched reluctance drive become a high performance vector drive but a complex coordinate transformation is unnecessary making the implementation very simple. For multiply excited operation and for high power requirements, in order to achieve the sliding mode control of total phase power, a space vector controlled split-link converter is accomplished.

A sliding mode speed controller with d.c. link power feedforward is added to the variable structure space vector controlled split-link converter to achieve a robust servo drive. The proposed switched reluctance drive can achieve fast and robust servo performance even under a high load and highly dangerous electric braking conditions.

LIST OF FIGURES AND TABLES

Chapter 6

CHAPTER 1

INTRODUCTION

1.1 INTRODUCTION

For a long time d.c. brush motors were used extensively in areas where variable-speed industrial applications were required. This motor could be controlled easily by the field and armature current. In particular, the separately excited d.c. motor has been used mainly for applications where there was a requirement of fast response and four-quadrant operation with very high performance. However, d.c. motors have certain disadvantages, which are due to the existence of the commutator and the brushes. So, they require periodic maintenance and also cannot be used in explosive or corrosive environments. To overcome these problems, alternating current asynchronous induction and permanent magnet synchronous motors, which can have simple and rugged structure, high reliability and efficiency have replaced dc motors in many variable speed applications. These brushless motors can be used in highly dangerous environments without maintenance. However, energy density, inertia, efficiency and cost are the main criteria for the selection of many variable speed products. The induction motor is the simplest of the brushless ac motors. It will run without any electronic control when directly connected to an appropriate d.c. supply. When operated in association with an inverter with vector control, the induction motor can be controlled with a high degree of accuracy as a high performance servo drive. The permanent magnet brushless d.c. motor also requires an inverter or electronic commutator and can offer very high performance. Unfortunately, its cost is high due to the need for expensive magnetic material in the rotor. On the contrary, another motor, the switched reluctance motor, is a very good

candidate suitable for variable speed industrial applications because it has the attributes to meet the requirements of variable speed applications. The main drawback of the switched reluctance motor has been acoustic noise and vibration such that it has not been popularly accepted. These two problems are related to high torque ripple. In normal operation of a switched reluctance motor it is not uncommon to have periods of negative torque between blocks of positive torque. This increases vibration and acoustic noise. Therefore, the main aim of this thesis is to solve this problem and provide an effective solution, namely, the author will show the possibility that Variable Structure Space Vector theory can be applied to switched reluctance servo drives. Application of Variable Structure Control (VSC) theory to the field of control of DC servo motors (Sabanovic and Vujovic 1984) [1], PM synchronous servo motors (Venkataramanan et al. 1986, Harashima et. 1986) [3], Slotine 1985 [4]), (Chen and Yeung, Ito 1991) [5] has been reported. Many other works, which survey the possibility of application of VSC theory in high-performance servo drives, have been published in the literature. It is well known that the characteristics of VSC are insensitivity to the variation of system parameters and external disturbances. However, how can it be applied to switched reluctance motors and related drives ? These involve the real spirit of VSC theory and the understanding of the plant system. In this case, the author creates a novel VSC, which is suitable for any phase switched reluctance motor and drive, so that the performance of the drive is very robust and its implementation is very simple. In this thesis there are a total of seven chapters to sequentially describe the novel drive including effective control schemes to achieve high-performance and a robust servo drive.

1.2 FORMAT OF THE THESIS

Chapter 1 is an introductory chapter, briefly describing the motivation of VSC theory applied to switched reluctance drives. After chapter 1, the arrangement of the thesis is as follows.

In Chapter 2, the characteristics and operating principle of the switched reluctance motor are described. Basically, the switched reluctance motor is derived from the synchronous reluctance motor but has typically higher motor efficiency. However, whilst it is increased the salient pole structure introduces high harmonics in the electromagnetic torque. Control is necessary to avoid generating negative torque. The main operating principles of the existing switched reluctance motor are described. How to obtain an effective improvement are discussed in this chapter.

In Chapter 3, power converters for a switched reluctance motor are described. Some famous power converters, such as asymmetric half-bridge converter, split DC link converter, C dump converter, Miller's converter, and Pollock's converter are briefly discussed. This chapter shows that in order to provide simpler and better performance of the drive, a novel control strategy must be added to the converter to achieve an excellent vector drive. In the next chapters, chapters 4, 5-phase split-link converter for a switched reluctance flux vector drive is studied.

Following Chapter 4, in Chapter 5, the variable structure space vector control of 4-phase split-link converter and the principle of sliding mode total phase power control are described.

In Chapter 6, which is the most important part in this thesis, a robust speed control schemes and a variable structure space vector controlled flux vector servo drive with sliding slope feedforward and integral compensation are studied.

Finally, in Chapter 7, some conclusions about the author's research will be summarised. The author's main contributions and proposed effective solutions to the variable speed industrial applications are described.

CHAPTER 2

CHARACTERISTICS AND OPERATING PRINCIPLE OF THE SWITCHED RELUCTANCE MOTOR

A switched reluctance motor has its history stretching back 166 years to the first "Electromagnetic Engines". In the last two decades this new type of electrical drive has been introduced again. The first commercially available switched reluctance motor was launched by TASC Drives in 1983. Even though the principle of operation of switched reluctance motor was established in the 1830's, it could not be implemented in practice until recently with to the progress of advanced power semiconductor devices. The new generation of power converters, based on IGBTs as power semiconductor switches and a digital application specific integrated circuit (ASIC) has overcome the reliability problem of the drive. Moreover, the computer aided design of the motor has made it possible to reduce the noise produced by the motor. Various applications of switched reluctance drives are under investigation at the moment. Smaller size switched reluctance motors have found applications in factory automation, positioning servos and variable speed drives. In medium and higher sizes, it has found application, such as centrifugal pumps and compressor drives. With its high efficiency throughout the operating range, simple unipolar converter, absence of rotor windings, it has considerable potential over the inverter fed induction motor. Understanding of its basic characteristics and operating principles is necessary to get the best out of the drive. Some basic operating principles of the switched reluctance motor are well established in the literatures [6-8]. In this

thesis, more advanced operating methods are described. Firstly the basic structure and operation of the drive are reviewed.

2-1 THE STRUCTURE OF THE SWITCHED RELUCTANCE MOTOR [9-11]

The switched reluctance motor is a doubly salient motor. Basically, it is a synchronous motor improved from the synchronous reluctance motor. In order to optimize efficiency, energy density, magnetic material and cost, the motor is generally designed using a 'finite element analysis' approach though many alternative techniques have been proposed. Usually the rotor poles and the stator poles are symmetrical about their centre-line and are equally spaced around the rotor and the stator, respectively. For a typical four-phase switched reluctance motor, this simple machine has six rotor poles and eight stator poles. A coil is wound around each stator pole. The coils on diametrically opposite poles may be connected in series or parallel to form a phase winding so that when current flows in the winding, one pole acts as north magnetic pole, the other as a south magnetic pole. The reluctance of the flux path between two diagonally opposite stator poles varies as a pair of rotor poles moves in and out of alignment. There are no magnets in the rotor, as shown in Fig. 2-1. The laminations shown are made of magnetically-soft, low-loss steel. The machine shown in Fig. 2-1 has four phases 1, 2, 3, and 4 as shown. When any pair of rotor poles is exactly aligned with the stator poles, that phase is said to be in the aligned position. If current is flowing in that phase winding, there is no torque at that position because no Back EMF is produced since there is no variation of incremental inductance. In this aligned position, the phase inductance is at maximum because the magnetic reluctance of the flux path is at its lowest. When the interpolar axis of the

rotor is aligned with the stator pole of a phase, that position is called the unaligned position, as shown in Fig. 2-2. In the unaligned position the phase inductance is at its minimum because the magnetic reluctance of the flux path is at its highest. The low inductance in this position means that there is rapid current rise during high speed running and commutation.

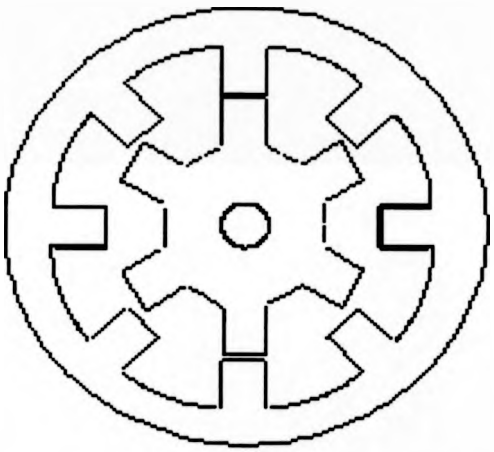

Fig. 2-1. Rotor is located at aligned position.

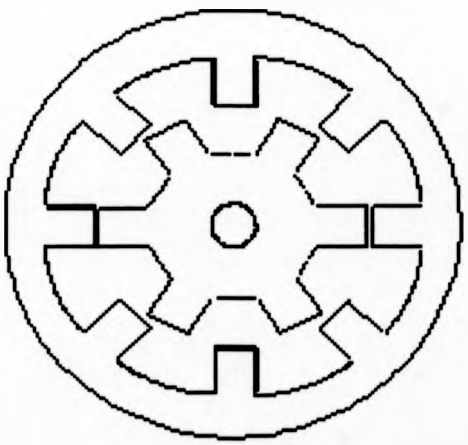

Fig. 2-2. Rotor pole is located at unaligned position.

2-2 ENERGY CONVERSION PRINCIPLE OF THE SWITCHED RELUCTANCE MOTOR [11-12]

Electromechanical systems are generally composed of an electrical system, a mechanical system, and a means whereby the electrical and mechanical system can interact. Both electrostatic and electromagnetic coupling fields may exist simultaneously. Losses will occur in all of the components of the electromechanical system. Heat loss will occur in the mechanical system due to friction and the electrical system will dissipate heat due to the resistance of the current-carrying conductors. Eddy current and hysteresis losses occur in the ferromagnetic material of all magnetic fields while dielectric losses occur in all electric materials. If W_E is the total energy supplied by the electrical source and W_M the total energy supplied by the mechanical source, then the energy distribution could be expressed as

$$W_E = W_e + W_{eL} + W_{eS} \tag{2-1}$$

$$W_M = W_m + W_{mL} + W_{mS} \tag{2-2}$$

where W_e is the energy transferred to the coupling fields by the electrical system. W_{eL} are the heat losses which are associated with the electrical system and W_{es} is the energy stored in the electric or magnetic fields which are not coupled with the mechanical system. W_{mL} is the energy losses of the mechanical system in the form of heat, W_{mS} is the energy stored in the moving device of the mechanical system, and W_m the energy transferred to the coupling field.

If W_F is defined as the total energy transferred to the coupling field, then

$$W_F = W_f + W_{fL} \tag{2-3}$$

where W_f is energy stored in the coupling field and W_{fL} is the energy dissipated in the form of heat due to losses within the coupling field(eddy current, hysteresis, or

dielectric losses). According to the law of conservation of energy, the electromechanical system must obey the following equation

$$W_f + W_{fL} = (W_E - W_{eL} - W_{eS}) + (W_M - W_{mL} - W_{mS}) \quad (2\text{-}4)$$

Equation (2-4) can be rewritten as

$$W_f + W_{fL} = W_e + W_m \quad (2\text{-}5)$$

This energy relationship can be shown as Fig. 2-3.

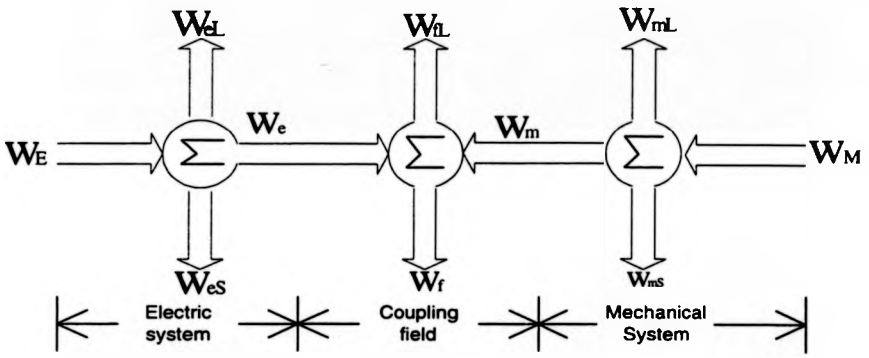

Fig. 2-3. Energy balance relationship between electric system and mechanical system.

If the losses of the coupling field can be neglected, then the field is conservative and the equation (2-5) becomes

$$W_f = W_e + W_m \quad (2\text{-}6)$$

For a switched reluctance motor, the voltage equation which describes the electrical system may be expressed as follows

$$v = r\,i + L\frac{d\,i}{d\,t} + E_f \quad (2\text{-}7)$$

where E_f is the voltage drop across the coupling field, r is the resistance of motor and circuit system, L is the inductance of circuit system and i is the phase current

flowing through motor phase winding. The electromagnetic torque can be expressed as

$$\tau = J\frac{d^2\theta}{dt^2} + B\frac{d\theta}{dt} + \tau_L \tag{2-8}$$

where J is the inertia constant, B is the viscous constant, θ is the rotational displacement of the rotor, τ is electromagnetic torque and τ_L is the load torque.

The total energy supplied by the electric source during time dt is

$$W_E = \int v\, i\, dt \tag{2-9}$$

The total energy supplied by the switched reluctance motor is

$$W_M = \int \tau d\theta \tag{2-10}$$

which may also be expressed as

$$W_M = \int \tau(\frac{d\theta}{dt})dt \tag{2-11}$$

Substituting (2-7) into (2-9) yields

$$W_E = r\int i^2 dt + L\int i\frac{d\,i}{d\,t}dt + \int E_f\, i\, dt \tag{2-12}$$

The first term on the right-hand side of (2-12) represents the energy loss due to the resistance of the switched reluctance motor circuit (W_{eL}). The second term represents the energy stored in the electromagnetic field external to the coupling field (W_{es}). So, the total energy transferred to the coupling field from the electric system is

$$W_e = \int E_f\, i\, dt \tag{2-13}$$

Similarly, for the mechanical system

$$W_M = J\int \frac{d^2\theta}{dt^2}d\theta + B\int (\frac{d\theta}{dt})^2 dt - \int \tau_L d\theta \tag{2-14}$$

The first term on the right-hand side of (2-14) represent the kinetic energy stored in the inertia of the switched reluctance motor. The second term is the heat loss due to friction (W_{mL}). Thus, the total energy transferred to the coupling field from the mechanical system is

$$W_m = -\int \tau_L \, d\theta \tag{2-15}$$

It is important to note that a positive torque τ_L is assumed to be in the same rotational direction as a positive rotational displacement $d\theta$.

Substituting (2-13) and (2-15) into (2-6), yields

$$W_f = \int E_f \, i \, dt - \int \tau_L \, d\theta \tag{2-16}$$

For a switched reluctance motor, E_f is the back EMF, denoting the variation of the stator flux linkage, i.e. $E_f = d\lambda/dt$, where λ is the stator flux linkage. Substituting E_f into (2-16), yields

$$W_f = \int i \, d\lambda - \int \tau_L \, d\theta \tag{2-17}$$

If there is no mechanical rotational displacement, the (2-17) becomes

$$W_f = \int i \, d\lambda \tag{2-18}$$

This coupling field energy corresponds to the area to the left of the $\lambda - i$ curve shown in Fig. 2-4, which represents the energy stored in the field at the instant when $\lambda = \lambda_a$ and $i = i_a$. The area to the right of the $\lambda - i$ curve is called the coenergy, which can be expressed as follows

$$W_c = \int \lambda \, di \qquad \text{with mechanical rotational displacement } d\theta = 0 \tag{2-19}$$

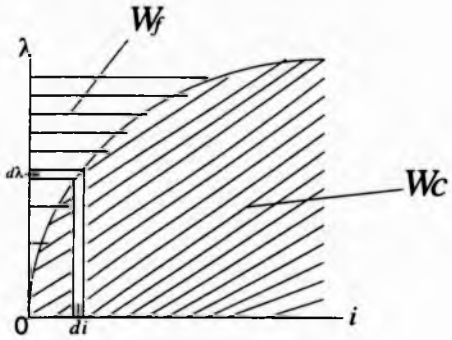

Fig. 2-4. Stored energy and coenergy in the magnetic field of the switched reluctance motor.

From Fig. 2-4, it can be seen that the sum of W_f and W_c is λ times i, namely,

$$\lambda i = W_c + W_f \tag{2-20}$$

Taking the partial derivative with respect to the rotational displacement on the both side of the equation (2-20), yields

$$\lambda \frac{di}{d\theta} + i\frac{d\lambda}{d\theta} = \frac{\partial W_c}{\partial \theta} + \frac{\partial W_f}{\partial \theta} \tag{2-21}$$

From (2-9),(2-10), (2-17), (2-19) and (2-21), the equation (2-22) can be obtained.

$$\frac{\partial W_c}{\partial \theta} = \tau = \lambda \frac{di}{d\theta} + i\frac{d\lambda}{d\theta} - \frac{\partial W_f}{\partial \theta} \tag{2-22}$$

The equation (2-22) is the most general expression for the torque produced by the switched reluctance motor. From this equation, one very important concept can be obtained, i.e. the electromagnetic torque can be decomposed into two parts: One is from the variation of the current with respect to the rotational displacement, another is exactly so-called moving load torque. If there is no variation of the current or rotation, then the electromagnetic torque of the switched reluctance motor system must be

equivalent to the load torque. In this case, the load or external disturbance torque can be estimated as being equivalent to the electromagnetic torque under sliding mode current control. This feature will be described fully in chapter 4. It should be noted that for a net electromagnetic torque to be present in the motor system, there must be either current variation or the rotational displacement.

2-3 OPERATING METHOD

A. Constant Torque Operation - Chopping Mode

This mode is generally used at low speed, which is necessary to control the flux linkage or phase current. This mode can be subdivided by three type: 'open loop voltage PWM' and ' current regulated PWM', dependent on controller. Each operating mode can be subdivided into 'soft chopping' and 'hard chopping', dependent on the converter used. For voltage PWM-soft chopping, the asymmetric half-bridge converter is suitable. Thus one switch can be left on and the other one can be switched on and off at a high frequency with a fixed duty-cycle over the switching cycle. As for voltage PWM- hard chopping, it can be carried out in a power converter with either one switch or two switches per phase. For asymmetric converter, both switches can be switched together at high frequency. For split-link converter, only one switch is switching in a similar way. This operating method is generally not suitable for motoring operation because it will increase the current ripple by a large factor but it is suitable for regenerating or braking operation to control current. Another chopping technique: current regulation - soft chopping can be used in the regulation of the phase current. By this method, power switches can be switched on or off according

as the current is greater or less than a reference current. Usually a hysteresis-type current regulator is used. Fixed frequency-type current modulation techniques can also be employed.

B. Control of Voltage conduction angle

This is a popular method suitable for medium and high speed operation but it is not suitable for low speed and lightly loaded cases. This is because torque pulsation is obvious during low speed and light load, but since the time period is short at high speed so that pulsing torque does not cause an obvious mechanical oscillation. Generally, the turn-off angle is fixed at a point prior to the aligned position to avoid negative torque and the turn-on angle is adjustable. With larger load, the conduction angle can be increased by advancing turn-on angle and fixing turn-off angle appropriately.

C. Constant power operation - Single pulse mode

During high speed operation, the turn-on angle and turn-off angle needs to be advanced, otherwise there would be substantial negative torque produced in the switched reluctance motor system at the end of each pulse. This has the effect of increasing the phase angle of the current with respect to the rotor. To achieve this aim, field-weakening is necessary. It is preferable to use single pulse excitation in the phase windings to avoid producing negative torque. Also, by phase advancing, the flux linkage becomes lower and the induced Back EMF is not higher than the supply source. Thus both the Back EMF and phase current can be maintained at maximum

level so that maximum constant power can be obtained. By phase advancing and employing single pulse operation of the phase current, flux linkage can be weakened and the speed can be increased rapidly and the motor run at very high speed. The switched reluctance drive can therefore operate over a very wide speed range with good power output characteristics.

D. Modulation Of Current Conduction Angle

Another simple control operation is the modulation of total current conduction angle with turn on and turn off angles with respect to the rotor position by modulation of the current level. Using the method, the maximum conduction angle can be modulated according to the PWM voltage level or by current chopping technology.

E. Sliding Mode dc link power control with phase current feedforward

This approach is the author's invention, and is described later. Since the switched reluctance drive system is a highly non-linear dynamic system, it is very difficult to predict and estimate the effects of changes in the system. In this case, conventional control methods struggle to satisfy the requirement of a real system. Even if a general closed loop controller is used, the performance is still not acceptable. However, from the point of view of energy conservation, if the power delivered to the drive system can be controlled by a good control scheme, then the drive system and its related performance could be significantly improved. In the later chapters, this principle is described. By d.c. link power control and a phase current feedforward technique the electromagnetic torque during sliding mode can be reduced to a very simple equation.

electromagnetic torque during sliding mode can be reduced to a very simple equation. Combined with a variable structure speed controller, the drive system become highly robust.

2.4 ANALYSIS AND SIMULATION OF SWITCHED RELUCTANCE MOTOR CHARACTERISTICS

According to equation (2-7), the general voltage equation of a switched reluctance phase winding can be rewritten as follows:

$$v = R\,i + L(\theta,i)\frac{d\,i}{d\,t} + i\frac{dL(\theta,i)}{d\,t} + M(\theta,i)\frac{d\,i_p}{d\,t} + i_p\frac{dM\theta,i)}{d\,t} \qquad (2\text{-}23)$$

where R is the sum of the stator winding and switch resistance, $L(\theta,i)$ is the phase inductance, i_p is the algebraic sum of the instantaneous phase current in previously excited phase and the instantaneous current from other phases, $M(\theta,i)$ is the mutual inductance between this phase and another phase, p, θ is the angular position of the rotor and ω is the angular frequency of the rotor. Other parameters are the same as in the equation (2-7). Therefore, the switched reluctance motor can be represented by an equivalent circuit shown in Fig. 2-5.

$$\text{where} \quad e = i\frac{dL(\theta,i)}{d\,t} + M(\theta,i)\frac{d\,i_p}{d\,t} + i_p\frac{dM\theta,i)}{d\,t}$$

$$= \left[i\frac{dL(\theta,i)}{d\,\theta} + M(\theta,i)\frac{d\,i_p}{d\,\theta} + i_p\frac{dM\theta,i)}{d\,\theta}\right]\omega \qquad (2\text{-}24)$$

From equation (2-24), it can be seen that that e is proportional to ω, denoting the back EMF.

Generally, $M(\theta,i)$ can be neglected since the mutual coupling in most switched reluctance drives is amall. Furthermore, it is not uncommon to have only one phase carrying current at any one time. So the equation (2-23) can be simplified as

$$v = R\,i + L(\theta,i)\frac{d\,i}{d\,t} + \omega\, i\frac{dL(\theta,i)}{d\,\theta} \qquad (2\text{-}25)$$

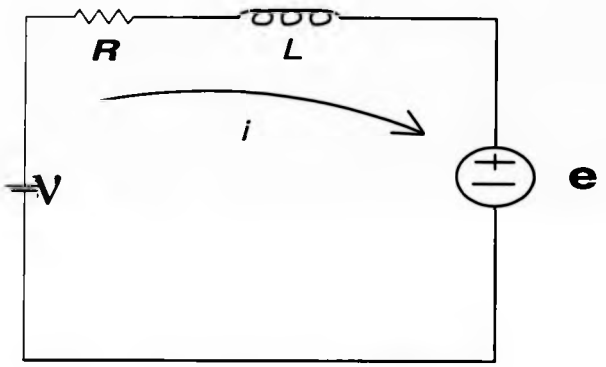

Fig. 2-5. Equivalent circuit of the switched reluctance motor

According to the equation (2-25), the phase current can be found if d.c. supply voltage v, the parameter R, L and e in the equivalent circuit shown in Fig. 2-5 are given. Although the real mutual inductance between the phase windings can be nearly neglected, the self inductance in the phase winding is not fixed, and is related to the rotor position and the level of the phase current. So the equation (2-25) is a difficult non-linear differential equation. However, the characteristics of the circuit can be defined for a computer simulation. In this context, by a simulation package, VISIM, the phase current and the related torque can be solved and its characteristics can be understood. In the equation (2-25), $\frac{dL(\theta,i)}{d\,\theta}$ plays a very important role. From the

geometry structure of the motor lamination, the self inductance profile can be conveniently approximated by a sinusoidal function plus a d.c. component. So, for a 8/6 four phase switched reluctance motor, the inductance can be expressed as follows:

$$L = L_0 + L_1 \sin 6\theta \qquad (2\text{-}26)$$

where L_0 is the d.c. component of the self inductance and L_1 is the amplitude of the fundamental component of the self inductance.

Figure 2-6 is the block diagram of the self inductance using VISIM package. In this diagram, L_0 = 0.0375 h and L_1 = 0.035 h, the angular frequency is 1256.637 Hz the inductance profile is edited by a modified sinusoidal function. Combined with the figure 2-6, the equation (2-25) can be implemented by the block diagram shown in Fig. 2-7. In the Fig. 2-7, the resistance is 4 ohm,and the input d.c. supply is 300 V. It is assumed that a split d.c. converter is used so that the voltage used for each phase is 150 V. Fig. 2-8 shows the simulated results which the motor is operated at 500 r/min. Fig. 2-8(a) is the simulated phase inductance in henries. Fig. 2-8(b) shows the simulated phase voltage (V). Fig. 2-8(c) shoes the simulated phase current (A) and Fig. 2-8(d) shows the simulated phase torque (Nm). From Fig. 2-8(c), it can be seen that there is a regenerative tendancy in the phase current. In the simulated phase torque, there is a negative torque during decreasing inductance region. This result shows that the phase current must be operated within the increasing inductance region to produce an effective positive torque and to avoid negative torque. Therefore, the phase current must be advanced to avoid producing negative when the motor is operated under high speed. This fact can be seen from the simulated results shown in Fig. 2-9(a) ~ Fig. 2-9(d), operation here is at 3000 r/min, whose turn-off phase angle is advanced.

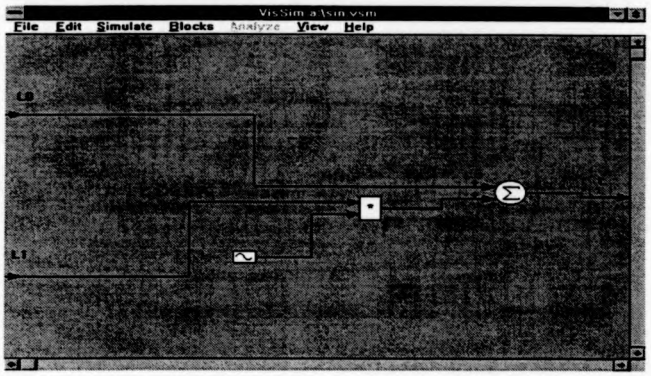

Fig. 2-6. An inductance profile of the switched reluctance motor.

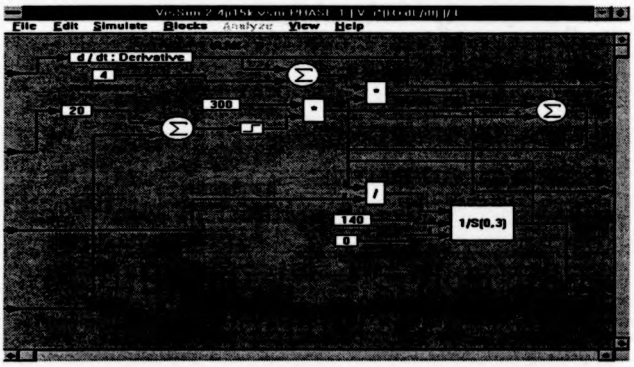

Fig. 2-7. Block diagram of the equivalent circuit in each phase winding.

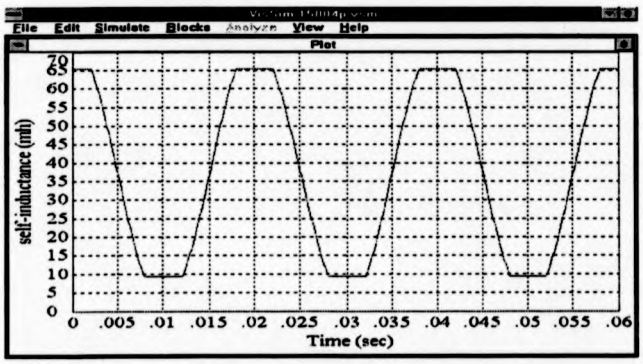

Fig. 2-8(a) A simulated self inductance under 500 r/min.

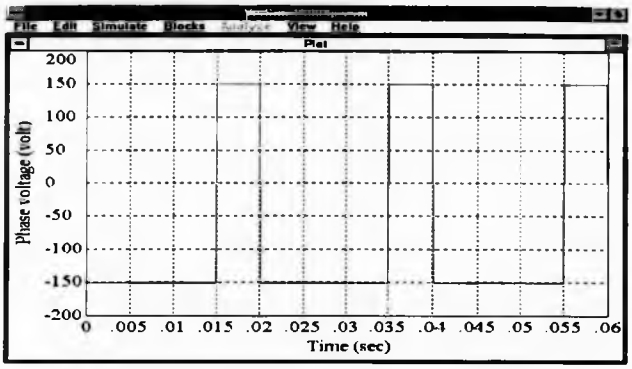

Fig. 2-8(b) A simulated phase voltage at 500 r/min.

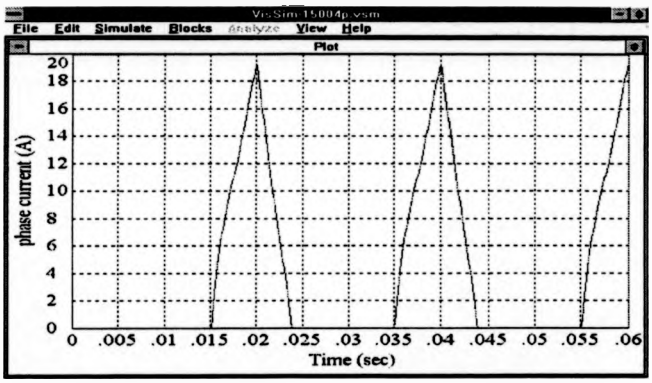

Fig. 2-8(c) A simulated phase current at 500 r/min.

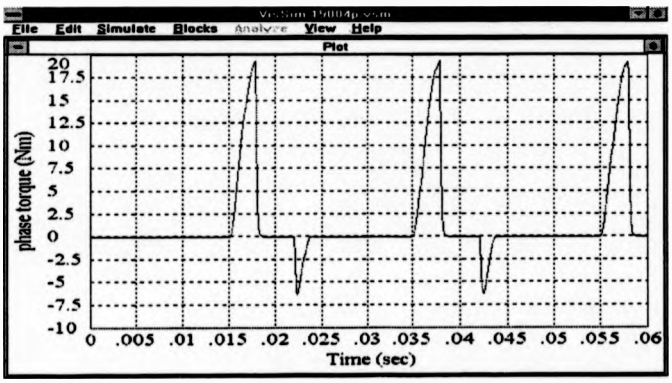

Fig. 2-8(d) A simulated phase torque at 500 r/min.

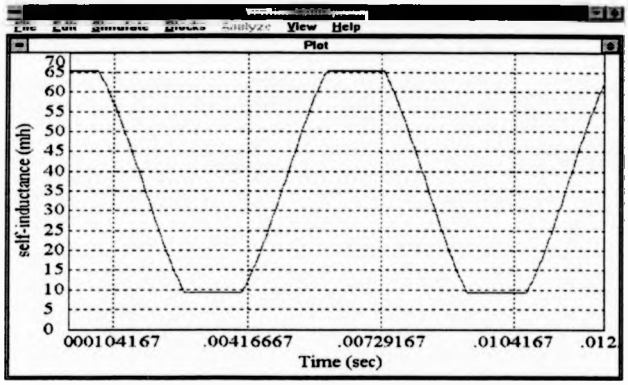

Fig. 2-9(a) A simulated phase self inductance at 3000 r/min.

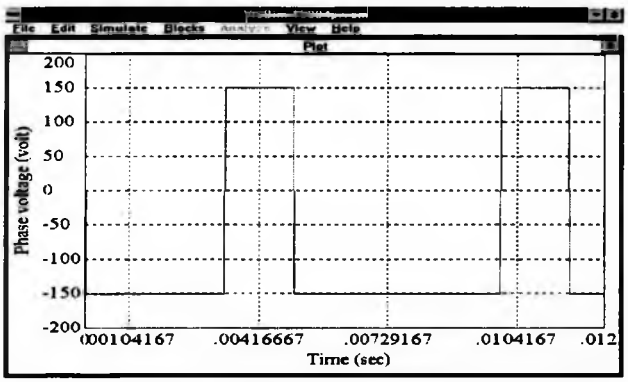

Fig. 2-9(b) A simulated phase voltage at 3000 r/min.

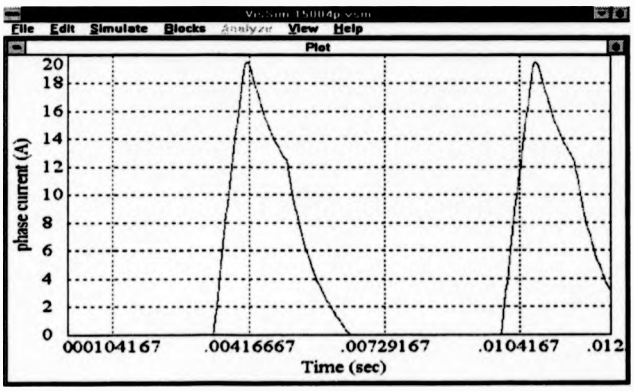

Fig. 2-9(c). A simulated phase current at 3000 r/min.

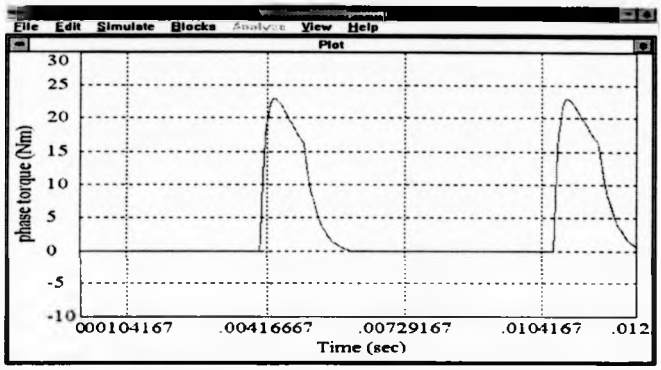

Fig. 2-9(d). A simulated phase torque at 3000 r/min.

2.5 EXPERIMENTAL INVESTIGATION OF SPLIT-LINK POWER CONVERTER

In order to develop a high performance Split-link converter for a switched reluctance servo drive, a conventional Split-link converter was modified to satisfy the required operation performance. Firstly, the basic chopping mode for singly-excitated and multiply-excited operation must be achieved. Secondly, the capability to operate in the highly difficult regenerative mode must be achieved. Thirdly, motoring and regenerative operation during high speed must be achieved. The following illustrations are some experimental investigation to show the high performance of the developed split-link converter.

Using a conventional four phase split-link converter, the normal chopping operation is carried out under 500 r/min. The experimental result is shown in Fig. 2-10(a). From this picture, it can be seen that the basic chopping mode has been achieved at 500 r/min. The regenerative experiment was done at 500 r/min. This result is shown in Fig. 2-10(b). When the operated rotor speed is increased up to 2380 r/min, the

chopping performance disappears but doubly-excitation operation under phase flux advancing is carried out. This result is shown in Fig. 2-11(a). From this figure, the real phase current in channel one and channel two can not be chopped at the prescribed reference level but the corresponding phase voltage waveform in channel three and four show that the modulation of the phase flux can still be partly achieved. The corresponding regenerative operation, running around 2380 r/min, was carried out. The result is shown in Fig. 2-11(b).

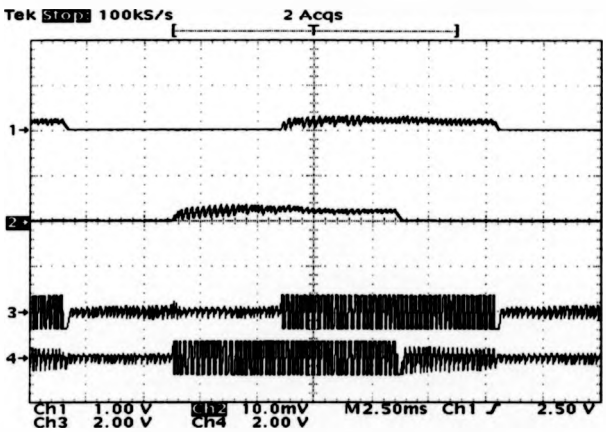

Fig. 2-10(a) Phase current and voltage waveforms during motoring state.

Ch1: phase-1 current, 10 A/div; Ch3: Phase- voltage, 400 V/div;

Ch2: phase-2 current, 10 A/div; 400 V/div; Ch4: phase-2 voltage, 400 V/div.

Time : 2.5 ms/div

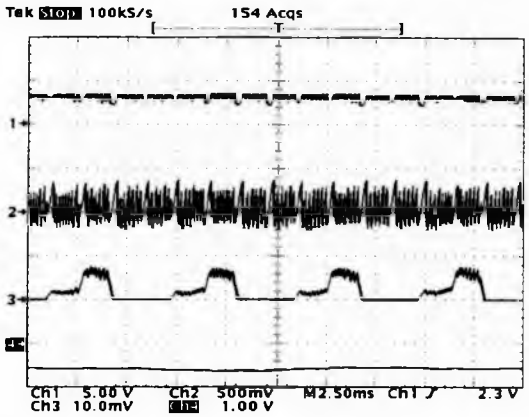

Fig. 2-10(b). Phase current and voltage waveforms during regenerative state.

Ch1: total som of all phase currents,12.5 A/div; Ch3:phase-1 current, 10 A/div;

Ch2: d.c. link current, 5 A/div; Ch4:shaft speed, 500 r/min.

Time: 2.5 ms/div.

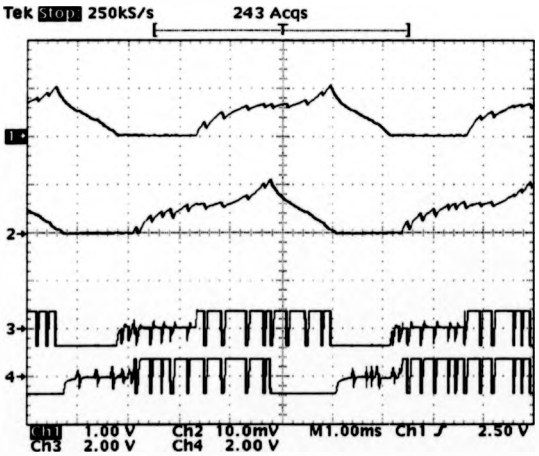

Fig. 2-11(a) Phase current and voltage waveforms during motoring state.

Ch1: phase-1 current, 10 A/div; Ch3: Phase-1 voltage, 400 V/div;

Ch2: phase-2 current, 10 A/div; Ch4: phase-2 voltage, 400 V/div.

Time: 1 ms/div.

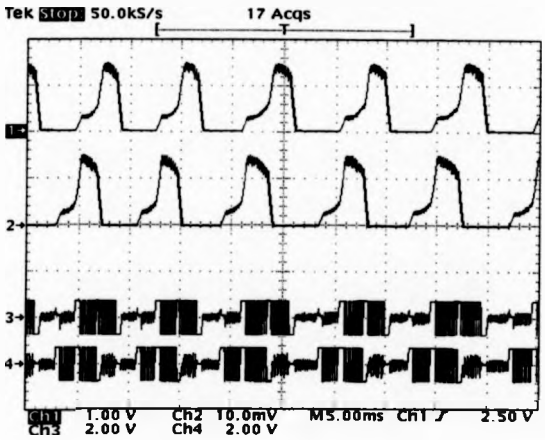

Fig. 2-11(b). Phase current and voltage waveforms during regenerative state.

Ch1: phase-1 current, 10 A/div; Ch3: Phase-1 voltage, 400 V/div; 10 A/div;

Ch2:phase-2 current, 10 A/div; Ch4: phase-2 voltage, 400 V/div.

Time: 5 ms/div.

These tests show that the basic operation of the converter has been proven. The author will now go on to develop the advanced control algorithms that lead to increased performance from the drive.

CHAPTER 3

POWER CONVERTER AND SWITCHED RELUCTANCE DRIVE

3-1. Introduction

There are several well known power converters which be used in a practical switched reluctance drives such as the Dump-Resistor converter, the asymmetric half bridge converter, the C-Dump, Miller, Pollock, and split-link converter. In this chapter, several frequently used power converters are described. In addition, a simple and effective control scheme is added to a power converter to achieve synchronously singly-excited, switched reluctance drive. As for more advanced power converter for a switched reluctance flux vector drive is described, in detail, in the next chapter and chapter five.

3-2. Existing Power Converter [12-24]

A. Dump-Resistor Converter

The circuit is shown in Fig. 3.1 for a three-phase switched reluctance motor. Only a snubber circuit and one dump resistor are necessary. Only one power supply is required for all the gate drive circuits because all the switches share a common point. When a phase switch is turned on, a dc-link voltage is applied to the phase winding. Energy is transferred from dc-link source to the motor. Part of energy is converted to mechanical energy, some is stored in the magnetic field. When the phase switch is

turned off, the stored energy freewheels via the winding, the freewheeling diode, and the dump resistor so that part of the energy is dissipated in the dump resistor and winding resistance while the rest is converted into mechanical energy. During this operating period, the voltage across the switch equals the sum of the voltage drop across the dump resistor and dc-link supply. This advantage of the circuit is simple in its converter topology but its disadvantage is the high energy losses in the Dump-resistor if high frequency switching is required under high load.

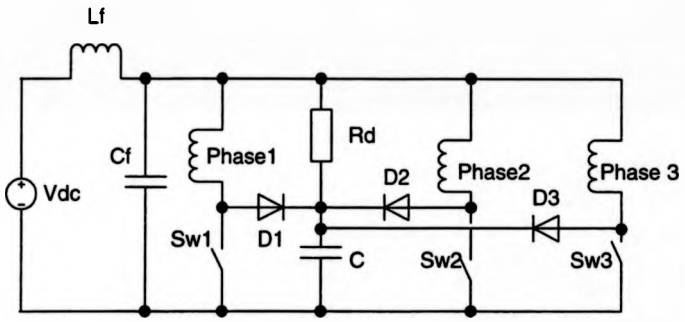

Fig. 3-1. 3-phase dump-resistor converter.

B. Asymmetric half-bridge converter

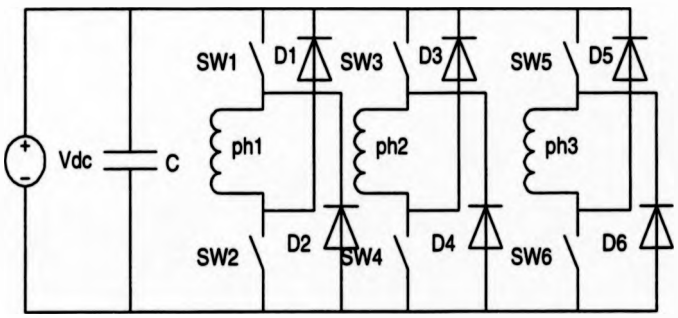

Fig. 3-2. Asymmetric half-bridge converter

This circuit uses two power semiconductor switches and two fast recovery diodes for each phase winding, as shown in Fig. 3-2. In the converter, there are three

conventional modes of operation which can be used. The first one is the positive voltage loop, which occurs when both power switches are simultaneously turned on. In this state, the supply voltage is connected across the related phase winding and the current in the phase winding is produced. The second operation is called 'zero voltage loop', which occurs if either of two power switches is turned off when current is flowing in the phase winding. In this case the phase current continues to flow through the power switch and the corresponding freewheel diode. During this operating state, the Back EMF induced in that phase winding becomes the power source and the current flowing in this loop gradually decreases due to the power dissipation in the phase winding resistance. The third operating state is called 'negative voltage loop', which occurs when both power switches are simultaneously turned off. In this case, the current is forced flow through both freewheel diodes and the dc power supply loop. The current decreases rapidly because the energy stored in the motor is returned to dc supply. Selected power switches and freewheel diodes must be sufficiently rated to withstand the transient votage and currents. The main disadvantages of the circuit is that it requires two power switches and two freewheel diodes per phase. Too many power switches and diodes will increase the switching losses during switching state. So, this circuit is not suitable for high frequency switching operation. However, its main advantages are :

(1) The rated positive dc power supply voltage can be used to increase the phase current during positive voltage loop so that the current level can reach the required value quickly.

(2) The rated negative dc power supply voltage can be used to decrease the phase current during a negative voltage loop to return excessive energy from the motor to dc power source.

(3) The phase current can usually be maintained at the required level by zero voltage loop when chopping mode is necessary.

C. C-Dump converter

a. C-Dump converter with resonant energy recovery

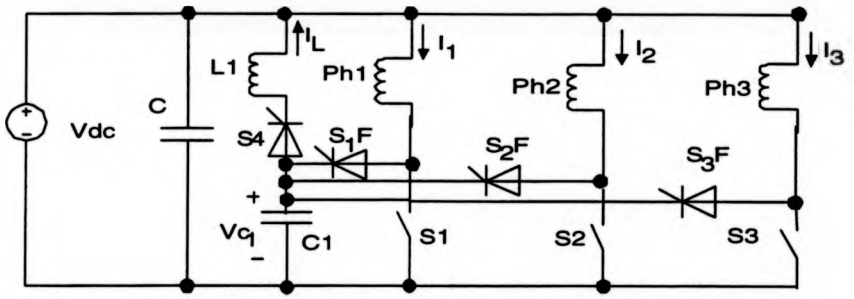

Fig. 3-3. C-Dump converter with resonant energy recovery

Referring to the circuit shown in Fig. 3-3, the circuit is called 'the C-dump converter' because the trapped energy is dumped into a capacitor before being returned to the dc supply by a resonant circuit. In this circuit, there is only one switch per phase, and it uses a single rail dc supply. When S_1 switches off, the phase current i_1 which was flowing through S_1 commutates to D_{1F} and begins to charge capacitor C_1. As the voltage in the capacitor is increased, the phase current decreases rapidly. Eventually, all the trapped energy is stored on the capacitor. If energy is required to return to the dc source, S_4 can be fired, thus C_1 will discharge its energy resonantly via L_1 into the

dc source capacitor C. S_4 turns off when i_L reaches zero. However, during the resonant recovery, the freewheeling SCR's become forward biased when $v_{c1} = V_{dc}$.

b. C-Dump converter with damped energy recovery

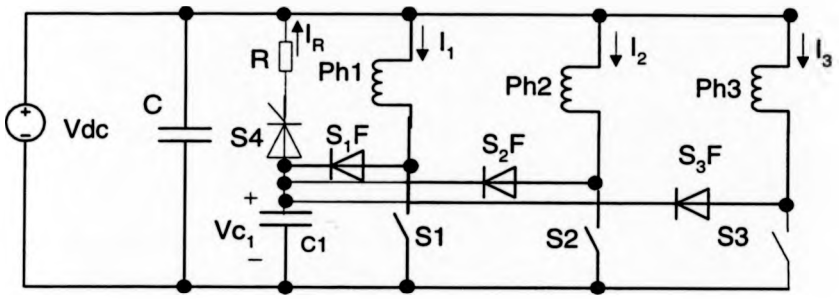

Fig.3-4. C-Dump converter with damped energy recovery

In Fig. 3-3 the difficulties of the circuit is that v_{c1} falls, well below V_{dc}, making it necessary to use the free-wheeling thristor rather than a free-wheel diode. It is desirable to maintain the capacitor voltage v_{c1} above the supply voltage. This can be achieved by the circuit shown in Fig. 3-4. The resistor prevents v_{c1} from dipping below V_{dc}, but the resistor also dissipates part of the energy being recovered.

c. C-Dump converter with chopping energy recovery

The circuit in Fig. 3-4 can recover part of the trapped energy while still permanently maintaining the dump capacitor voltage above the supply voltage. However, the amount of energy lost during the recovery cycle would be unacceptable. Another improved topology is shown in Fig. 3-5., which provides a low-loss means of recovering the stored energy while permanently maintaining the capacitor above the supply voltage. When the chopper switch is closed, the dump capacitor C_1 begins to

discharge. After the chopper switch is opened, the stored energy in L is returned to the source through the free-wheeling diode D.

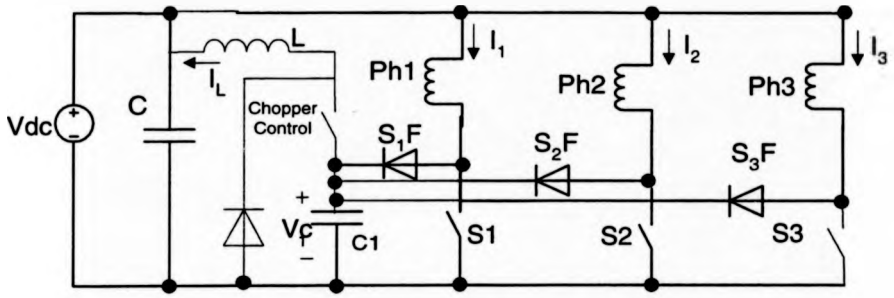

Fig. 3-5. C-Dump converter with chopping energy recovery.

D. Miller Converter

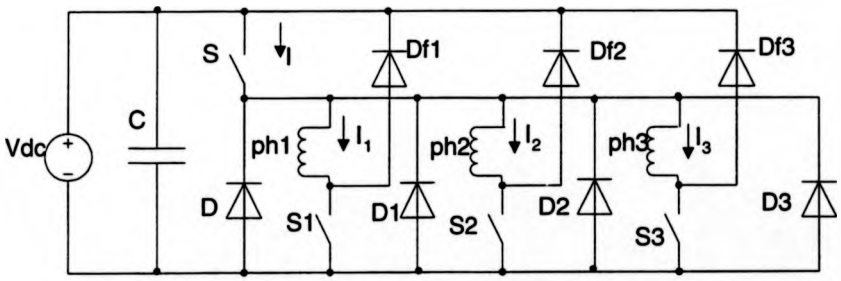

Fig.3-6(a). A 3-phase miller's converter.

Although the asymmetric half-bridge converter is a good power converter, allowing three types of operating modes, it is unsuitable for multiple phase motors because it needs many switches and freewheel diodes. Therefore, an improved design was developed by Miller [12]. The circuit shown in Fig. 3-6(a) is its typical circuit for three-phase switched reluctance motors. The upper transistor S serves all three phases, while the lower switches control each phase. S must be operated with a sufficiently low duty-cycle so that when one phase is turning off, it has sufficient reverse voltage.

A useful variant uses one upper switch between each pair of phases in a 4-phase drive, giving a total of six transistors, as shown in Fig. 3-6(b). If the chopping transistors are connected to phase 1 & 3 and 2 & 4 respectively, the problem of overlap is greatly reduced and all phases can have the maximum reverse voltage during turn-off. However, the improved circuits are suitable for only single excitation. According to author's research, Miller's converters are not appropriate for simultaneous, multiple excitation because the shared top switch will be burned down during high speed or regenerative state unless a very high current rating switch is used.

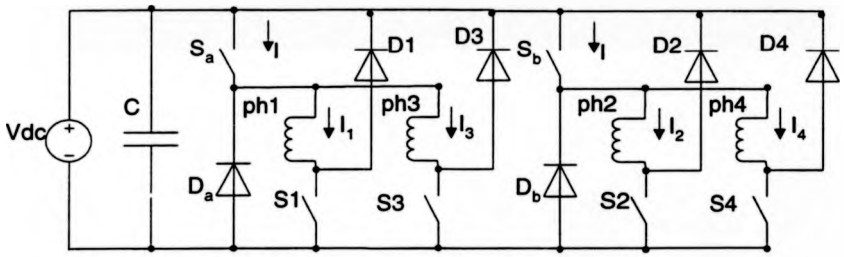

Fig.3-6(b). A 4-phase power converter.

E. Pollock Converter [19]

This circuit for a four-phase is shown in Fig. 3-7. It contains two power switches, S_b and S_d, each one connecting two of the phase windings to the positive supply rail, and two further switches, S_a and S_c, to connect the other ends of the phase windings to the lower supply rail. Each phase winding is connected to a different pair of top and bottom switches. This circuit has the switch to motor voltage ratio of the asymmetric half-bridge and yet has only one switch per phase winding. The current rating of each switch is higher to allow for the additional current through it.

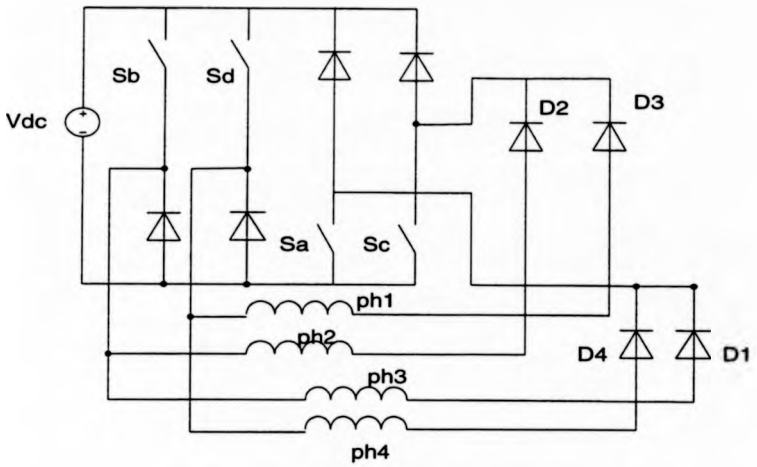

Fig. 3-7. 4-phase Pollock's converter

In this circuit, each switch is connected to two phase windings. The flow of current in both the phase windings is affected if the state of the switch is changed. Namely, a positive voltage loop in one phase winding cannot be accomplished by a negative voltage loop in the adjacent phase winding. Sequentially excited phase windings share a common switch. When the current is flowing in phase winding 1. Switch S_b can be kept on all the time, while switch S_a can be chopped at high frequency with an adjustable duty ratio or it can be chopped by current feedback. Phase winding 2 is next to be energized to continue the rotation of the rotor in an anticlockwise direction. By closing switch S_c the current can build up in phase winding 2. When this current reaches the required value it can be chopped using switch S_c independently of the current in the first phase. Some time later it is necessary to decrease the current in phase winding 1, while maintaining the current level in second phase winding. This can be achieved by turning off switch S_a and interchanging the operation of S_b and S_c. The chopping of the current in the phase winding 2 is controlled by switch S_b.

When S_b is on, the current in phase winding 1 decays slowly in a zero voltage loop, and when it is off, this current falls much faster in a negative voltage loop. The switching sequence is identical for other switches.

F. Split-link converter [12],[19]

This converter is a very simple and popular power converter, and is as shown in Fig. 3-8. Its advantages are that it has the minimum number of power switches and energy can be returned to the power source during turn-off period. The DC link voltage is split with two capacitors so that only half of the full voltage from the input source can be used. Therefore, the converter is usually suitable for only low speed operation because the phase current cannot be chopped during high speed and the half of the full voltage limits the maximum back EMF induced in the phase winding so that the highest rotor speed is limited. Another disadvantage in the converter is that it cannot be used in odd-phase motors because an unbalanced phase voltage across each phase winding will occur.

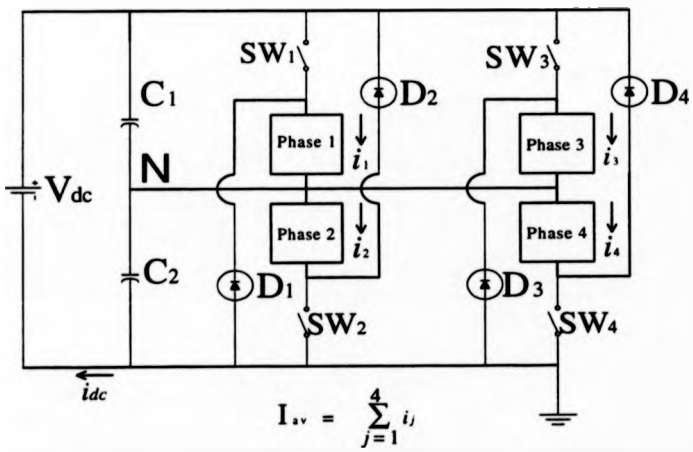

Fig. 3-8. A 4 phase split-link converter for a switched reluctance motor.

3-3 Space vector controlled split-link converters

This converter developed by the author is basically a split-link converter but its performance is absolutely different from the conventional one. It retains the advantage of traditional split-link converters but it can also be used with odd-phase motors. This is one of author's significant contributions to switched reluctance power converters. Used in odd-phase switched reluctance motors, the unbalanced supply voltage problem can be overcome even under high load conditions because a feedforward current controller or a phase power controller can be used to solve this problem. In chapter four and five, space voltage vectors will be suitably selected to regulate flux linkage by a variable structure controller with sliding mode. Thus the proposed split-link converter can not only be used in low speed operation but also in high speed operation. Under multiply-excited operation or even in regenerative mode, it can still work well.

3-4. SYCHRONOUS SINGLY-EXCIED POWER CONVERTER

The switched reluctance motor is a doubly salient machine, which has a nonuniform air gap between the stator and the rotor, giving a nonlinear variation in inductance of the stator winding as the rotor rotates. The higher the speed is, the quicker the variation of the inductance becomes, making a rapid dynamic nonlinear time-varying system. In this situation, the torque developed by the switched reluctance motor is determined by the angular position and the amplitude of the phase current [25]-[30]. Conventionally, the phase current controller for the switched reluctance motor has been designed only considering the current control, ignoring the requirement of the load. Such a current controller may not be particularily good when load disturbances exist in the real drive system [25]-[30]. The most obvious problem is that the current waveform is distorted during load variation even if it is under light load. Another example is that the drive system can easily oscillate because of variation of the mechanical load. Owing to the shortage of load regulation, a drive using a conventional current chopper can easily oscillate at the mechanical natural frequency even when closed loop speed control is added. In this section, the author propose a simple synchronous singly-excited phase current controller for a switched reluctance drive. The current controller is different from the conventional current chopper because it can regulate load angle such that the relative electric angle between the phase current and rotor pole is located between $\pi/8$ and $3\pi/8$. When the relative angle is located between $\pi/8$ and $3\pi/8$, the current controller will become a current chopper under the normal motoring operation. Therefore, the time-varying coordinate transformation in a traditional field-oriented

a.c. machine becomes unnecessary and the simple split-link power converter can be used to achieve high-performance switched reluctance drive..

3. 4-1 BASIC ANALYTICAL MODEL AND CONTROL PRINCIPLE

A. Control Characteristics of Singly-excited Switched Reluctance Drives

The general voltage equation for each phase winding in the conventional power converter circuit of the switched reluctance motor, as shown in Fig. 3-10 , is given by

$$\upsilon = r\, i + \frac{d\lambda}{dt} \tag{3-1}$$

where υ is the voltage applied to the phase winding and r is the resistance, i the current , and λ the stator flux linkage associate with the switched reluctance motor phase coil, respectively. The flux linkage equation can be expressed as

$$\lambda = L(\theta, i)\, i \tag{3-2}$$

where $L(\theta,i)$ is the instantaneous inductance of phase windings, through which phase current i is flowing, at angular position θr. By neglecting the voltage drop on the resistance and substituting (3-2) into (3-1), we get

$$\upsilon = L(\theta, i)\frac{di}{dt} + \omega\, i\, \frac{dL(\theta, i)}{d\theta} \tag{3-3}$$

where $\omega = \frac{d\theta}{dt}$ is the angular frequency of the rotor.

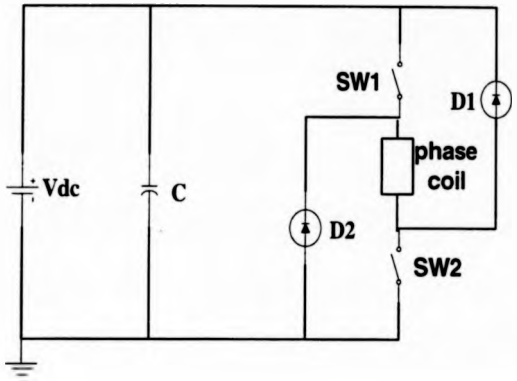

Fig. 3-9. The Switched Reluctance power converter for each phase winding.

Equation (3-3) shows that the phase current is dependent on the phase voltage, $L(\theta,i)$ and $dL(\theta,i)/d\theta$, but the solution of equation (3-3) to find the current is very difficult because $L(\theta,i)$ and $dL(\theta,i)/d\theta$ are nonlinear functions of the position θr and current i. To simplify the control of phase current, it is appropriate to control di/dt. If over a switching cycle the change in current, Δi, can be controlled to be small, then di/dt can be approximately to zero. Therefore, equation (3-3) becomes

$$i = \frac{\upsilon}{\omega \, dL(\theta,i)/d\theta} \tag{3-4}$$

From (3-4), it can be seen that the phase current i depends on ω. If the shaft speed, ω, is high such that back EMF, $\omega \, dL(\theta,i)/d\theta$, is sometime larger than power supply voltage V_{dc}, then phase current i will decrease. Thus the phase current waveform will be distorted or will become uncontrollable in this situation. Therefore, phase current must be limited to a maximum value at rated speed. Assume this value is labeled as I_m, then conventional current chopper naturally can be appropriately

operated so that demand of phase current is not larger than I_m. However, $dL(\theta,i)/d\theta$, the inductance variation with respect to position, is not constant unless the phase current is maintained in the linear region. In general, a switched reluctance motor is operated in saturation to increase its efficiency. Therefore, a dynamic nonlinear current controller is required to satisfy the practical requirements. Meanwhile, the system also needs a speed controller, otherwise the phase current can not be controlled effectively and satisfactorily. Fortunately, there is a position sensor for phase commutation in a switched reluctance drive system. If the phase current can be controlled so that it is synchronous to the rotor position, then the control of the phase current in the stator phase winding will be simplified as it will only be related to two variables. One is the amplitude of phase current, the other is the load torque angle, i.e. the relative angular position between the rotor position without load and the rotor position with load. The control of the load torque angle is unnecessary because it can be converted into the indirect speed error control. This idea greatly simplifies the phase current controller so that only speed error compensation and amplitude regulation of the phase current are sufficient in a real switched reluctance motor current controller.

B. The Principle of Load Torque angle Control

For an ideal switched reluctance motor, the rotor flux distribution would be sinusoidal in space. Unfortunately, the salient pole structure in switched reluctance motors do not always produce this feature. However, first of all, we can study an ideal rotor flux distribution under unsaturated condition and use the flux without load as the "flux component Reference Model", then adaptively regulate the phase current according to torque formula under ideal unsaturation case until the real rotor position with load is

aligned with the rotor position without load. When the switched reluctance drive system is loaded by a dynamic load, the on-line measurement of the rotor flux vector with load is difficult. However, knowing that the real rotor position is the same as position of the rotor flux vector under no load simplifies the design of the load torque angle controller. For a unknown dynamic load, when the phase current is regulated until there is no speed error, then the real rotor flux vector leads the real rotor position by the load torque angle. The real rotor position is the same as position of the rotor flux vector without load. If it is the case, the current controller will now force the rotor pole to follow the rotor flux vector rotating with reference speed.

Since the switched reluctance motor has a periodic stator and rotor flux distribution [24], with minimum flux in unaligned position and has maximum flux in the aligned position, so the ideal stator flux and rotor flux can be simplified and can be approximately expressed as

$$\begin{aligned} \lambda_s &= L_{ls}\, i + \lambda_r \\ &= L_{ls}\, i + \{ L_A - L_B \cos [2(\omega_r t + \delta)] \}\, i \end{aligned} \tag{3-5}$$

where λ_s and λ_r denote the stator and rotor flux vector, respectively.

L_{ls} is the leakage inductance

$\omega_r t$ is the electrical angular displacement of the rotor flux vector

$\omega_r t + \delta$ is the electrical angular displacement of each rotor pole

δ is the torque angle between each rotor pole and its corresponding rotor flux vector.

δ_m denotes the maximum torque angle when the phase winding is excited by the maximum phase current, Im.

$L_A = (L_d + L_q)/2$ and $L_B = (L_d - L_q)/2$.

Ld is the maximum inductance when the rotor and the stator are aligned, which corresponds to $\omega_r t = \pi/2$ & $\delta = \delta_m$

L_q is the minimum inductance when the rotor and the stator are unaligned, which corresponds to $\omega_r t = 0$ & $\delta = \delta_m$.

Since the phase current is synchronous with rotor flux vector, their angular frequencies are same but the angle between them is not fixed because load is not always constant. Obviously, the leading electrical angular displacement of the rotor flux vector with respect to the rotor pole is not always fixed. Therefore, if the angle between the phase current and rotor pole is fixed, the real rotor position can be controlled by regulating the amplitude of the phase current. If the rotor pole is located at the minimum inductance position for t = 0, then the electrical angular position of the rotor pole at time t , θr , can be defined as

$$\omega_r t = \theta_r = \frac{N_r}{2}\theta_{rm} \qquad (3\text{-}6)$$

where is the number of rotor poles, θ_{rm} is the mechanical position of the rotor pole at N_r time t . From (3-4) and (3-5), because L_{ls} is essentially constant, if the mutual inductance between phase windings and the voltage drop on the resistance are neglected, and the angular frequency of the rotor flux vector is also controlled so that

it can maintain at constant value, ω, during some short time period, then the differential equation governing the phase current will be same as (3-3). By (3-2), (3-4) and (3-5), the phase current can be found as follow.

$$i = \frac{\upsilon}{\omega\,[2\,L_B\ \mathrm{SIN}\ 2(\theta_r+\delta)]} \tag{3-7}$$

Therefore, neglecting saturation case, the approximate average electromagnetic torque over a short switching cycle becomes [38]

$$T = \frac{\upsilon\, i}{2\,\omega}\Big|_{i\ =\ \text{constant}} = [\,L_B\ \mathrm{SIN}\ 2(\theta_r+\delta)\,]\,i^2 \tag{3-8}$$

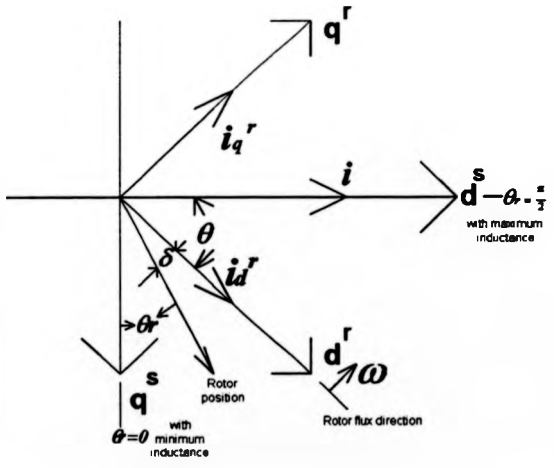

Fig. 3-10. Rotor Flux Field-Oriented Vector Diagram.

If the phase current vector i in the stator winding is selected as the d^s axis of the stator reference frame and the minimum inductance position is selected as q^s axis, the radial direction of the rotor flux vector is selected as the d^r axis of the rotor reference

frame and its tangent direction is selected as the q^r axis, as shown in Fig. 3-10. From Fig. 3-10, one can get the following equations

$$i_d{}^r = i\,COS\,\theta = i\,SIN\,(\theta_r+\delta)$$

$$i_q{}^r = i\,SIN\,\theta = i\,COS\,(\theta_r+\delta) \qquad (3\text{-}9)$$

Choosing $\lambda_r' = L_B\, i_d{}^r$, from equation (3-9) and Fig. 3-11, one can obtain the electromagnetic torque in the rotor reference frame as follows:

$$T^r = \lambda_R \times i = \lambda_r'\, i_q{}^r$$

$$= [\,L_B\,SIN\,2(\theta_r+\delta)]\,i^2 \qquad (3\text{-}10)$$

where λ_R denotes the modified rotor flux vector and $\lambda_r' = L_B\, i_d$ does its magnitude , " $\times$ " does vector product. From equation (3-8) and (3-10) one can see that the electromagnetic torque in the rotor reference frame, T^r, is equivalent to that in the stator reference frame, T. This means that the field-oriented rotor flux component and torque component can be decoupled and the torque applied on the rotor to change the real electrical angular position of the rotor pole. However, from the equation (3-8) it can be seen that the torque is dependent on the real rotor position θ_r, the load torque angle δ, and the amplitude of the phase current. In other word, the control of the phase current is determined by the real rotor position θ_r, the load torque angle δ and the demand torque. If T_c denotes the required command torque in the switched reluctance drive, then providing $(\theta_r+\delta)$ is not equal to 0 or $\pi/2$, the exciting current i can be found as follow.

$$i = \sqrt{\frac{Tc}{L_B \, SIN \, 2(\theta_r + \delta)}} = \sqrt{\frac{q \, T_m \, cosec \, 2(\theta_r + \delta)}{L_B}} \qquad (3\text{-}11)$$

where T_m is the maximum torque when the maximum phase current, I_m, is excited at $(\theta r + \delta) = \pi/4$ and $\delta = \delta m$. $q = T_c/T_m$, is a weighting factor. Since I_m denotes the maximum exciting current corresponding to T_m, so $I_m = \sqrt{T_m/L_B}$. Thus, substituting I_m into equ. (3-11) yields

$$i = I_m \sqrt{q} \sqrt{cosec \, 2(\theta r + \delta)} \qquad (3\text{-}12)$$

From equation (3-12) one can see that if $(\theta_r + \delta)$ is either 0 or $\pi/2$, then i will become very large to obtain the required torque, T_c (unless q is small). Equation (3-12) can only be implemented in real time if the torque angle is known. To simplify the phase current controller, a good approximation is to modify equation (3-12) — replacing the torque angle by the increment of phase current, as shown by equation (3-13), and then limiting the excited electrical angle of the phase current to be only inside the region, $\pi/8 \leq \theta_r \leq 3\pi/8$, and within each position of the rotor pole regulating Δq until it is aligned with the demand position. In other words, it means that the turn-on electrical angle of each phase winding is at $\pi/8$, while its turn-off electrical angle is at $3\pi/8$. The main reason using the phase current increment to replace the torque angle is that the torque angle is dynamic and uncertain and the accurate rotor flux position is difficult to find, but through iterative regulation of the phase current the real rotor position will be forced to track the position of the rotor flux vector under no load so that it can smoothly rotate by the reference angular frequency, ω.

$$i = \sqrt{q + \Delta q}\ I_m \sqrt{\text{cosec } 2\theta_r}$$

$$= 1.118\, I_m \sqrt{q + \Delta q} \qquad \text{for } \pi/8 \le \theta_r \le 3\pi/8 \qquad (3\text{-}13)$$

where 1.118 is the average value of $\sqrt{\text{cosec } 2\theta_r}$ in the region , $\pi/8 \le \theta_r \le 3\pi/8$. If so, the phase current ripple can be largely reduced and the phase current can be approximately controlled just by regulating q value according to speed error because $1 \le \sqrt{\text{cosec } 2\theta_r} \le 1.189$ holds and its average value is 1.118 for $\pi/8 \le \theta_r \le 3\pi/8$. Thus both the electrical noise emission and the vibration in the switched reluctance motor can be largely reduced. Meanwhile, torque control can be also greatly simplified so that it can become just a phase current control. As a result, even a low cost 8-bit microcomputer can be used for implementation of the high performance switched reluctance drive.

C. Synchronous Phase Current Amplitude Control

From above theoretical analysis, obviously the phase current in the stator phase winding plays the most important roles in the switched reluctance drive system. According to equation (3-13), the amplitude of the phase current can be approximately constant for $\pi/8 \le \theta_r \le 3\pi/8$ and depends on I_m and $\sqrt{q + \Delta q}$. Therefore, a real-time phase current controller to track $1.118\ I_m \sqrt{q + \Delta q}$ is necessary. Once the controller is accomplished, then control of the phase current will become just the control of $\sqrt{q}$. The real-time phase current controller can be realized by a " Model Reference Adaptive Current Controller " combined with a " PWM voltage modulator ", in which the phase current with adjustable switching frequency has to be

synchronized to each rotor position signal according to the field oriented theory. This technology can result in a more stable, accurate, and no drift real-time current from the rotor flux reference frame.

The PWM switching frequency can be adjusted to 20 KHz or more higher frequency if required and then compared with the demand current signal. The PWM switching signal can be designed as digital pulse trains. The positive edge of each pulse triggers and turns on the corresponding power switch in Fig. 3-9 until the real phase current reaches its reference value. When the real current reaches this reference value, the negative edge signal from a comparator immediately triggers and turns off corresponding power switch. When the power switch is turned on the positive d.c. voltage is supplied and when it is turned off the zero d.c. voltage is supplied if it is operated before commutation, but the negative d.c. voltage is supplied after commutation Mathematically, these phase voltage can be written as

$$V_i = S_i * V_{dc} \tag{3-14}$$

where V_i is the voltage of the i th phase winding and S_i is the corresponding switching logic function in the power inverter, subscript i is the phase symbol, for example a, b, c, and d for 4 phase switched reluctance motor. Therefore, the control law for each phase current can be described by the following equation

$$\begin{aligned} S_i &= 1 \quad \text{when } t = t_k \\ S_i &= 0 \quad \text{when } i = i_{ref} \\ S_i &= -1 \quad \text{after commutation} \end{aligned} \tag{3-15}$$

where t_k denotes the time when the k th pulse of the PWM switching signal transits from low to high, i does the measured phase current and i_{ref} does its reference phase current. If $i(t_k)$ denotes the phase current at t_k and the time from $i(t_k)$ to $i = i_{ref}$ is labeled by ΔT_k, then equation (3-4) can be rewritten as

$$i = \frac{(\frac{\Delta T_K \ Vdc}{2\pi})}{\frac{\Delta L(\theta, i)}{\Delta \theta}} \quad \text{for } t = t_k \text{ to } t = t_{k+1} \tag{3-16}$$

where $\Delta L(\theta, i)$ is the change in inductance from $t = t_k$ to $t = t_{k+1}$.

Obviously, if $\Delta L(\theta, i)$ in equation (3-16) is not zero or $\Delta L(\theta, i)/\Delta\theta \neq 0$, the phase current can be controlled by controlling ΔT_k even if $L(\theta, i)$ is unknown and is changing because the real phase current is linearly proportional to $dL(\theta, i)/dt$ over a switching cycle and $dL(\theta, i)/dt$ is a fixed constant over the same switching cycle. Therefore, providing the conduction region of the switched reluctance motor is not located in the region : $dL(\theta, i)/d\theta \cong 0$ and the demand phase current is not larger than I_m, then the phase current can be adaptively controlled by equation (3-15). Normally the region , $dL(\theta, i)/d\theta \cong 0$, is near maximum inductance or minimum inductance position and no back EMF is induced in the phase winding.at these points. These must be avoided to control the phase current effectively. Equation (3-15) means that as soon as the positive edge of PWM switching signal arrives the phase winding is supplied by the d.c. voltage, $+V_{dc}$, while once the real phase current reaches the reference demand value then it is grounded. However, the phase winding will be supplied by the negative d.c. voltage after commutation. So the turn-off angle must be appropriately selected to prevent the motor from producing negative torque. From equations (3-15) and (3-16), the simple current controller can force the measured phase current to track the

reference demand current as long as the PWM switching frequency is high enough and the current is less than I_m. Actually, according to author's works, it is like "A variable structure current controller", but it is more simple and more adaptive. The reference demand current signal can be considered as a switching function located on the switching plane. The switching voltage, V_i, will force the measured phase current to slide along reference demand current signal according to the switching function, S_i.

3-5. IMPLEMENTATION OF THE SYNCHRONOUS PHASE CURRENT CONTROLLER

Fig. 3-11 is the complete system block diagram used to control the phase current of the switched reluctance motor. Now its mode of operation is briefly stated as follows.

Demand speed is compared with the real rotor speed and then speed error is found. By using the load torque angle controller, speed error can be converted into $\sqrt{q + \Delta q}$ corresponding to load torque angle. After this value is multiplied by 1.118 I_m, which is obtained from adaptive phase current amplitude controller, it is again compared with the real phase current by the high speed comparator. Its error is sent to the Flip-flop to limit the real phase current. A 8051 microcomputer decodes the signal from the position sensors to detect q^s axis and the rotor pole position and generates an accurate switching function Si to drive power converter shown in Fig. 3-9. It also monitors the whole system to protect the drive from overcurrent, overvoltage and abnormal operation.

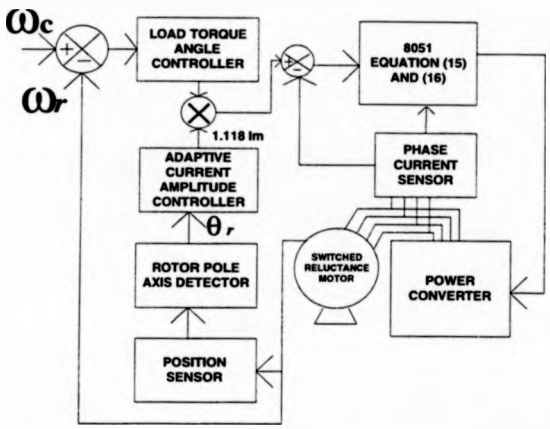

Fig. 3-11. An adaptive synchronous phase current controller block diagram.

A. The Synchronous Phase Current Amplitude Controller

The synchronous phase current amplitude controller can be implemented by hardware or software. Here it is accomplished by an Intel microcomputer, 8051, Its program is extremely simple involving just two timers, T0 and T1. T0 generates the PWM switching signal for the flip-flop, which is programmed at 20 KHz and is maintained in synchronous with the rotor position sensor. T1 is used as the timer to measured the time error between tc and tr. One bit of port 2, P2.5, is used as a output pin to produce the PWM switching signal. This is programmed as the switching function Si and its function is accomplished in the interrupt service routine of the timer 0. As soon as the positive edge of the PWM signal arrive P2.5 sends logic "HI", while the switching function is zero, i.e. Si = 0 it signal becomes "LOW". The reference current signal is generated by a D/A converter, DAC 08. The output of DAC 08 is compared with the voltage from the current sensor through a high speed comparator, LM311. The resultant output signal is clamped at +5 Volt through a pull-up resistor. In the normal

state(no over-current or over-voltage) the logic signal is programmed at "LOW" but when abnormal state occurs it will be switched to logic "HI" to protect the system. Thus this simple software can implement the amplitude control of the adaptive synchronous phase current controller because the complex coordinate transformation computation is unnecessary and its implementation is achieved by 8051 assembly language.

B. Load Torque Angle Regulation

From a previous discussion, it has been shown that the torque is the function of two parameters. One is the amplitude of the phase current, the other is the load torque angle between the rotor flux vector and the rotor pole. The load torque angle depends on the load. Controlling the amplitude of the phase current alone can not garantee the success of the current controller. To regulate the load torque angle, it is a good approach to fix the turn-on electrical angular position. In general, when the rotor moves to minimum inductance position the phase coil is excited. This means that the phase current vector leads the rotor by 90° electrical angle when $\theta_r = 0$. To get the maximum torque, this leading angle can be chosen as $\pi/4$. During high speed the larger angle should be selected to prevent the switched reluctance motor from generating negative torque. Once the leading angle is fixed, it is equivalent to fix the position of the rotor flux vector. While the real rotor position is not aligned with this position, there will be an angle error, which is firstly converted into the time error and then is measured by the timer 1 in the 8051 microcomputer. Using a PI controller the time error is converted into the q value in equation (3-13) and then by DAC 08 the reference phase current signal , given by equation (3-13), is set so that the real phase current can track the

reference current by the switching of each voltage vector, V_i, as specified by equation (3-14)-(3-16). Hence the real-time load torque angle control law can be implemented as follows:

(1) STEP 1 : Find time error corresponding to the torque angle

If ω_c denotes the command speed of Switched Reluctance Motor and real rotor speed is ω_r, then we can convert them into t_c and t_r, respectively. A measure of their error can be expressed as

$$\Delta t = t_c - t_r$$

where t_c denotes the command time period corresponding to ω_c and t_r does the time period corresponding to ω_r. The trigger time of t_c and t_r is at the same time and are synchronous to the positive edge of the PWM switching signal.

(2) STEP 2 : Find the amplitude of phase current

To make torque angle control more robust , we can set an allowable time error band, ΔB. When the time error goes outside the band, real-time phase current regulation has to be made. As previous theoretical analysis and symbols, the phase current control algorithm can be stated as follow:

(A) $i = 1.118\ I_m \sqrt{q + \Delta q}$, when $\Delta t < \Delta B$

where $q = K_p\ \Delta t$ and $\Delta q = k_i \sum \Delta t$, K_p is a proportional gain constant and k_i is the proportional integral gain constant.

(B) $i = 1.118\, I_m \sqrt{q}$, when $\Delta t > \Delta B$ and $\Delta t > 0$

where $q = K_p \Delta t$

(C) $i = 0$, when $\Delta t > \Delta B$ and $\Delta t < 0$

(3) STEP 3 : An certain if the rotor speed is correct

(A) If $\omega_r \cong \omega_c$, then keep the exciting current i and go to step (3)

(B) otherwise go to step (1)

The whole control algorithm mentioned above is implemented just by one Intel 8051 microcomputer and one current sensor thus meeting the industry applications.

3. 5-2 EXPERIMENT RESULTS

To confirm the feasibility of the phase current controller proposed in this chapter, some experiments have been performed and their results are shown in Fig.3-12 ~ Fig. 3-13.. In these experiments, the load is one 7 KVA d.c. generator with adjustable d.c. field current.. The d.c. armature current is dumped into a resistance load. In the no-load condition the switched reluctance motor is turning the d.c. generator but there is no armature current. The system is installed with one dynamic torque transducer, one speed transducer, and one vibration sensor on the stator surface of switched reluctance motor. Firstly, the system is operated under no load and the d.c. supplied voltage is +300 volts and its result is shown in Fig. 3-12(a). From the diagram one can see that the overshoot of the phase current near turn-on electrical angle is quite large though its

associated vibration is not obvious. The overshoot can be attributed to the selection of the turn-on angle, i.e. advancing the phase angle, because the angle is near " 0 " electrical angular position, where nearly no rotor flux variation, i.e. $d\lambda/dt \cong 0$. It also verifies the accuracy of the equation (3-12), where $\theta_r = 0$ & $\delta = 0$, the amplitude of the demand phase current, $\sqrt{q}\ I_m$, is 2 A. In this experiment the load is very small, so $\delta = 0$. Even if the demand phase current is just 2 A, the real phase current has large overshoot because $\sqrt{\text{cosec } 0}$ is quite large. Its physical explanation is that there exists no back EMF near maximum reluctance position,"0". When the d.c.field current in the d.c. generator is increased to 5 A, the overshoot of the phase current becomes small and the vibration is still small, as shown in Fig. 3-12(b). This phenomenum is still governed by the equation (3-12) because the load torque angle, δ, increases although the switched reluctance motor is turn on at the same electrical angular position, $\theta r = 0$. Therefore, the transient phase current is closely related to the load torque angle. Fig. 3-12(c) is the result got from $\theta_r \neq 0$ and $\delta = 0$, that is, under no load. One can see that the phase current in Fig. 3-12(b) is improved due to the increased load torque angle, but Fig.3-12(c) is superior to Fig. 3-12(a) and Fig. 3-12(b) because no overshoot appears under no load.

It shows that the overshoot of the phase current is closely related to the rotor flux vector position , not to the real position of the rotor. As for the vibration, Fig. 3-12(c) appears larger but it is because the phase current in Fig. 3-12(c) provides a larger shaft torque and the phase current is not regulated. Two quite obvious vibration signals are shown in Fig. 3-12(d) and Fig. 3-12(e), respectively. Fig. 3-12(d) is operated at 1300 rpm under no load and Fig. 3-12(e) is operated at 1950 rpm with 2 A d.c. generator

excited field current. Both phase currents are turn on at zero electrical degree. These results show that the switched reluctance drive system will oscillate when the frequency of the phase current approaches the natural frequency of the whole drive system even under no load. Therefore, the conventional current chopper must be avoided as possible the turn-on angle near "0" or "$\pi/2$ " unless under high speed operation. In a real drive system, the load is unknown and uncertain. To drive the switched reluctance drive system, a constant torque control law is not practical. Without an advanced control algorithm it is difficult to get a good performance drive. When the d.c. excited field current in d.c. generator load is increased up to 5 A and the proposed phase current controller is run under a periodic load disturbance, the result are shown in Fig. 3-13(a). The results obtained under operation of a larger load disturbance over a short time is shown Fig. 3-13(b). It can be seen that the phase currents in both diagrams are dynamically regulated so that the steady state rotor speed can maintain the demand value, 1000 rpm, even there exist unknown load disturbance. The same phase current controller was applied to another 4 KW 4-phase switched reluctance drive. The input d.c. voltage was also +300 V and the d.c. generator was operated at 7 A d.c. excited field current load. The results of the transient phase current, shaft speed, and shaft torque, following a step response from 0 rpm to 730 rpm and from 0 rpm to 1360 rpm, are shown in Fig. 3-14(a) and Fig. 3-14(b), respectively. Run/Stop and Step speed trigger signals from zero speed to 730 rpm and those from zero speed to 1360 rpm were used to trigger an oscillosope. Although the d.c. generator load and its inertia were large, the speed response time was still fast. From Fig. 3-14(a) and Fig. 3-14(b), it can be seen that the time from zero speed to demanded speed can be controlled within one second by increasing the phase current and maintaining a

constant torque angle. Obviously, if a larger current switched reluctance drive was used to increase phase current and the shaft torque, a very quick speed response can be expected.

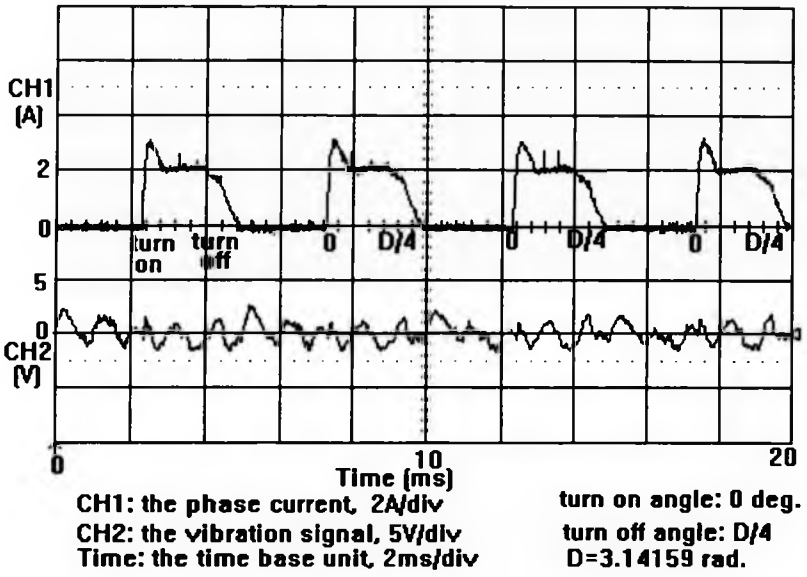

Fig. 3-12(a). The periodic pulse phase current response under no load.

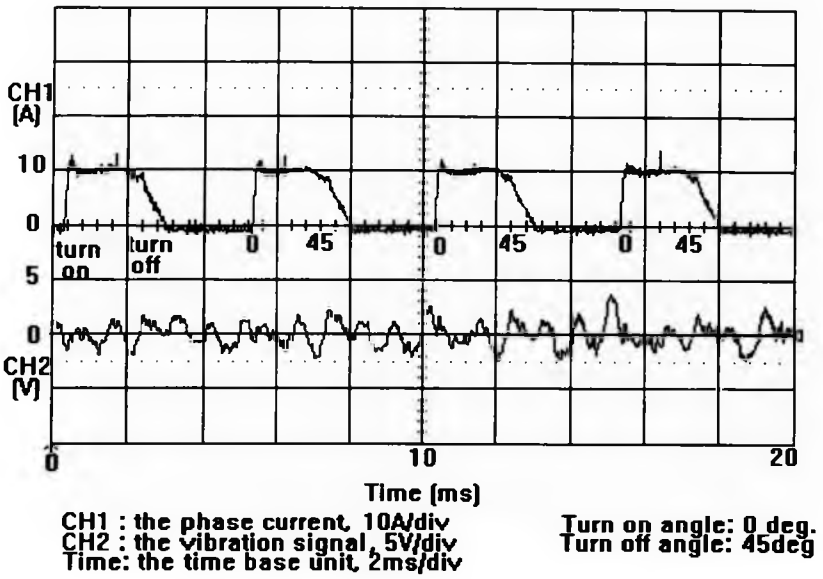

Fig. 3-12(b). The periodic pulse phase current response under load.

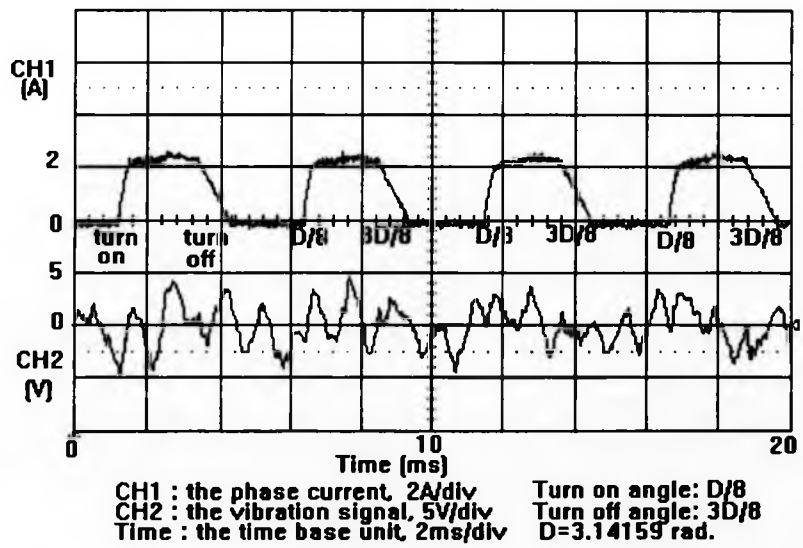

Fig.3-12(c). The periodic pulse phase current response under no load.

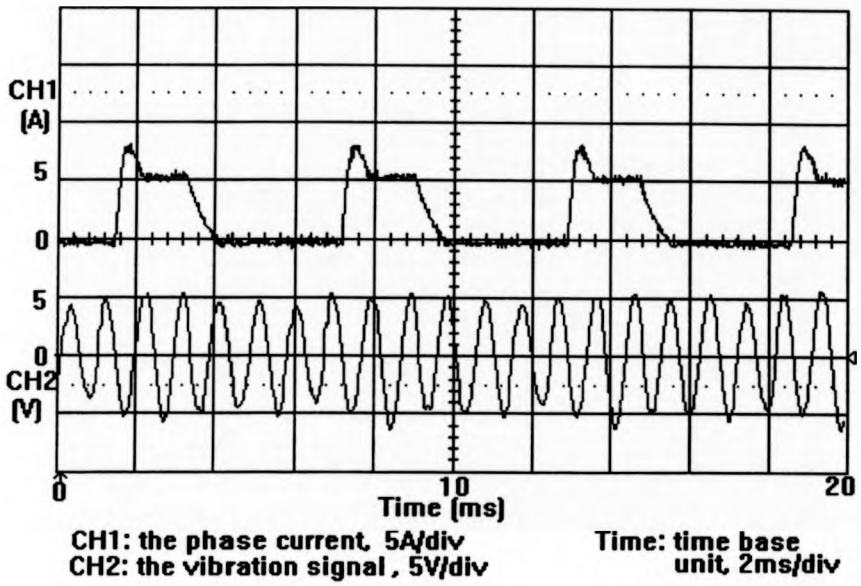

Fig. 3-12(d). The periodic pulse phase current response under no load.

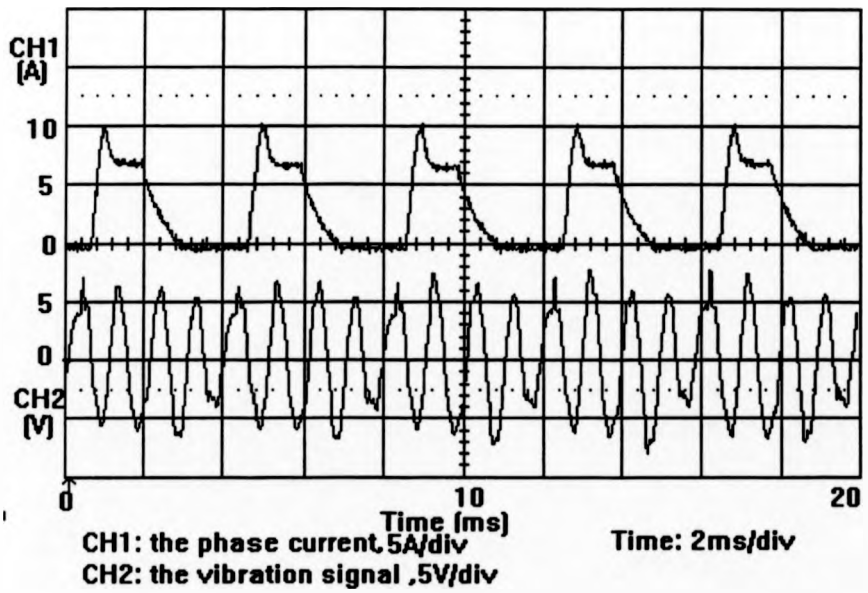

Fig. 3-12(e). The pulse phase current response during high speed.

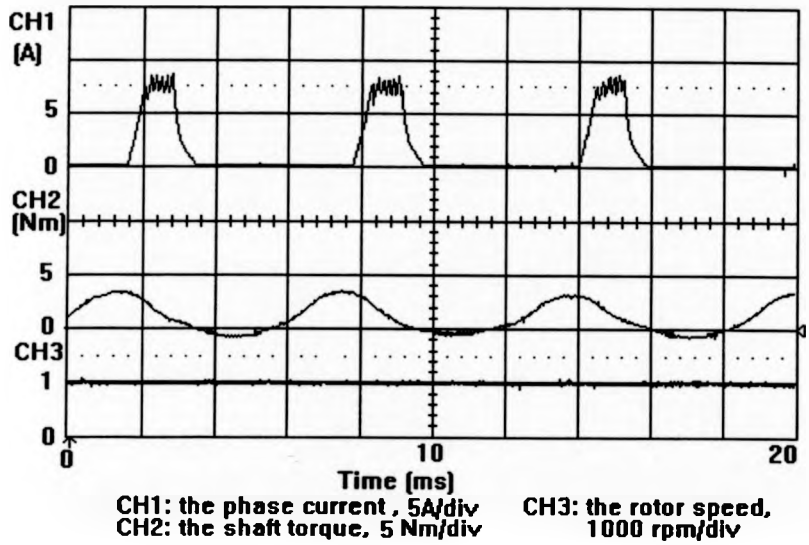

Fig. 3-13(a). Adaptive synchronous phase current and steady state speed response under periodic load disturbance.

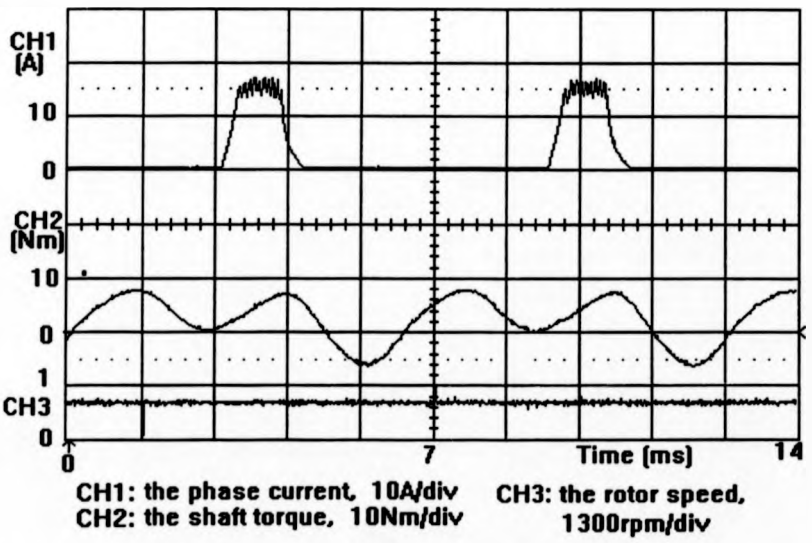

Fig. 3-13(b). Adaptive synchronous phase current and steady state speed response under larger load disturbance.

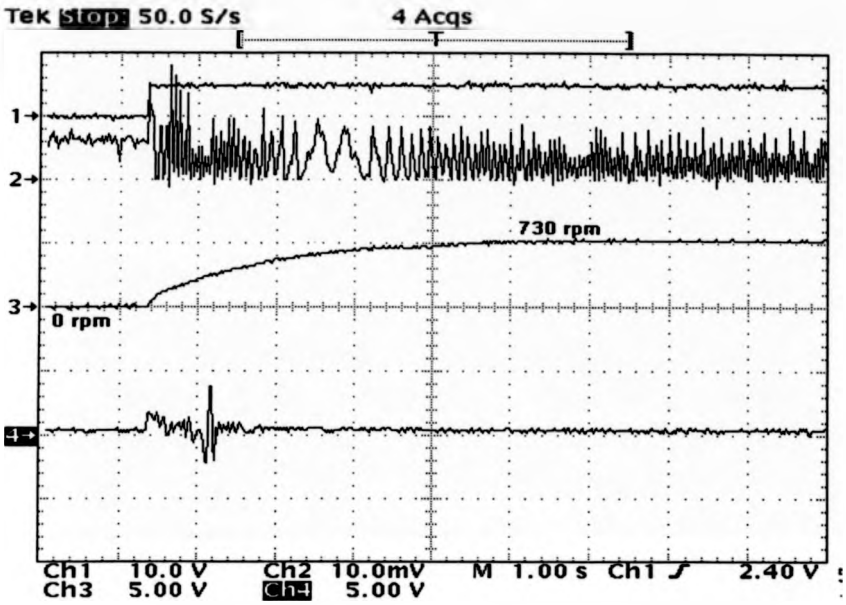

Fig. 3-14(a). Phase current, shaft speed, and shaft torque step response from zero speed to 730 rpm.

Ch1: Step speed command signal from zero speed to 730 rpm, 10 V/div Ch2: Phase current, 10 A/div Ch3: Shaft speed, 730 rpm/div Ch4: Shaft torque, 50 Nm/div M: time base, 1 s/div

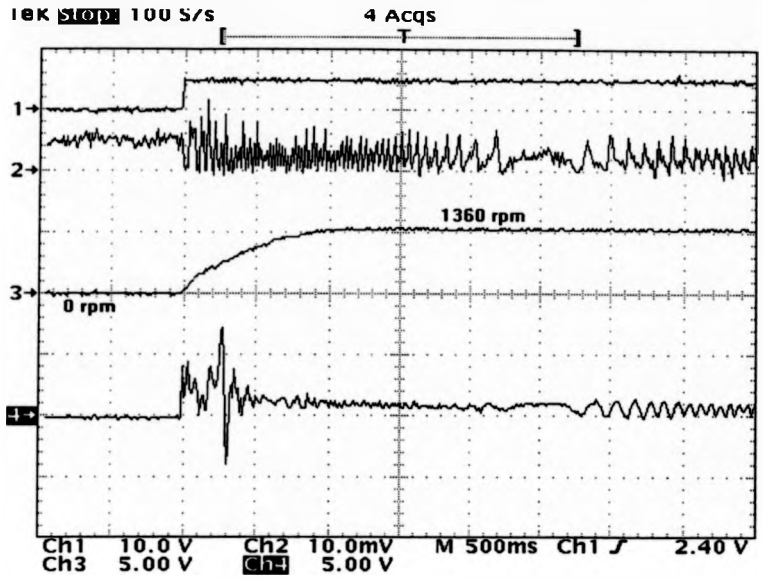

Fig. 3-14(b). Phase current, shaft speed, and shaft torque step response from zero speed to 1360 rpm.

Ch1: Step speed command signal from zero speed to 1360 rpm, 10 V/div Ch2: Phase current, 20 A/div Ch3: Shaft speed, 1300 rpm/div Ch4: Shaft torque, 50 Nm/div M: time base, 500 ms/div

3. 5-3 DISCUSSION AND CONCLUSION

In this chapter, "Synchronous load torque angle control" has been applied to the phase current controller in the singly-excited switched reluctance motor drive system. Its successful experimental results prove the feasibility of the phase current controller. Because the conduction region is limited to between $\pi/8$ and turn-off electrical angle $3\pi/8$, it is impossible for rotor flux vector or the real rotor pole to move to maximum

inductance position, even if this case were possible it can be overcome by the commutation action since the excited phase current would be switched to the new excited phase early at $3\pi/8$. Therefore, the drive would not provide negative torque unless it is operated at very high speed. During high speed, the controller would have to select a new excited phase to supply a larger leading angle. Traditional coordinate transformation computation associated with a vector drive is unnecessary. Furthermorem because singly-excitation is used, one current sensor only is required so that the current controller becomes very simple. System vibration or oscillation problems are also minimized by the adaptive current controller. Therefore, one can draw the following conclusions:

(1) The phase current is significantly affected by the variation of the inductance during rotor rotation, not by the inductance itself. It is also affected by the loads.

(2) The value of the phase current is closely related to the position of the rotor flux vector but not to the real position of the rotor. That is, it is absolutely related to load. The load torque angle is an extremely important parameter in the switching reluctance drive system.

(3) Turn-on and turn-off electrical angles play quite important roles in the singly-exited switching reluctance motor. If these angles are selected unsuitably, vibration will appear when the frequency of the phase current approaches the natural frequency of the switched reluctance drive system. The condition of no rotor flux variation, $d\lambda/dt = 0$, should be avoided. Normally this corresponds to the positions 0 or $\pi/2$. Optimum conduction region should be chosen between $\pi/8$ and $3\pi/8$ so as to generate smooth positive torque.

(4) The phase current at turn-on angle has to be controlled to synchronize to rotor position to get stable load torque angle regulation and to obtain high-performance switched reluctance drive .

(5) Although the phase current in the singly-excited switched reluctance motor cannot be maintained constant during commutation, especially at turn-off instant, one current sensor is enough if the adaptive phase current controller is used .

(6) Speed response can be increased by increasing phase current under constant torque angle.

CHAPTER 4

A Variable Structure Space Voltage Vector Controlled 5-phase Split-Link Converter

4-1 INTRODUCTION

In chapter 3, some power converters were described and only singly-excited switched reluctance drive was studied. For low power switched reluctance drive, the performance of the drive with single excitation is enough. However, for high power drive with two or more motor phase power converter must be able to deliver current to at least two phases at one time.

From the literature there is no control scheme which has been described which offers a high performance without involving high cost, computationally intensive, control schemes or the storage and manipulation of extensive characterizing data of the motor. None of the published vector control schemes are suitable for implementation in a high power, high performance commercial switched reluctance converter and that is where the work of this chapter makes a significant contribution. In this chapter a novel power converter is described for a five phase motor and the model and control theory of the converter system are then developed. Experimental implementation and test results are presented for a five phase switched reluctance drive.

4-2 THE SPACE VOLTAGE VECTOR CONTROLLED SPLIT-LINK CONVERTER

A. 5-phase split dc link converter

The split d.c. link converter has been known as one of the many possible power converters for switched reluctance drives and its use has been widely reported [23-30]. The total dc supply is split by two equal series connected capacitors to create a center point to which one end of all phase windings are connected. One switch and one diode is connected to the other end of each phase winding to supply power from one of the halves of the split dc supply. The circuit therefore offers the possibility of only one switch per phase. It is however accepted that the circuit suffers from the disadvantage that the number of phase windings should be even.

Paper [31] has described a 5 phase switched reluctance motor which has 10 stator poles and 8 rotor poles, designed specifically for very high efficiency. The high efficiency is achieved from a short flux loop excitation pattern. The poles of adjacent phases, when simultaneously excited, are arranged to have opposite magnetic polarity such that a very short magnetic path is created. Higher air-gap flux is obtained from a given stator phase current and motor efficiencies in excess of 90 % (@ 4 kW) have been reported [31]. The use of an asymmetric half bridge power converter is seen as inappropriate for such a motor in a commercial drive since 10 switches would be needed though the use of the shared switch asymmetric half bridge reduces this number to 6 [31].

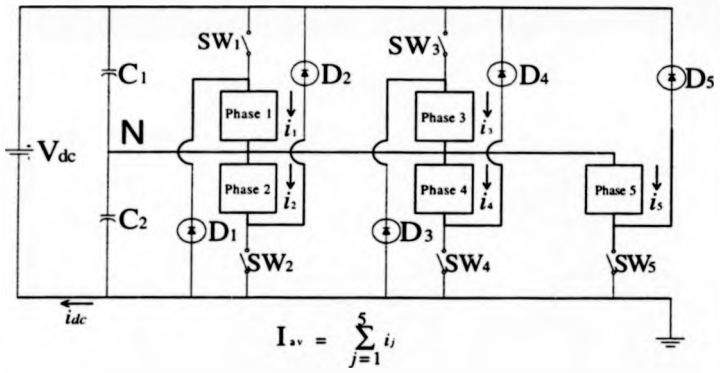

Fig. 4-1. Split-Link Converter for a 5-phase switched reluctance motor.

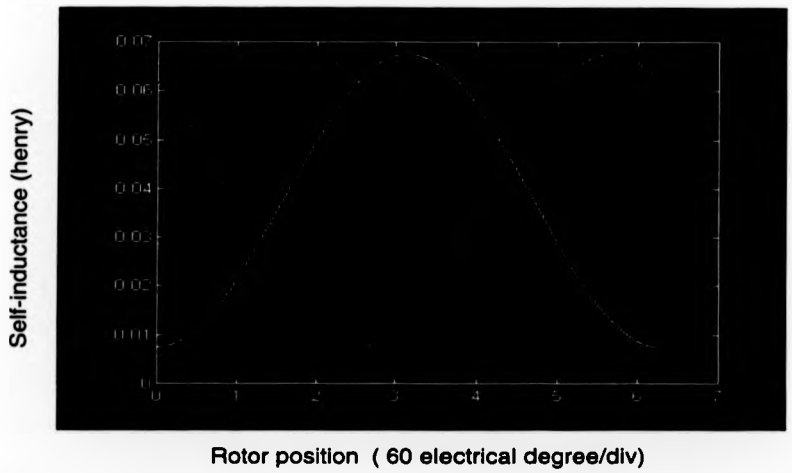

Fig. 4-2 Relationship between phase inductance for each of the 5 phase and rotor position.

The use of the split d.c. link converter for this motor would produce the power converter shown in Fig. 4-1. This would be a very cost effective solution requiring only 5 switches but the motor control scheme would have to maintain the center point voltage as close as possible to the mid-point. The converter must be carefully

controlled particularly under dynamic conditions to avoid deviations from the ideal center point. The control scheme which achieves this is described in the section III of this chapter. The use of the split d.c. link power converter allows complete flexibility and independence between phases. Unlike other circuits with one switch per phase there are no additional circuits for energy recovery and there are no restrictions on the number or sequence of phases which can be excited simultaneously. This is particularly important for the five phase motor since it can be seen from the inductance profiles shown in Fig. 4-2 that up to three phases could be conducting at one time, all producing positive torque.

B. The space voltage vector split-link converter

Table 4-1 Space voltage vectors of a 5 phase switched reluctance motor

S_5	S_4	S_3	S_2	S_1	**Excited phase windings**	**Equilibrium Vectors**	**Position codes of reference rotor pole**
0	0	0	0	1	1	V_1	1C
0	0	0	1	1	1 & 2	V_1+V_2	18
0	0	0	1	0	2	V_2	19
0	0	1	1	0	2 & 3	V_2+V_3	11
0	0	1	0	0	3	V_3	13
0	1	1	0	0	3 & 4	V_3+V_4	03
0	1	0	0	0	4	V_4	07
1	1	0	0	0	4 & 5	V_4+V_5	06
1	0	0	0	0	5	V_5	0E
1	0	0	0	1	5 & 1	V_5+V_1	0C

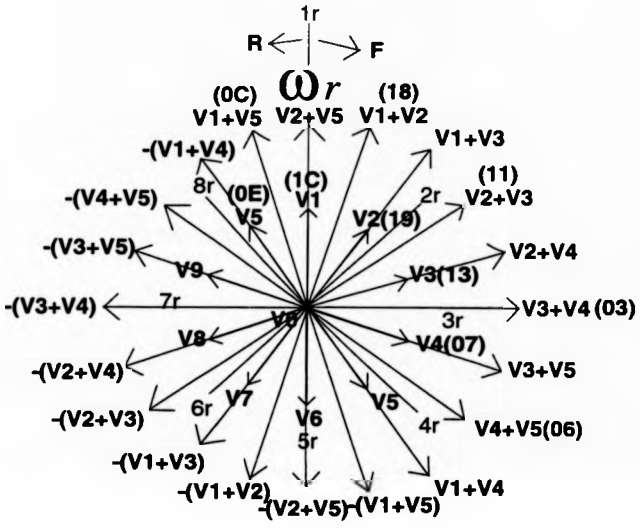

Fig. 4-3. Space voltage vector diagram of a 5-phase switched reluctance motor .

Table 4-2a Doubly-excited combinative vectors during forward rotational state

Rotational State	Rotor pole position codes	Excited phases (Vector)	S_5	S_4	S_3	S_2	S_1
Motoring	0E	(V_3+V_4)	0	1	1	0	0
Motoring	0C	(V_3+V_4)	0	1	1	0	0
Motoring	1C	(V_4+V_5)	1	1	0	0	0
Motoring	18	(V_4+V_5)	1	1	0	0	0
Motoring	19	(V_5+V_1)	1	0	0	0	1
Motoring	11	(V_5+V_1)	1	0	0	0	1
Motoring	13	(V_1+V_2)	0	0	0	1	1
Motoring	03	(V_1+V_2)	0	0	0	1	1
Motoring	07	(V_2+V_3)	0	0	1	1	0
Motoring	06	(V_2+V_3)	0	0	1	1	0
Regeneration	0E	(V_1+V_2)	0	0	0	1	1
Regeneration	0C	(V_1+V_2)	0	0	0	1	1
Regeneration	1C	(V_2+V_3)	0	0	1	1	0
Regeneration	18	(V_2+V_3)	0	0	1	1	0
Regeneration	19	(V_3+V_4)	0	1	1	0	0
Regeneration	11	(V_3+V_4)	0	1	1	0	0
Regeneration	13	(V_4+V_5)	1	1	0	0	0
Regeneration	03	(V_4+V_5)	1	1	0	0	0
Regeneration	07	(V_5+V_1)	1	0	0	0	1
Regeneration	06	(V_5+V_1)	1	0	0	0	1

Table-4-2b (Doubly- excited combinative vectors during reverse rotational state)

Rotational State	Rotor pole position codes	Excited phases (Vectors)	S_5	S_4	S_3	S_2	S_1
Motoring	19	(V_3+V_4)	0	1	1	0	0
Motoring	11	(V_3+V_4)	0	1	1	0	0
Motoring	13	(V_4+V_5)	1	1	0	0	0
Motoring	03	(V_4+V_5)	1	1	0	0	0
Motoring	07	(V_5+V_1)	1	0	0	0	1
Motoring	06	(V_5+V_1)	1	0	0	0	1
Motoring	0E	(V_1+V_2)	0	0	0	1	1
Motoring	0C	(V_1+V_2)	0	0	0	1	1
Motoring	1C	(V_2+V_3)	0	0	1	1	0
Motoring	18	(V_2+V_3)	0	0	1	1	0
Regeneration	13	(V_1+V_2)	0	0	0	1	1
Regeneration	03	(V_1+V_2)	0	0	0	1	1
Regeneration	07	(V_2+V_3)	0	0	1	1	0
Regeneration	06	(V_2+V_3)	0	0	1	1	0
Regeneration	0E	(V_3+V_4)	0	1	1	0	0
Regeneration	0C	(V_3+V_4)	0	1	1	0	0
Regeneration	1C	(V_4+V_5)	1	1	0	0	0
Regeneration	18	(V_4+V_5)	1	1	0	0	0
Regeneration	19	(V_5+V_1)	1	0	0	0	1
Regeneration	11	(V_5+V_1)	1	0	0	0	1

Table 4-3 (The electrical regenerative vectors which all switches are turned off)

Excited phase	Excited vectors	Regenerative Vectors	S_5	S_4	S_3	S_2	S_1
1	V_1	V_6	0	0	0	0	0
2	V_2	V_7	0	0	0	0	0
3	V_3	V_8	0	0	0	0	0
4	V_4	V_9	0	0	0	0	0
5	V_5	$-V_5$	0	0	0	0	0
1, 2	(V_1+V_2)	$-(V_1+V_2)$	0	0	0	0	0
2, 3	(V_2+V_3)	$-(V_2+V_3)$	0	0	0	0	0
3, 4	(V_3+V_4)	$-(V_3+V_4)$	0	0	0	0	0
4, 5	(V_4+V_5)	$-(V_4+V_5)$	0	0	0	0	0
5, 1	(V_5+V_1)	$-(V_5+V_1)$	0	0	0	0	0
No excited current	V_0	No regenerative vector	0	0	0	0	0

From Fig. 4-2 and table 4-1, it can be seen that, one or two phase windings are firstly excited, then the rotor will take up a position according to Fig. 4-2. The position code from the rotor position decoder can be found. When only one phase is excited, the excited stator pole is exactly aligned with the corresponding rotor position, which is exactly the so-called aligned position for that phase and there exits maximum self-inductance in this position. When two phase are simultaneously excited, the corresponding rotor pole will move to a position where reluctance is equal for both phase windings. In table 4-1 there are ten sets of rotor pole position codes which correspond to ten sets of excitation phase windings. In order to produce effective positive torque rather than negative torque, the region corresponding to increasing inductance needs to be identified and then the appropriate phase windings can be correctly excited. To do that, from table 4-1 one can get ten sets of optimum phase excitations during forward rotation state. Conversely, another ten sets of optimum phase excitations can be found for reverse rotation or regenerative operation, and are shown in table 4-2.

C. Representation of the switched reluctance output voltage as a space vector

If the common terminal M of all motor phase windings is connected to the neutral N of split-link converter, as shown in Fig.4-1, then table 4-2 gives ten conduction states of the converter. Each time when the corresponding phase switches are turn off, there are another ten sets of excited phase states because their excited sources are switched to another voltage source of opposite polarity from two capacitors in the d.c. link. Therefore, at any rotor pole position in table 4-2 the converter output voltage can be

represented as a complex-vector. Firstly for the phases connected through an upper switch

$$U_k = +V_{cU} \exp(jk\pi / 5) \qquad \text{when k= 1, 3 turn on} \qquad (4\text{-}1)$$

A positive voltage vector acting to increase the flux in the k th stator pole.

$$U_k = -V_{cD} \exp(jk\pi / 5) \qquad \text{when k= 1, 3 turn off} \qquad (4\text{-}2)$$

A negative voltage vector acting to reduce the flux in the k th stator pole.

For the phases connected to a lower switch

$$V_k = +V_{cD} \exp(jk\pi / 5) \qquad \text{for k= 2, 4, 5 turn on} \qquad (4\text{-}3)$$

$$V_{k+5} = -V_{cU} \exp(jk\pi / 5) \qquad \text{for k= 2, 4, 5 turn off} \qquad (4\text{-}4)$$

$$V_{cU} + V_{cD} = V_{dc} \qquad (4\text{-}5)$$

where k is the symbol of phase windings or phase switches in Fig.1, V_k, V_{k+5} denotes the voltage vector across the k th phase winding, V_{cU} and V_{cD} denote the voltage across upper and lower capacitor in d.c. link, respectively. V_{dc} is the total voltage across d.c. link source.

Theoretically there should have 2^{10} combinations of stator space vectors for forward or reverse rotation but the optimum combination of doubly-excited vectors for a 5-phase switched reluctance motor must be selected according to the high-efficiency magnetic path and the geometric structure between the stator and the rotor. To simplify system and generate high torque output, two phase simultaneous excitation is used in the control scheme of the converter motor system. From the equilibrium vectors from table 4-1 and equations (4-1)-(4-5), it can be seen that there exist thirty one instantaneous space voltage vectors for the control of the converter during each electric cycle, as shown in Fig.4-3.

4-3 THE CONTROL MODEL OF 5-PHASE SPLI-LINK CONVERTER

A. The Principle of Total Phase Power Control

The general voltage equation for a phase winding of a switched reluctance motor is given by

$$\upsilon = r\, i + \frac{d\lambda_s}{dt} = r\, i + \frac{\partial \lambda_s}{\partial i}\frac{d i}{d t} + \frac{\partial \lambda_s}{\partial \theta}\omega_r \qquad (4\text{-}6)$$

where υ is the voltage across the phase winding when the switches of the power converter are turned on or turn off so that the corresponding voltage vectors in the equations (4-1) ~ (4-4) are applied to their phase windings, and r is the equivalent resistance in the circuit - including the conducting resistance of the switches, i is the phase current, and λ_s is the stator flux linkage associated with the switched reluctance motor phase coil. ω_r is the rotor speed.

From equation (4-6), the stator flux linkage can be expressed as

$$\lambda_s = \int \upsilon\, dt - r \int i\, dt \qquad (4\text{-}7)$$

if the switching frequency of each switch is fixed, and its corresponding switching period is denoted by T and the state of each switch is expressed by a switching function, then the voltage vector across each phase winding can be written as

$$V_j = S_j * V_{c\,j} \qquad \text{for } j = 1, \cdots, 5 \qquad (4\text{-}8)$$

where j denotes a particular phase winding in the motor, S_j denotes a switching function in the phase plane of variable structure system and $V_{c\,j}$ denotes the voltage across the capacitor, which is paralled with the j th phase switching circuit , and

$S_j = 1$ when switch SW_j for the j th phase is turned on.

$S_j = -1$ when the j th switch SW_j is turned off and the current is still flowing through the phase winding via recovery diode D_j. (4-9)

If it is assumed that the power converter is operating with fixed PWM switching frequency, f, (period, T) and is alternating between the state $S_j = 1$ (for time T_{on}) and the state $S_j = -1$ (for time T_{off}), where $T = T_{on} + T_{off}$, then equation (7) can be rewritten as

$$[\lambda_{sj}(t_k) - \lambda_{sj}(t_{k-1})] = [V_j T_{on} + (V_{j+5})T_{off}] - rT[i_j(t_k) + i_j(t_{k-1})]/2$$

for $j = 1, \cdots, 5$ (4-10)

By equations (4-1) ~ (4-4) and (4-8) ~ 4-(9) the equation (4-10) can be expressed as

$$[\lambda_{sj}(t_k) - \lambda_{sj}(t_{k-1})] = [V_{cj} T_{on} - (V_{dc} - V_{cj})T_{off}] - rT[i_j(t_k) + i_j(t_{k-1})]/2$$

for $j = 1, \cdots, 5$ (4-11)

where $\lambda_{sj}(t_{k-1})$ and $i_j(t_{k-1})$ denote the initial stator flux linkage and the sampled current of the j th phase winding at the start of the k th switching cycle, while $\lambda_{sj}(t_k)$ and $i_j(t_k)$ denote the stator flux linkage and the sampled current of the same phase winding at the end of the k th switching cycle. From equations (4-5) and (11), if two adjacent phase windings are excited simultaneously, then the following expressions can be derived.

$$\sum_{j=1}^{m}[\lambda_{sj}(t_k)] - \sum_{j=1}^{m}[\lambda_{sj}(t_{k-1})] = \{[2D(t_k)-1]V_{dc} - r I_{av}(t_k)\}T$$

for $m = 2$ (4-12)

where $D(t_k) = [T_{on}(t_k) / T]$, $I_{av}(t_k)$ denotes the average of the sum of all phase currents between tk-1 to tk.

If both sides of equations (4-12) are divided by the switching period T, an expression for the average total phase voltage applied to the motor from t_{k-1} to t_k is obtained

$$V_{av}(t_k) = [2D(t_k)-1]V_{dc} - r\, I_{av}(t_k) \qquad (4\text{-}13)$$

where $D(t_k) = [T_{on}(t_k) / T]$. Therefore, the average value of the total power delivered to all of phase windings is given by

$$P_{av}(t_k) = [2D(t_k)-1]V_{dc}\, I_{av}(t_k) - r\, I_{av}^2(t_k)$$

$$= V_{av}(t_k)\, I_{av}(t_k) - r\, I_{av}^2(t_k) \qquad (4\text{-}14)$$

where $V_{av}(t_k)$ denotes the equivalent average voltage across the equivalent circuit of all phase windings between t_{k-1} and t_k. Now equation (4-14) can be rewritten as

$$P_{av}(t_k) = V_{dc}\, i_{dc}(t_k) - r\,\{ i_{dc}(t_k) / [2D(t_k) - 1]\}^2 \qquad (4\text{-}15)$$

where $i_{dc}(t_k) = [2D(t_k)-1]I_{av}(t_k)$ denotes the equivalent average current flowing through d.c. source between t_{k-1} to t_k

From the equation (4-15), it can be seen that the control of the average power $P_{av}(t_k)$ just needs the measurement and control of the d.c.source link current $i_{dc}(t_k)$ if resistor voltage drop can be neglected. This dramatically simplify the control of phase power to d.c. source link current control. However, if this technology is used in high power control, especially under the regenerative conditions it is very dangerous because the equivalent input resistance and the large capacitanceof the two capacitors would produce a large time constant and slow down the response of the power flow. Therefore this method is only suitable for near steady state operation. During transient state, the control of total phase power must be based on the equation (4-14).

B. Variable Structure Control Of total phase Power [32,33]

The conventional current chopping technique is only suitable for low speed operation and a phase advancing technique can be used in the high speed case. With phase advancing there are some difficulties, i.e. the region without back EMF, there would be no torque during the early part of the conduction cycle. Secondly, a known problem of high torque ripple is difficult to eliminate during the transition from one phase to the subsequent phase. This problem is caused by forcing independent control of individual phase current. If the design of the converter is based on the view point of the whole system, then this problem can be effectively improved. Another problem with the conventional current chopping technique is that it is just a bang-bang control, the operating speed range is narrow because the back EMF depends on speed and current. However, if space voltage vectors are appropriately selected and combined with the variable structure phase power control using single d.c. link current sensor technology, problems described above will be effectively improved.

If the switching time period T in the equation (4-13) approaches zero theoretically, then $I_{av}(t_k)$ will approach to the instantaneous sum of all phase currents $\sum_{j=1}^{5} i_j$. The sum of the 'equivalent back EMF' and the voltage induced by the 'equivalent inductance' is equivalent to the instantaneous total phase voltage by equation (4-6), giving the following equation

$$\lim_{T\to 0} V_{av}(tk) = \upsilon = \lim_{T\to 0} \left[L_{eq}(\theta) \frac{d\, i_{dc}(t_k)}{d\, t} + i_{dc}(t_k)\, \omega_r \frac{d\, L_{eq}(\theta_r)}{d\, \theta_r} \right] \quad (4\text{-}16)$$

where $L_{eq}(\theta_r)$ is the 'equivalent inductance' of a single imaginary coil which represents all simultaneously excited coils in the motor when the rotor is in a position θ_r, ω_r is the angular frequency of the rotor, and υ is the corresponding instantaneous total phase voltage. Thus the equation (16) can be rewritten as

$$\frac{d\, i_{dc}(t)}{d\, t} = [\upsilon - i_{dc}(t)\, \omega_r \frac{d\, L_{eq}(\theta_r)}{d\, \theta_r}] / L_{eq}(\theta_r) \qquad (4\text{-}17)$$

Therefore, to control the summation of all of phase currents to track the reference current sliding mode is required. In this case one can select the following switching function in the phase plane

$$\wp = i_{dc}(t) - I_c(t) \qquad (4\text{-}18)$$

where $I_c(t)$ is the reference current at the time instance t and $i_{dc}(t)$ is the equivalent d.c. link current at the same time. So, to satisfy $\lim_{\wp \to 0} \wp \frac{d\,\wp}{d\,t} < 0$, the control law can be designed as follow

$$\upsilon = +V_{dc} \quad \text{if } \wp < 0$$
$$\upsilon = -V_{dc} \quad \text{if } \wp > 0 \qquad (4\text{-}19)$$

To track the reference current, the control law in the equation (4-12) needs to generate the appropriate T_{on} and T_{off} time signals in each independent phase winding to achieve control of the summation of all of phase currents so that equivalent average voltage satisfies the equation (4-6). This can be realized by a digital PWM current controller, which is described in part A. a of section IV. By substituting (4-18) into $d\wp/d\,t = 0$, the equivalent voltage becomes

$$\upsilon_{eq} = i_{dc}(t)\, \omega_r \frac{d\, L_{eq}(\theta_r)}{d\, \theta_r} = V_{dc} \lim_{T \to 0} [2\, D(t_k) - 1] \qquad (4\text{-}20)$$

and the existence condition of the sliding regime is

$$|\upsilon_{eq}| < |V_{dc}| \qquad (4\text{-}21)$$

In this case, by equation (4-14) and (4-20), the corresponding equivalent power becomes

$$P_{eq}(t) = i^2_{dc}(t)\left(\omega_r \frac{d L_{eq}(\theta_r)}{d \theta_r}\right) = V_{dc} \lim_{T \to 0}\{[2 D(t_k)-1] I_{av}(t_k)\} - \lim_{T \to 0}[r I_{av}^2(t_k)]$$

$$= V_{dc} i_{dc}(t) - r i^2_{dc}(t) \qquad (4\text{-}22)$$

By equation (4-14) and (4-16), it is noted that not in case of the sliding mode, the equivalent power is

$$P_{eq}(t) = i^2_{dc}(t)\left(\omega_r \frac{d L_{eq}(\theta_r)}{d \theta_r}\right) + L_{eq}(\theta_r) i_{dc}(t) \frac{d i_{dc}(t)}{d t} = V_{dc} i_{dc}(t) - r i^2_{dc}(t) \qquad (4\text{-}23)$$

C. Stator flux Phase Shifting Approach

The variable structure control of input power described in part B would appear to be another form of a current chopper but actually it is not because it is a vector controlled phase power chopper. The significant difference from the conventional current chopper is that the controller of total phase power is based on the space voltage vector. In this paper, the procedure to produce larger torque and to maximize the efficiency of the 5 phase drive double-excitation is described. It is noted that the rotor pole reference frame is slightly different from that of single-excition. The coordinate axis of the switched rotor pole reference frame is located at the middle line between two adjacent rotor pole cordinate axes. This middle line separates space plane into two half plane - one side is for forward rotation and the other side is for reverse rotation. From Fig 3. it can be seen that the criteria of vector selection is based on the phase of vectors located at the switched rotor pole frame. When the rotor pole rotates to the aligned position if low speed is required, then the vector close to minimum reluctance is selected. On the contrary, if high speed is required, the vector close to the larger

reluctance is chosen. By the selected vector from the switching table the phase of stator flux vector relative to the rotor is easily adavanced or retarded. When the total phase power reaches the reference upper limit, a regenerative vector, which is the negative split d.c. voltage from the converter, is selected. When the total phase power is smaller than the reference lower limit the suitable switching vector from switching table is selected to increase the total phase power. Therefore, the stator flux vector can accelerate or deaccelerate to quickly orient the rotor pole and achieve the required speed by the variable structure power control. In low speed the doubly-excited voltage vector with larger radial rotor flux linkage is selected but at high speed the doubly-excited vector with larger tangential rotor flux linkage is selected. During super high speed only a singly-excited vector with minimum rotor flux linkage is chosen. If reverse mechanical rotation is required, the suitable regenerative vector is selected to quickly remove the machanical kinetic energy and follow the command power. This phase shifting of stator flux vectors not only simplify the control of the converter system but also greatly increase the response of the rotor speed. Owing to this, as phase power can be controlled, the shaft torque during steady state would be smooth if rotor speed is accurately controlled. The related vibration and acoustic noise can be greatly improved.

4-4 IMPLEMENTATION OF THE CONVERTER SYSTEM

(A) Sliding Mode Total Phase Power Controller

a. Digital PWM current controller

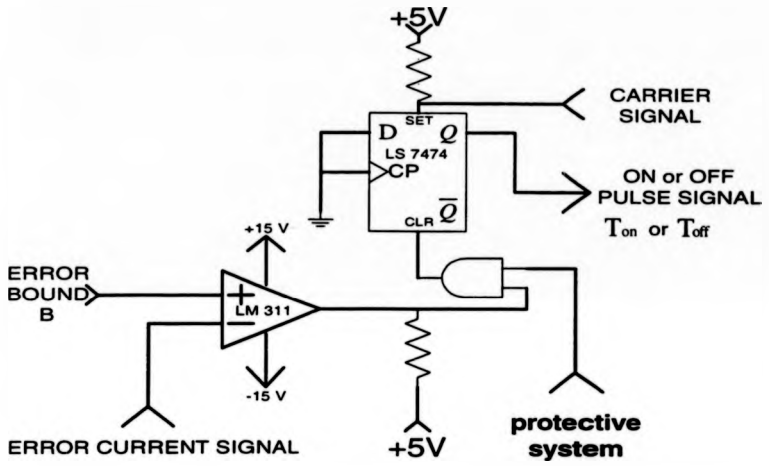

Fig. 4-4. Digital pulse width modulator for the sliding mode power controller.

Sliding mode total phase power control can be simplified as the control of the summation of all phase currents if the input d.c. voltage is fixed as described by section 4-3. In implementation, it can be acchieved using one current sensor. Using a comparator, a flip-flop and a timer, the current controller can be easily realized. LM 311, TTL 7474 and the internal timer T0 in a 8751 microcomputer are used to implement this controller. Timer T0 generates the clock signal for the flip-flop, (frequency programmed to be near 20 kHz) and is synchronously locked to the rotor position sensor. The real current is compared with the reference current through LM 311 comparator and the error of current can be obtained. The error current is amplified by the PI controller and then it is modulated according to equation (4-14) and the

switching table 4-2 to drive five IGBT module in the split-link converter. A detail block diagram of split-link converter controller is as shown in Fig.4-4. If load current is too large because of high load, the current controller with a fixed hysteristic band is unsuitable. In the proposed controller, it only necessary to adjust the frequency of the carrier. The PWM switching frequency can be very easily reduced or increased to regulate the real load current according to load.

(B) Stator Flux Vector Phase Shifting Approach

To extend operating range of rotor speed, total phase power can only be controlled under low speed by a variable structure current controller. During high speed the converter needs to choose appropriate space voltage vectors to avoid operating in the decreasing inductance region. Without using the conventional phase advancing technique, a feasible approach is to reduce the amplitude of rotor flux linkage. To do that, an effective way is to change the exciting phase. That is, select a suitable combination of phase excitations. According to space structure of phase windings, one can get many combinations but the optimum space votage vector can be found as shown table 4-2. Table 4-2a is one example for foward rotation and table 4-2b is another example for reverse rotation.

4-5. EXPERIMENTAL RESULTS

To present the feasibility of the converter for odd-phase switched reluctance motors, a split-link converter for a 4 kw 5-phase switched reluctance motor was constructed. In these experiments, the load is a 7 KVA d.c. generator. The system is installed with a torque and a speed transducer. The input d.c. voltage is adjustable, its maximum value is + 550 V and the maximum peak d.c. link current is limited to 60 A. Fig. 4-5 shows the experimental result when the converter is operated under unbalanced loads uneven loading of the two capacitors and the rotor speed is 470 r/min. In Fig. 4-5(a)~ Fig 4-5(c) the current of phase 1 is used as the reference signal. All phase currents are synchronized to their individual position sensor and the signal of position 1 is used as the oscilloscope trigger signal. The current of phase 5 and total sum of all instantaneous phase currents are shown in Fig. 4-5(d). From Fig. 4-5 it can be seen that all phase currents are asymmetrical to one another at a particular instant due to saturation but the total sum of all phase currents is controlled within tolerable error band and the netural voltage is about 160 volts. Compared with the ideal voltage (150 V), the error of this is 6.6 % but the error of a.c.voltage drift is very small. This shows that variable structure phase power controller is effective even under unbalanced loads.and two different supply voltages. Fig 4-6 is the result when the converter is operated under higher load and speed. One can see that the total sum of all the phase currents is different from Fig. 4-5 because the variable structure controller is invalid when the tested motor is run at high speed without flux weakening or phase advancing. However, the netural voltage in Fig. 4-6 is about 140 V. This still shows that the error of d.c. voltage drift is around 6.6 % and a.c. voltage drift is very small.

of the tested motor is designed at 1500 r/min and the experimental results in Fig. 4-6 shows that the conventional chopping technique cannot be operated above 1500 r/min without using phase advancing techniques. The stator flux vector shifting approach was tested and results are shown in Fig 4-7. It is seen that the operating speed is 6048 r/min. The power meter shows that real power was 1.2 kW. The neutral voltage in Fig. 4-7 was about 143 volts, and under these condition the motor ran well. This confirms that stator flux vector phase shifting approach can be speeded up to several times base speed. Fig.4-8 shows the steady state response of phase currents and the shaft torque, when the motor was operated at 1090 r/min, under very high load and without a speed controller. Although the voltage is square a.c. waveform, shaft torque is smooth. This is attributed to the selected space voltage vectors so that space phase shifting approach was used instead of chopping phase current. Fig. 4-9 shows the transient response of total phase power and shaft torque when operated at 810 r/min, and demonstrates the fast response performance of the split-link converter with the proposed controller. When the converter was combined with a sliding mode speed controller, the speed control is quite robust. Fig. 4-10 shows a typical experimental result. The motor was originally operated at 980 r/min with a load of 20 Nm but its speed is increased up 1000 r/min under unknown and uncertain load perturbation. From torque and speed meter the recorded shaft torque was 16.2 Nm and speed was 1000 r/min. i.e. an error speed of about 2 %. These results show that split-link converter can be used in doubly-excited odd phase switched reluctance motor with the minimum switches and with energy recovery. The center point voltage can be controlled within acceptable limits without sacrificing control of the individual phases.

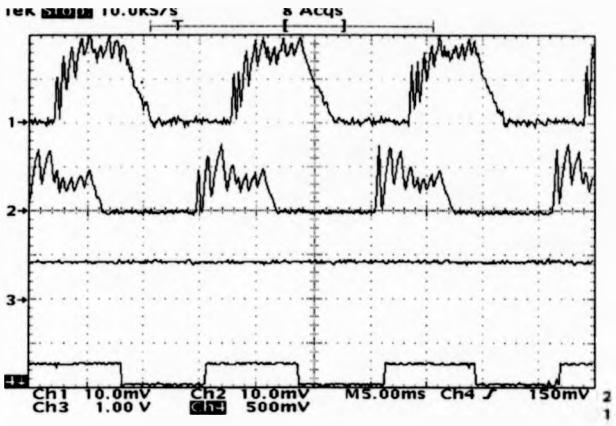

Fig. 4-5(a) Neutral voltage and phase current waveforms under unbalanced loads Ch1: the current waveform of phase 1, 10 A/div; Ch2: the current waveform of phase 2, 10 A/div; Ch3: neutral voltage, 200V/div; Ch 4: synchronously triggering signal, 10 V/div. Time: 5.00 ms/div.

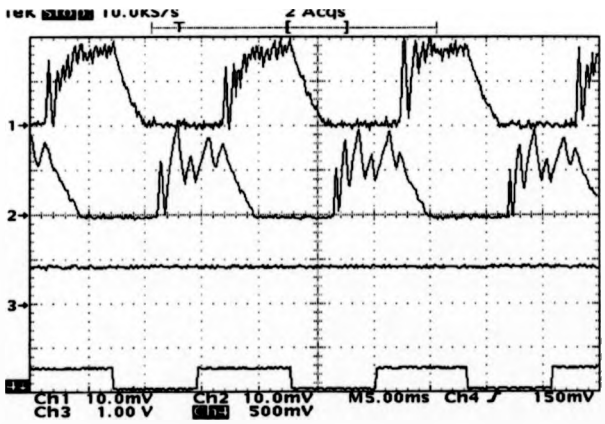

Fig. 4-5(b) Neutral voltage and phase current waveforms under unbalanced loads ; Ch1: the current waveform of phase 1, 10 A/div; Ch2: the current waveform of phase 3, 10 A/div; Ch3: neutral voltage, 200 V/div; Ch4: synchronously triggering signal, 10 V/div. Time: 5.00 ms/div.

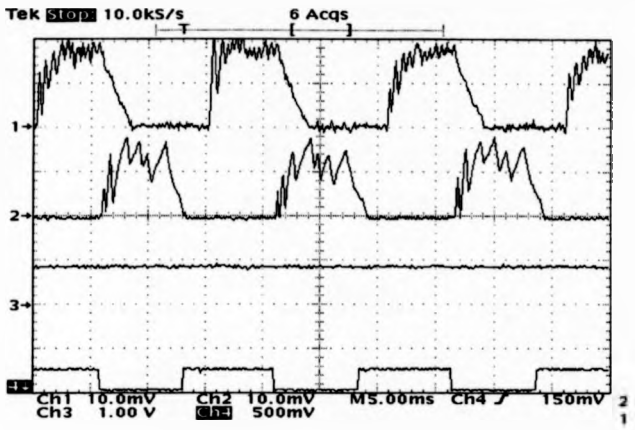

Fig.4-5(c) Neutral voltage and phase current waveforms under unbalanced loads; Ch1: the current waveform of phase 1, 10 A/div; Ch2: the current waveform of phase 4, 10 A/div; Ch3: neutral voltage, 200 V/div; Ch 4: synchronously triggering signal, 10 V/div. Time: 5.00 ms/div.

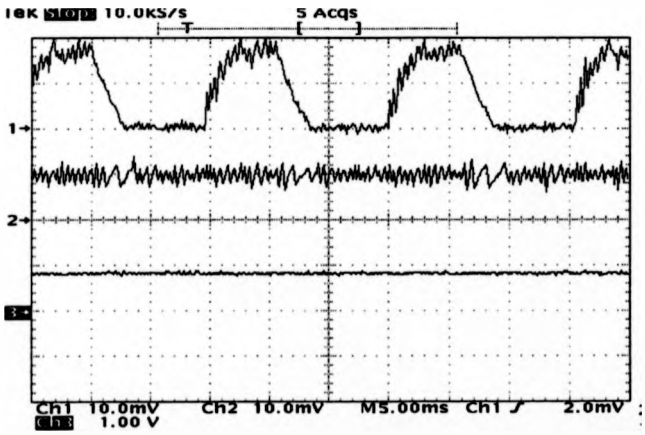

Fig. 4-5(d) Phase current, the scalar sum of all instantaneous phase current, and neutral voltage waveforms under unbalanced loads

Ch1: the current waveform of phase 5, 10 A/div; Ch2: the scalar sum of all instantaneous phase current, 20 A/div; Ch3: neutral voltage, 200 V/div. Time : 5.00 ms/div.

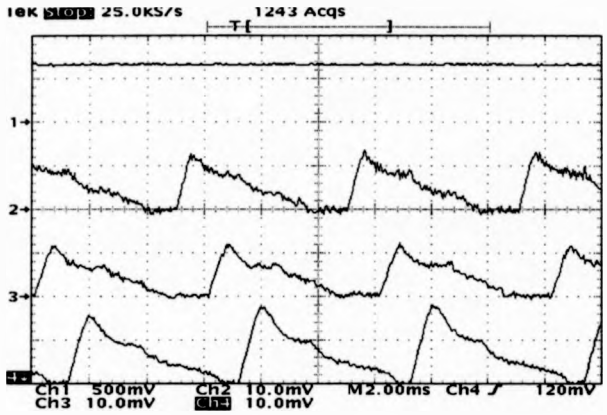

Fig. 4-6(a). Steady state response of neutral voltage and phase current operated at 1230 r/min and high load. Ch1: neutral voltage, 100 V/div; Ch2: the current waveform of phase 1, 10 A/div; Ch3: the current waveform of phase 2, 10 A/div; Ch4: the current waveform of phase 3, 10A/div. Time : 2.00 ms/div.

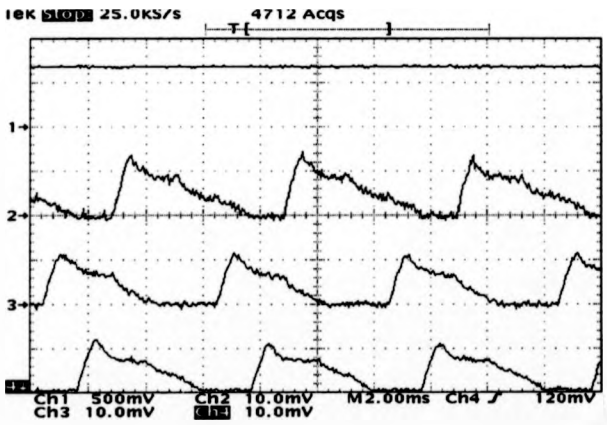

Fig.4-6(b). Steady state response waveforms of neutral voltage and phase operated at 1230 r/min and high load. Ch1: neutral voltage, 100 V/div; Ch2: the current waveform of phase 1, 10 A/div; Ch3: the current waveform of phase 4, 10 A/div; Ch4: the current waveform of phase 5, 10A/div. Time : 2.00 ms/div.

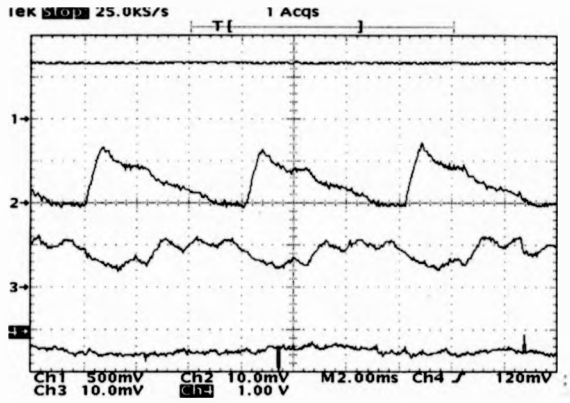

Fig. 4-6(c). Steady state response waveforms of neutral voltage, phase current, the scalar sum of all instantaneous phase current, and shaft torque operated at 1230 r/min and high load. Ch 1: Neutral voltage, 100 V/div; Ch 2: the current waveform of Phase 1, 10 A/div; Ch3: the scalar sum of all instantaneous phase currents, 20 A/div; Ch 4: shaft torque, 10 Nm/div. Time : 2.00 ms/div.

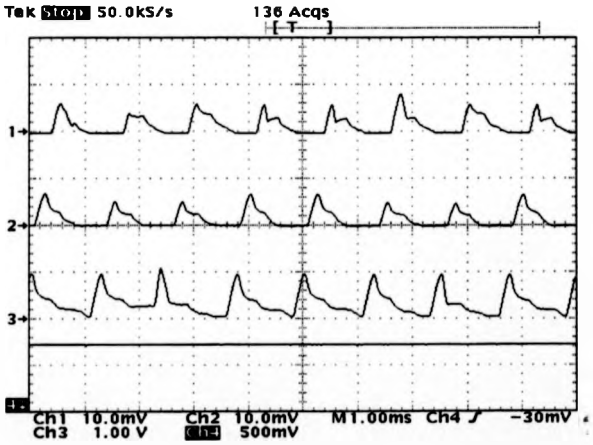

Fig. 4-7(a). High speed response waveforms of phase current and neutral voltage using stator flux vector phase shifting approach. Ch1: the current waveform of phase 1, 10 A/div; Ch2: the current waveform of phase 2, 10 A/div; Ch3: the current waveform of phase 3, 10A/div ; Ch4: neutral voltage, 100 V/div. Time : 2.00 ms/div.

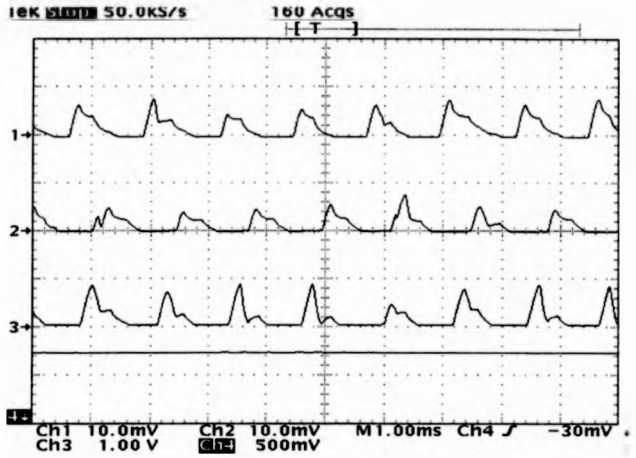

Fig. 4-7(b). High speed response waveforms of phase current and neutral voltage using stator flux vector phase shifting approach. Ch1: the current waveform of phase 1, 10 A/div; Ch2: the current waveform of phase 4, 10 A/div; Ch3: the current waveform of phase 5, 10A/div ; Ch4: neutral voltage, 100 V/div. Time: 1.00 ms/div.

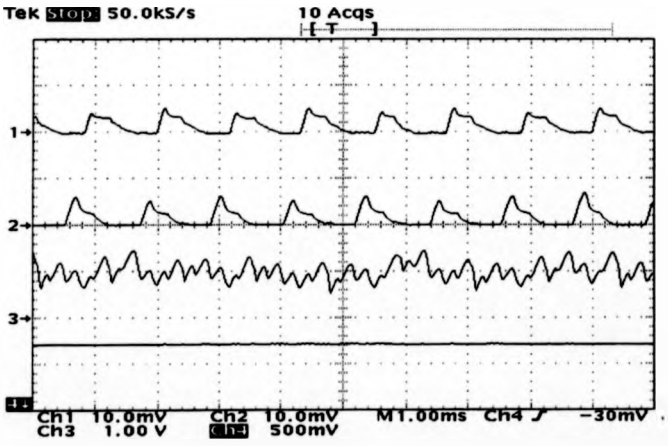

Fig. 4-7(c). High speed response waveforms of phase current, scalar sum of phase currents and neutral voltage using stator flux vector phase shifting approach. Ch1: the current waveform of phase 1, 10 A/div; Ch2: the current waveform of phase 2, 10 A/div; Ch3: total current waveform, 10A/div ; Ch4: neutral voltage, 100 V/div. Time : 5.00 ms/div.

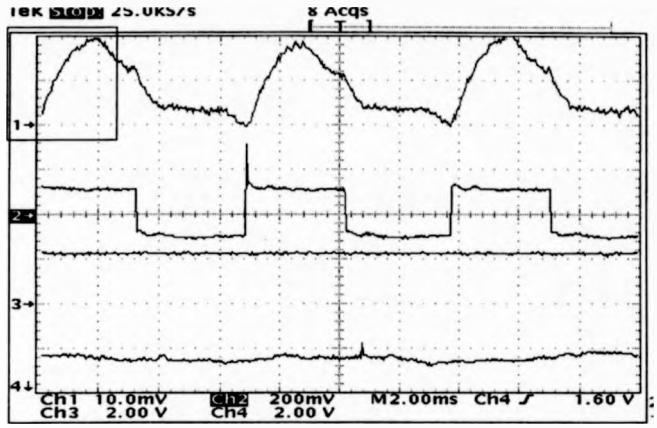

Fig.4-8. Steady state response waveform of the phase current, phase voltage, rotor speed and shaft torque operated at 1090 r/min. Ch1: phase current, 10 amp/div. Ch2: phase voltage, 300 volt/div. Ch3: shaft speed, 1000 r/min/div. Ch4: Shaft torque, 20 Nm/div. Time: 2.00 ms/div.

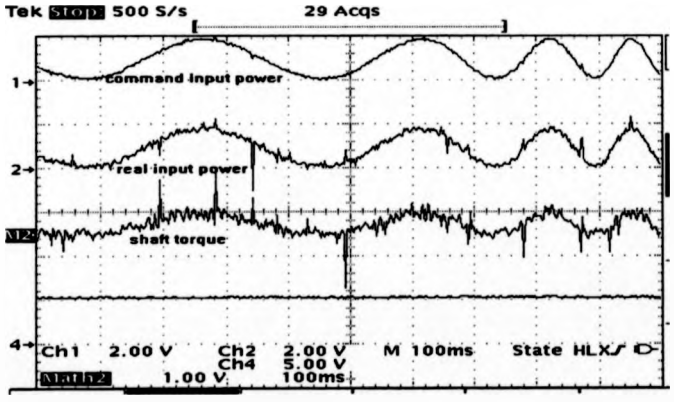

Fig. 4-9. The dynamic response of the instantaneous input power, shaft torque and shaft speed following a sinusoidal modulation of command input power. Ch1 : command input power, 600 W/div. Ch2: real input power, 600 W/div. Ch3 : shaft torque, 50 Nm/div. Ch4 : Shaft speed, 800 r/min/div. Time: 100.00 ms/div.

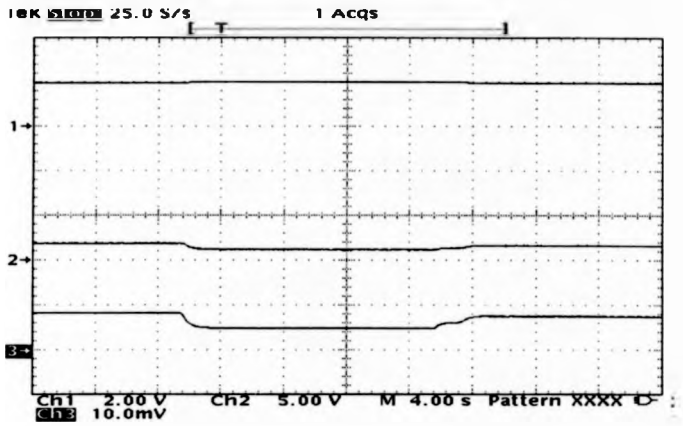

Fig. 4-10. Speed response of switched reluctance vector drive under sliding mode speed controller. Ch1: Rotor speed, 1000 r/min/div; Ch2: Shaft torque, 50 Nm/div; Ch3: Field excited current of a D.C. generator, 2 A/div. Time: 4.00 s/div.

4-6 . DISCUSSION AND CONCLUSION

In this chapter, a split-link converter for a doubly-excited 5-phase switched reluctance motor was presented. Conventionally, it is difficult for the split-link converter to be used in an odd-phase switched reluctance motor, especially for a multiply-excited switched reluctance motor. However, by variable structure control of total phase power combined with space voltage vectors, not only can this converter be used for an odd-phase motor but also it can be operated at very high speed. The implementation of the controller is dramatically simplified as a single current controller without any power or voltage sensor. The converter system does not include a speed controller but the shaft torque in steady state is

reasonably smooth. It is realized just by a 8-bit microcomputer and a few logic IC. It can be seen that it operates well in a high power 5-phase doubly-excited switched reluctance motor. The d.c voltage drift at neutral can be controlled within 6.6 % even under unbalanced loads or high speed and high load. This can be attributed to the excellent "variable structure space voltage vector controller". However, from the experimental waveforms it should be noted that perfect sliding-mode total phase current cannot be achieved because the design implementation was the simplest and lowest cost components, however, approximate sliding-mode, reaching mode, is accomplished. If the design used computationally intensive digital signal processor, its performance could be greatly improved. Under very high speed, perfect sliding-mode operation is invalid, but combined with stator flux vector phase shifting approach, the variable structure controller still operates well. This fact demonstrates the feasibility and potential of the odd-phase split-link converter, with the controller, in variable speed industrial applications, particularly in view of the fact that the implementation of 5-phase converter is so simple. No previous author has found a way of using a split d.c. converter with an odd number of phases

CHAPTER 5

Variable Structure Space Vector Controlled 4-phase Split-Link Converter

5-I INTRODUCTION

In the prvious chapter, a 5 phase split-link converter had been studied. It can been seen that even under high load, the voltage at the netual point deviates only 6.6 % and it still operats well. In this chapter same theory will be applied to introduce excellent performance, for instance, during the commutation or the regeneration period, where an approximate sliding mode total phase power can still be maintained. This performance is very important for generating smooth electromagnetic torque such that vibration and acoustic noise can be greatly reduced. Since split-link converter are simple and it can operate in a regenerate mode, it is very suitable for servo applications. To achieve this, the control of total power in all phases cannot use a conventional approach and the idea of whole system must be considered to satisfy the requirement in the transient state and in the steady state. Because the geometric structure of the motor is different for odd phase and even phase, the formula of the total phase power in 4-phase is different from the one in 5-phase described in the previous chapter, and it is closely related to the number of simultaneously excited phase. However, the end result and control theory are the same, since they both use phase current feedforward to tack the command total current. Furthermore, if the magnetic characteristics of the switched reluctance motor can be designed so that the variation of the inductance, with respect to rotor position, can be designed to be some

constant value, then the ripple of electromagnetic torque would be less because the torque will be depenent on only one parameter- the sum of the squares of all phase currents. However, under saturated conditions, the magnetic circuit becomes nonlinear, and torque is then determined by rotor position and current level. The control of torque for mininum ripple is then very different. However, the current can be controlled by chopping if the flux can be weakened. This will reduce the torque ripple because the component of rotor flux linkage and phase current can be approximatly decoupled. This theory will be explored in this chapter..

5-2 4-PHASE SPLIT-LINK CONVERTER AND SWITCHED RELUCTANCE MOTOR SYSTEM

A. Drive system description

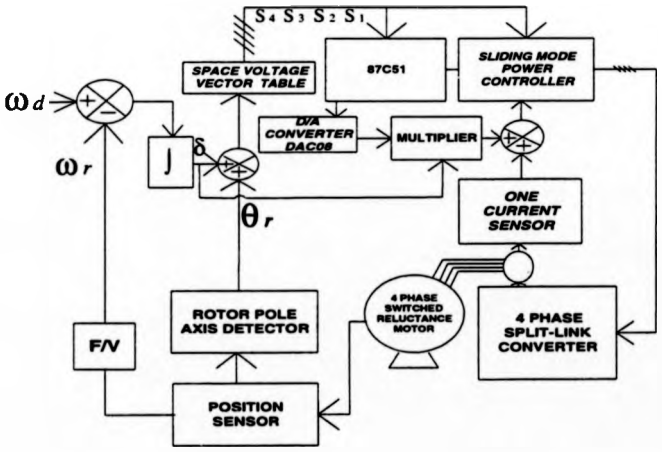

Fig. 5-1. Block diagram of sliding mode 4 phase switched reluctance flux vector drive.

The proposed switched reluctance motor drive is shown as Fig. 5-1. The drive system consists of four main components: a four phase switched reluctance motor, a four phase split dc link converter, sensors, and a control circuit. Tested motor is a 4 phase 4kW, 1500 r/min, 600 V switched reluctance motor. The power converter is a typical 4-phase split-link converter, which is implemented by four IGBT modules and driving circuits. Sensors are composed of a 4-bit position sensor, single d.c. link current sensor and a F/V speed converter. Control circuit is basically an eight bit microcomputer with a few simple logic IC. In the drive system, there is no need for off-line characterization of the phase winding inductance profile. Also, there is no previously known information of the load dynamics. The drive system requires no coordinate transformation computation but uses a dual sliding mode controller. The first is the sliding mode d.c. link power controller, the second is the sliding mode speed controller. Both have feedforward and integral compensation. The whole rotational space is divided into 48 sectors based on the position code of the rotor encoder. In each sector, the operation of the phase winding corresponds to a commutation. In each sector, one or two phase excitation can be used. The electrical cycle of each rotor pole occurs over eight sectors, with a complete revolution of the rotor taking 6 electrical cycle. Although the excited operation over eight sectors is different, these operations are repeated until the next electrical cycle occurs. These excited operations involves the modulation of the phase voltages to produce the required phase current or flux linkage. Since the modulated flux linkage is a function of the level and the phase of the excited phase voltages, so these selected phase voltages are called voltage vectors here. These excited voltages across the four phase

windings exhibit different space phase angle relationship with respect to the rotor, so these voltages are called space voltage vectors.

B. 4 Phase split-link converter

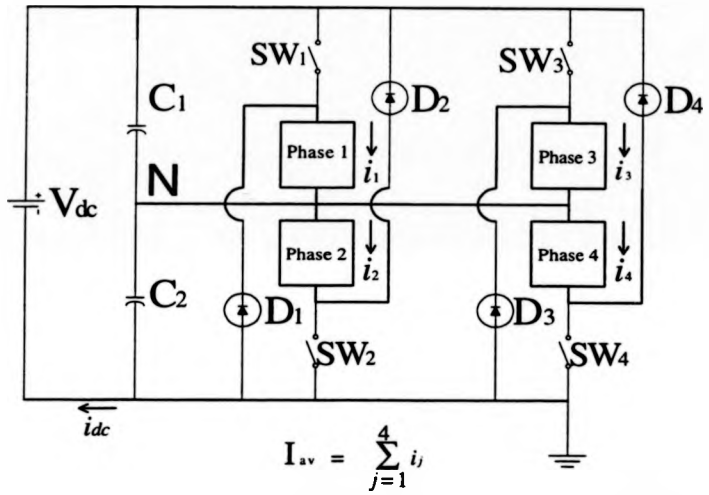

Fig. 5-2. 4 phase split-link converter for a switched reluctance motor.

Table 5-1 Space voltage vectors of a 4 phase switched reluctance motor

S_4	S_3	S_2	S_1	Excited phase windings	Equilibrium Vectors	Position codes of reference rotor pole
0	0	0	1	1	V_1	05
0	0	1	1	1 & 2	$V_{12}(V_1+V_2)$	01
0	0	1	0	2	V_2	00
0	1	1	0	2 & 3	$V_{23}(V_2+V_3)$	08
0	1	0	0	3	V_3	0A
1	1	0	0	3 & 4	$V_{34}(V_3+V_4)$	0E
1	0	0	0	4	V_4	0F
1	0	0	1	4 & 1	$V_{41}(V_4+V_1)$	07

Table 5-2a Doubly- excited combinative vectors during forward rotation

Rotational State	Rotor pole position region	Excited phases (Vectors)	S_4	S_3	S_2	S_1
Motoring	θ_6 (0F~07)	(V_1+V_4)	1	0	0	1
Motoring	θ_7 (07~05)	(V_1+V_2)	0	0	1	1
Motoring	θ_8 (05~01)	(V_1+V_2)	0	0	1	1
Motoring	θ_1 (01~00)	(V_2+V_3)	0	1	1	0
Motoring	θ_2 (00~08)	(V_2+V_3)	0	1	1	0
Motoring	θ_3 (08~0A)	(V_3+V_4)	1	1	0	0
Motoring	θ_4 (0A~0E)	(V_3+V_4)	1	1	0	0
Motoring	θ_5 (0E~08)	(V_1+V_4)	1	0	0	1
Regeneration	θ_3 (08~0A)	(V_1+V_2)	0	0	1	1
Regeneration	θ_2 (00~08)	(V_1+V_4)	1	0	0	1
Regeneration	θ_1 (01~00)	(V_1+V_4)	1	0	0	1
Regeneration	θ_8 (05~01)	(V_3+V_4)	1	1	0	0
Regeneration	θ_7 (07~05)	(V_3+V_4)	1	1	0	0
Regeneration	θ_6 (0F~07)	(V_2+V_3)	0	1	1	0
Regeneration	θ_5 (0E~08)	(V_2+V_3)	0	1	1	0
Regeneration	θ_4 (0A~0E)	(V_1+V_2)	0	0	1	1

Table 5-2b Doubly- excited combinative vectors during reverse rotation

Rotational State	Rotor pole position region	Excited phases (Vectors)	S_4	S_3	S_2	S_1
Motoring	θ_6 (0F~07)	(V_1+V_4)	1	0	0	1
Motoring	θ_7 (07~05)	(V_1+V_2)	0	0	1	1
Motoring	θ_8 (05~01)	(V_1+V_2)	0	0	1	1
Motoring	θ_1 (01~00)	(V_2+V_3)	0	1	1	0
Motoring	θ_2 (00~08)	(V_2+V_3)	0	1	1	0
Motoring	θ_3 (08~0A)	(V_3+V_4)	1	1	0	0
Motoring	θ_4 (0A~0E)	(V_3+V_4)	1	1	0	0
Motoring	θ_5 (0E~08)	(V_1+V_4)	1	0	0	1
Regeneration	θ_3 (08~0A)	(V_1+V_2)	0	0	1	1
Regeneration	θ_2 (00~08)	(V_1+V_4)	1	0	0	1
Regeneration	θ_1 (01~00)	(V_1+V_4)	1	0	0	1
Regeneration	θ_8 (05~01)	(V_3+V_4)	1	1	0	0
Regeneration	θ_7 (07~01)	(V_3+V_4)	1	1	0	0
Regeneration	θ_6 (0F~07)	(V_2+V_3)	0	1	1	0
Regeneration	θ_5 (0E~08)	(V_2+V_3)	0	1	1	0
Regeneration	θ_4 (0A~0E)	(V_1+V_2)	0	0	1	1

Table 5-3 (The electrical regenerative vectors which all switches are turned off)

Excited phase	Excited vectors	Regenerative Vectors	S_4	S_3	S_2	S_1
1	V_1	V_5 ($-V_1$)	0	0	0	0
2	V_2	V_6 ($-V_2$)	0	0	0	0
3	V_3	V_7 ($-V_3$)	0	0	0	0
4	V_4	V_8 ($-V_4$)	0	0	0	0
1, 2	(V_1+V_2)	$-(V_1+V_2)$	0	0	0	0
2, 3	(V_2+V_3)	$-(V_2+V_3)$	0	0	0	0
3, 4	(V_3+V_4)	$-(V_3+V_4)$	0	0	0	0
4, 1	(V_4+V_1)	$-(V_4+V_1)$	0	0	0	0
No excited current	V_0	No regenerative vector	0	0	0	0

A four phase split-link converter is shown in Fig. 5-2. The total dc supply is split by two equal series connected capacitors to create a center point to which the first ends of all phase windings are connected. One switch and one diode is connected to the other end of each phase winding to supply power from one of the halves of the split dc supply. This would be a very cost effective solution because it offers the characteristics of minimum switches and energy recovery.

In table 5-1, there are eight sets of rotor pole position codes (hex) which correspond to eight sets of phase winding excitations. Since these excitations are controlled by the switches of the split-link converter, they are denoted by S_j, denoting the state of j th switch in Fig.5-2. In order to produce effective positive torque, the regions corresponding to increasing inductance need to be identified and then suitable space voltage vectors can be excited. These vectors must be selected for motoring mode operation. Conversely, if negative torque is required to remove the mechanical kinetic energy of the motor and the load, the vectors corresponding to decreasing inductance must be excited. The operating mode is called regeneration. In Table 5-2a, there are

eight sets of optimum space voltage vectors to be selected for forward rotation during the motoring and the regeneration mode, respectively. Another eight sets of optimum space voltage vectors are selected for reverse rotation, as shown in table 5-2b. These available space voltage vectors are shown in Fig. 5-3(a). By appropriate modulation of the space voltage vectors, the equivalent flux vector, which corresponds to the sum of all phase flux linkages, can be decomposed into two components : One is aligned with the rotor pole and the other is orthogonal to the rotor pole, as shown in Fig. 5-3(b) [34-35]. Although they are similar to the d.c. machine, these two components are dependent on rotor positions and the current level. In this case, even if these two component are separated, they are still nonlinear and time-varying. Without an effective nonlinear controller, it is impossible for low level torque ripple to be realized in a high power multiply-excited switched reluctance drive. The desired average current vector and decoupled current vectors operated in the first sector, θ_1, are shown in Fig. 5-3(a).

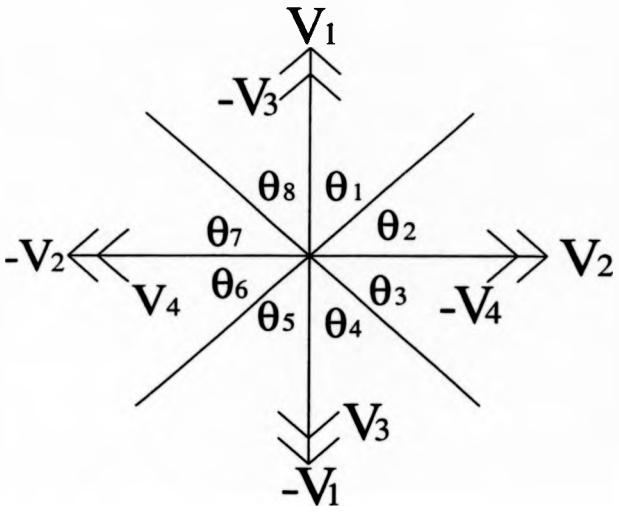

Fig.5-3(a). Available space voltage vectors and operating regions of a 4-phase switched reluctance motor.

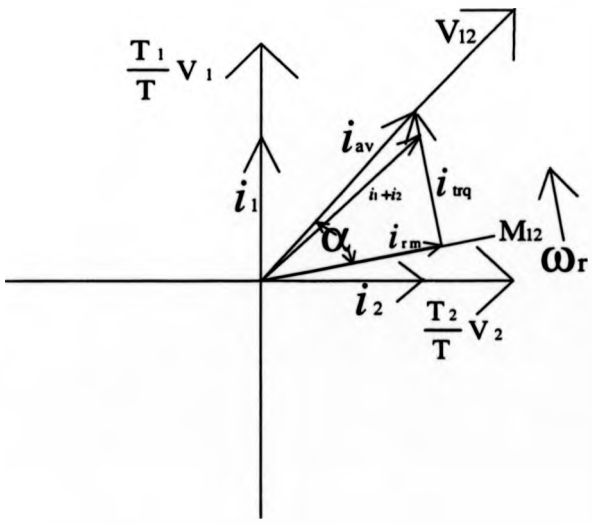

Fig. 5-3(b). Induced space current vectors and desired average current vector and decoupled current vectors operated in θ_1.

C. Vector Representation of 4-phase Split-link Converter Output Voltage [36-39]

If the common terminal of all motor phase windings is connected to the neutral N of the split-link converter, as shown in Fig. 5-2, then table 5-2a or table 5-2b just gives eight sets of voltage vectors during motoring state. For the split-link converter, each voltage vector corresponds to a positive phase voltage when the corresponding power switch is turned on. When the switch is turned off, the voltage is replaced by another negative voltage across the capacitor in the split-link. Therefore, at any rotor pole position, converter output voltage can be represented as a complex vector as follows:

$$V_k = +V_{cU} \exp(jk\pi/4) \quad \text{when k= 1, 3 turned on} \quad (5\text{-}1)$$

$$V_{k+4} = -V_{cD} \exp(jk\pi/4) \quad \text{when k= 1, 3 turned off} \quad (5\text{-}2)$$

$$V_k = +V_{cD} \exp(jk\pi/4) \quad \text{when k= 2, 4 turned on} \quad (5\text{-}3)$$

$$V_{k+4} = -V_{cU} \exp(jk\pi/4) \quad \text{when k= 2, 4 turned off} \quad (5\text{-}4)$$

$$V_{cU} + V_{cD} = V_{dc} \quad (5\text{-}5)$$

where, k is the symbol of phase windings or phase switches in Fig. 5-2, V_k and V_{k+4} denote the voltage vector across k th phase winding during conduction and regeneration, respectively. V_{cU} and V_{cD} denote the voltage level across upper and lower capacitors in the d.c. link, respectively. V_{dc} is d.c. voltage level across d.c. link source.

D. Motor and load dynamics

The electromagnetic dynamic model of a four phase switched reluctance motor can be expressed as follows :

$$\frac{d\,\omega_r}{d\,t} = -\,(B/J)\,\omega_r + (-\tau_L + \tau)/\,J \tag{5-6}$$

$$\upsilon = r\,i + \frac{d\,\lambda_s}{d\,t} \qquad \text{or} \tag{5-7a}$$

$$L(i,\theta_r)\frac{d\,i}{d\,t} = -[\,r + \frac{d\,L(i,\theta_r)}{d\,\theta_r}\,\omega_r\,]\,i + \upsilon \tag{5-7b}$$

where υ is the instantaneous voltage input of the phase winding when switches of the split-link converter are turned on or turned off so that its amplitude is equivalent to the level of the voltage vectors in the equations (5-1) ~ (5-4), and r is the equivalent resistance in the circuit - including the conducting resistance of the switches, i is the phase current, λ_s is the stator flux linkage associated with the switched reluctance motor phase coil, and $L(i,\theta_r)$ is corresponding stator phase inductance at position θ_r. ω_r is the rotor speed, τ is the electromagnetic torque of the motor, J is the inertia constant of the rotor and load, B is the viscous friction coefficient , and τ_L is load torque.

5-3 THE PHASE POWER CONTROL OF THE DRIVE SYSTEM

A. Space Vector Control Of Total Phase Power [8-12]

From equation (5-7a) the stator flux linkage can be rewritten as

$$\lambda_s = \int \upsilon\,dt - r\int i\,dt \tag{5-8}$$

if the switching frequency of each switch is fixed, and its corresponding switching period is denoted by T, and the state of each switch is expressed by a switching function, then the voltage vector across each phase winding can be written as

$$V_j = S_j * V_{c\,j} \qquad \text{for } j = 1,\cdots,4 \qquad (5\text{-}9)$$

where j denotes the symbol of a particular phase winding in the motor, S_j denotes the switching function which describes the switching state of j th switch and $V_{c\,j}$ (V_{cU} or V_{cD}) denotes the voltage across the capacitor, which is paralleled with the j th phase switching circuit , and

$S_j = 1$ when switch SW_j for the j th phase is turned on.

$S_j = -1$ when the j th switch SW_j is turned off and the current is still flowing through these winding via recovery diode D_j. (5-10)

If it is assumed that the power converter is operated with fixed switching frequency, f, (switching period is T) and is alternating between the state $S_j = 1$ (for time T_{on}) and $S_j = -1$ (for time T_{off}), where $T = T_{on} + T_{off}$, then by equations (5-1)-(5-4) equation (5-8) can be rewritten as

$$[\lambda_{s\,j}(t_k) - \lambda_{s\,j}(t_{k-1})] = [V_j T_{on} + (V_{j+4})T_{off}] - r T [i_j(t_k) + i_j(t_{k-1})]/2$$

$$\text{for } j = 1,\cdots,4 \qquad (5\text{-}11)$$

By equations (5-5), (5-9) and (5-10), equation (5-11) can be expressed as

$$[\lambda_{s\,j}(t_k) - \lambda_{s\,j}(t_{k-1})] = [V_{c\,j} T_{on} - (V_{dc} - V_{c\,j})T_{off}] - r T [i_j(t_k) + i_j(t_{k-1})]/2$$

$$\text{for } j = 1,\cdots,4 \qquad (5\text{-}12)$$

where $\lambda_{s\,j}(t_{k-1})$ and $i_j(t_{k-1})$ denote the initial stator flux linkage and the sampled current of the j th phase winding at the start of the k th switching cycle, while $\lambda_{s\,j}(t_k)$ and $i_j(t_k)$ denote the stator flux linkage and the sampled current of the same phase winding at the end of the k th switching cycle. From equations (5-5) and (5-12),

if two adjacent phase windings are excited simultaneously, then the following expression can be derived.

$$\sum_{j=1}^{2}[\lambda_{s\,j}(t_k)] - \sum_{j=1}^{2}\lambda_{s\,j}(t_{k-1})] = \{[2D(t_k)-1]V_{dc}(t_k) - r\,I_{av}(t_k)\}T \qquad (5\text{-}13)$$

where $D(t_k) = [T_{on}(t_k)/T]$, $I_{av}(t_k)$ denotes the average of the sum of all phase currents between t_{k-1} to t_k.

If both sides of equations (5-13) are divided by the switching period T, an expression for the average total phase voltage applied to the motor from t_{k-1} to t_k is given by

$$V_{av}(t_k) = [2D(t_k)-1]V_{dc}(t_k) - r\,I_{av}(t_k) \qquad (5\text{-}14)$$

Both sides of equation (5-14) are multiplied by $I_{av}(t_k)$, the average value of the total power delivered to the motor phase windings is given by

$$P_{av}(t_k) = [2D(t_k)-1]\,]V_{dc}(t_k)\,I_{av}(t_k) - r\,I_{av}^2(t_k)$$

$$= V_{av}(t_k)\,I_{av}(t_k) - r\,I_{av}^2(t_k) \qquad (5\text{-}15)$$

where $V_{av}(t_k)$ denotes the equivalent average voltage across the equivalent circuit of all phase windings between t_{k-1} and t_k.

B. Variable Structure Control of Total Phase Power [13-21]

According to the power invariance transformation, equation (5-15) can be rewritten as

$$P_{av}(t_k) = V_{dc}(t_k)\,i_{dc}(t_k) - R\,i_{dc}^2(t_k) \qquad (5\text{-}16)$$

where R denotes the equivalent input resistance from d.c. link and

$$i_{dc}(t_k) = [2D(t_k)-1]I_{av}(t_k)$$

denotes the equivalent average current flowing through dc source between tk-1 and tk .

If command d.c. link power and corresponding command d.c. link current, at time t_k, are denoted by $P_c(t_k)$ and $I_c(t_k)$, respectively, then when switching frequency is approaching an infinite large value, then the error rate between command d.c. link power and real d.c. link power becomes

$$\frac{d\, V_{dc}(t)\, i_{dc}(t)}{d\, t} = V_{dc}(t)\,[I_c(t) - i_{dc}(t)] + R\,[I_c^2(t) - i_{dc}^2(t)] \qquad (5\text{-}17)$$

where $I_c(t)$ and $i_{dc}(t)$ are the command and real d.c. link current at the time instance t, respectively.

Before sliding mode total phase power reaches, the error rate of the d.c. link current in (5-17) is not zero. Because the drive system has an unknown load and is subject to uncertain disturbances, the equivalent sliding mode total phase power is difficult to achieve unless the real loads and disturbances are known. However, according to singular perturbation theory, the steady state solution of the equation (5-17) — an integral manifold can be directly found from (5-7b), by letting $L(i,\theta_r) = 0$ and sloving (5-7b). Thus the total average phase power in sliding mode is found as follows

$$P_s(t) = \sum_{j=1}^{4} \upsilon_j\, i_j = \sum_{j=1}^{4} \left[r\, i + \frac{d\, L_j(i_j,\theta_r)}{d\,\theta_r}\, \omega_r \right] i_j^2 \qquad j = 1,..,4 \qquad (5\text{-}18)$$

where the parameters in (5-18) are same as those in (5-7b) but here they correspond to the jth phase.

Therefore, only if duty ratio $D(t_k)$ in (5-15) or $P_{av}(t_k)$ in (5-16) is controlled such that (5-18) is satisfied, then sliding total phase power can be achieved. In this case equation (5-19) will hold.

$$V_{dc}(t)\, i_{dc}(t) = V_{dc}(t)\, I_c(t) = P_s(t) \qquad (5\text{-}19)$$

Now, define a switching function as follows:

$$\sigma = V_{dc}(t) i_{dc}(t) - V_{dc}(t) I_c(t) \qquad (5\text{-}20)$$

In order to reduce d.c. link power chattering , a soft sliding mode control law can be designed as follows:

$$V_{dc}(t) i_{dc}(t) = V_{dc}(t) [I_c(t) + I_m] \quad \text{if} \quad \sigma \leq -\epsilon \text{ and } \frac{d\sigma}{dt} \leq -\eta$$

$$V_{dc}(t) i_{dc}(t) = V_{dc}(t) [I_c(t) - I_m] \quad \text{if} \quad \sigma \geq +\epsilon \text{ and } \frac{d\sigma}{dt} \geq \eta$$

$$V_{dc}(t) i_{dc}(t) = V_{dc}(t) \{ I_c(t) - I_m [L_p \sigma + L_i \int \sigma dt] \} \quad \text{if} \quad -\epsilon \leq \sigma \leq +\epsilon \qquad (5\text{-}21)$$

where, η and ϵ are positive real constant which are used to determine the tolerable range of the equivalent d.c. link current sliding along command reference current function; I_m is a limited maximum d.c. link current; $0<L_p<1$ and $0<L_i<1$ are proportional and integral constants, respectively. Therefore, the total phase power of the drive system in sliding mode is:

$$P(t) = V_{dc}(t) I_c(t) \qquad (5\text{-}22)$$

If $V_{dc}(t)$ is fixed as a d.c. power supply voltage, such as 300 V, then equation (5-22) becomes

$$P(t) = V_{dc} I_c(t) \qquad (5\text{-}23)$$

So, the total phase power control becomes the control of the equivalent d.c. link current.

5-4 EXPERIMENTAL INVESTIGATION OF AN APPROXIMATE SLIDING MODE TOTAL PHASE POWER CONTROL

Generally, a switched reluctance drive is designed to operate with excitation of only one phase during each conduction cycle. However, during commutation the effect of the previous phase current cannot be neglected, especially when the level of phase current is large. Furthermore, during the regenerative state, it is more difficult for a total sum of all phase currents to be controlled to be a constant. However, if the total sum of all phase currents is considered and the feedforward strategy is used to feedback individual phase currents and to cancel the error between the command total sum of all phase currents and the real total sum of all phase currents, then from equation (5-22) the total phase power, or the equivalent total phase power in the d.c. link, can be achieved by controlling the total sum of all phase currents, or the average d.c. link current.

To achieve total phase power control, the chopping condition of the phase current must be satified. This chopping condition is approximately the sliding mode in the variable structure current control scheme. However, even if all of the phase currents can be chopped, it can not be guaranteed that the total sum of all phase currents is a controllable constant. If there exists at least one of phase currents can be chopped, then the total sum of all phase currents can be chopped by feedforward of each phase current so that the real total sum of all phase currents can track the command value according to variable structure control theory and equations (5-15) ~ (5-23).

In order to achieve feedforward control the total sum of all phase currents, there should be exist at least one phase current which can be chopped by a PWM phase voltage controller. If this condition cannot be satisfied, it is impossible for the sliding mode phase power control to accomplish. In this case, the conventional phase angle advancing seems to be effective and the most effective way would be to advance each current (thus weakening flux linkage) and then taking their total sum and using the current feedforward control technology.

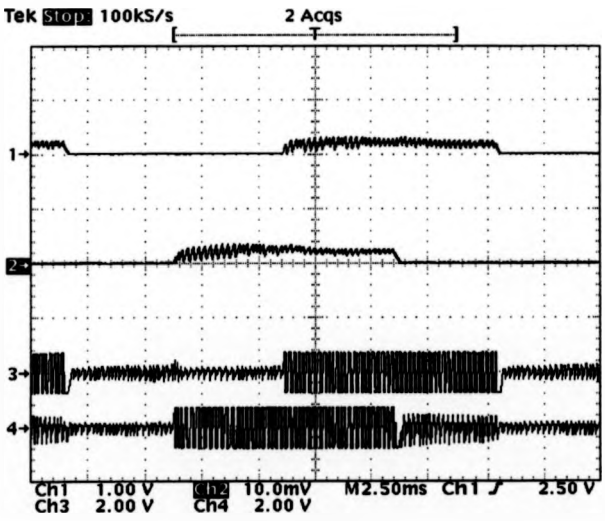

Fig. 5-4(a) Phase current and phase voltage waveforms during motoring state. Ch1: phase-1 current, 10 A/div; Ch2: phase-2 current, 10 A/div; Ch3: Phase-1 voltage, 400 V/div; Ch4: phase-2 voltage, 400 V/div. Time : 2.5 ms/div.

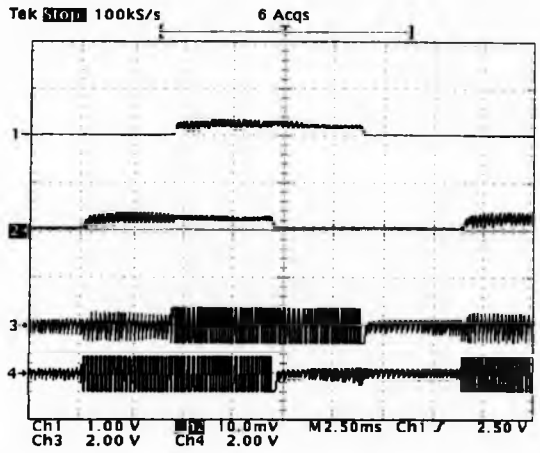

Fig. 5-4(b) Phase current and phase voltage waveforms during motoring state. Ch1: phase-3 current, 10 A/div; Ch2: phase-4 current, 10 A/div; Ch3: Phase-3 voltage, 400 V/div; Ch4: phase-4 voltage, 400 V/div. Time : 2.5ms/div.

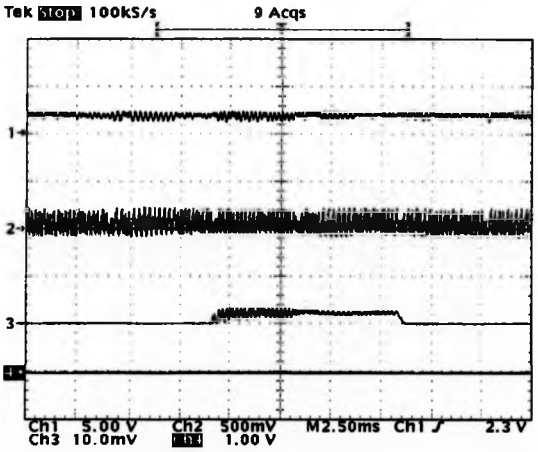

Fig. 5-4(c) Phase current and phase voltage waveforms during motoring state. Ch1: total som of all phase currents,12.5 A/div; Ch2: d.c. link current, 5 A/div; Ch3: phase-1 current, 10 A/div; Ch4: shaft speed, 500 r/min. Time: 2.5 ms/div.

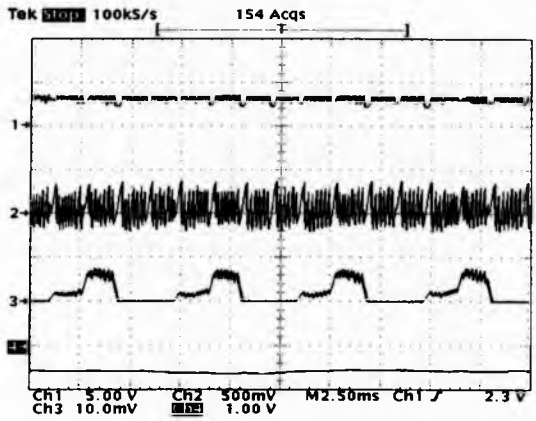

Fig. 5-4(d). Phase current and phase voltage waveforms during regenerative state. Ch1: total som of all phase currents,12.5 A/div; Ch2: d.c. link current, 5 A/div; Ch3:phase-1 current, 10 A/div; Ch4: shaft speed, 500 r/min. Time: 2.5 ms/div.

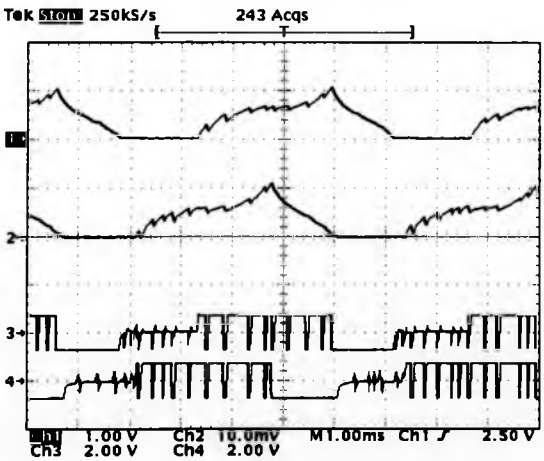

Fig. 5-5(a) Phase current and phase voltage waveforms during motoring state. Ch1: phase-1 current, 10 A/div; Ch2: phase-2 current, 10 A/div; Ch3: Phase-1 voltage, 400 V/div; Ch4: phase-2 voltage, 400 V/div. Time: 1 ms/div.

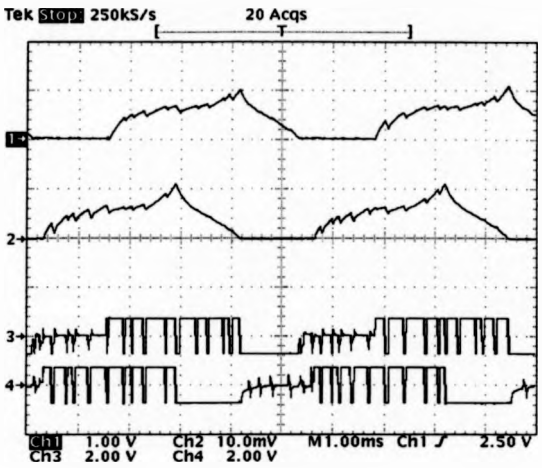

Fig. 5-5(b) Phase current and phase voltage waveforms during motoring state. Ch1: phase-3 current, 10 A/div; Ch2: phase-4 current, 10 A/div; Ch3: Phase-3 voltage, 400 V/div; Ch4: phase-4 voltage, 400 V/div. Time: 1ms/div.

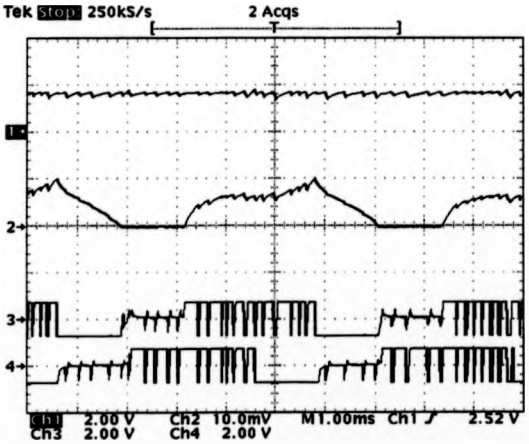

Fig. 5-5(c) Phase current and phase voltage waveforms during motoring state. Ch1: phase-1 current, 10 A/div; Ch2: phase-2 current, 10 A/div; Ch3: Phase-1 voltage, 400 V/div; Ch4: phase-2 voltage, 400 V/div. Time: 1ms/div.

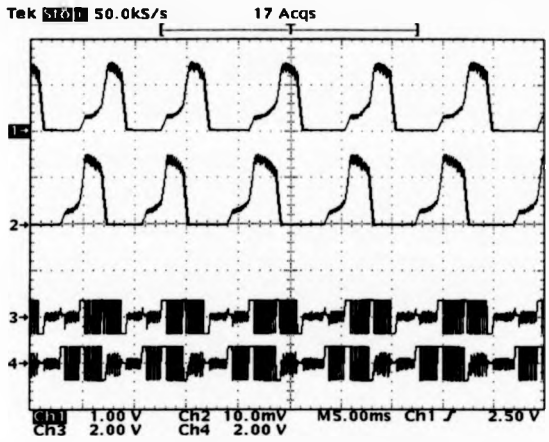

Fig. 5-5(d). Phase current and phase voltage waveforms during regenerative state.Ch1: phase-1 current, 10 A/div; Ch2: phase-2 current, 10 A/div; Ch3: Phase-1 voltage, 400 V/div; Ch4: phase-2 voltage, 400 V/div. Time: 5 ms/div.

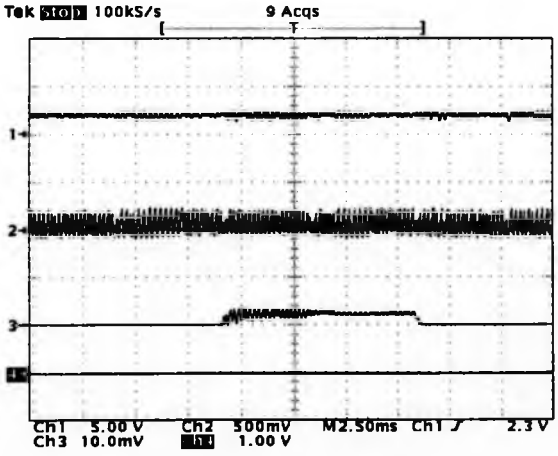

Fig.5-6(a). Current and phase voltage waveforms at 500 r/min. Ch1: total som of all phase currents,12.5 A/div; Ch2: d.c. link current, 5 A/div; Ch3:phase-1 current, 10 A/div; Ch4: shaft speed, 500 r/min. Time: 25 ms/div.

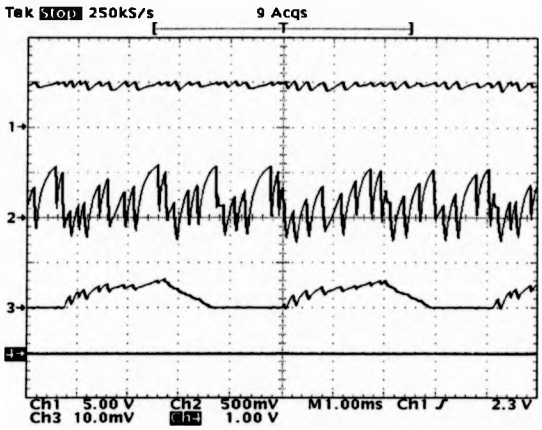

Fig. 5-6(b). Current and phase voltage waveforms at 2380 r/min.Ch1: total sum of all phase currents,12.5 A/div; Ch2: d.c. link current, 5 A/div; Ch3: phase-1 current, 10 A/div; Ch4: shaft speed, 2400 r/min. Time: 1 ms/div.

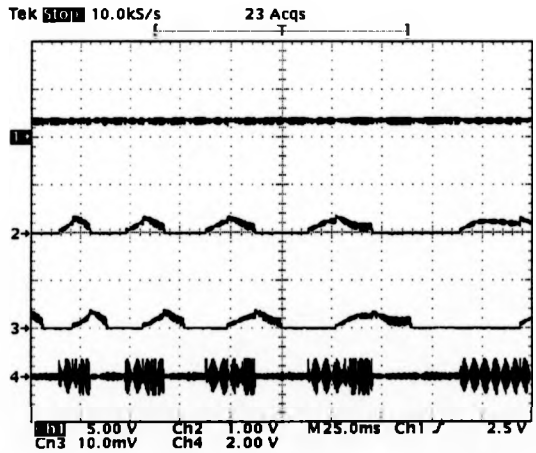

Fig. 5-6(c) Phase current and phase voltage waveforms during the transition from high speed to low speed state. Ch1: total sum of all phase currents,12.5 A/div; Ch2: phase-1 current, 10 A/div; Ch3:phase-2 current, 10 A/div; Ch4: phase-1 voltage 400 V/div. Time: 25 ms/div.

To show the effectiveness of the total phase power controller, some experiments have been carried out, usng the four-phase split link converter shown in Fig. 5-2 and space vectors in Table 5-2 and Table 5-3. According to equations (5-15) ~ (5-23), the total phase power can be controlled to track the command value. In Fig. 5-4(a), the current and voltage waveform of phase-1 and phase-2 have been recorded, when the motor was running at 500 r/min. Fig. 5-4(b) was the waveforms of phase-3 and phase-4 obtained again, running at 500 r/min. Fig. 5-4(c) shows the waveforms of total sum of all phase currents, running at the same operating condition. From this figure, it can seen that total sum of all phase currents during an approximate sliding mode can be achieved and the average level of the d.c. link current is fixed approximately if high level harmonics are neglected. In Fig. 5-4(d), a similar case is illustrated during a continued period of regeneration.

In Fig. 5-5, Some similar results can be obtained even if the operated speed is increased up 2380 r/min. Figure 5-6 are some experimental results which exhibit the control performannce of total phase power, running at 500 r/min, 2380 r/min and the regenerative state from 2380 r/min to 500 r/min, respectively.

From Fig. 5-5 ~ Fig. 5-6, it can be seen that the total sum of all phase current is an approximate constant no matter speed is low, high or under regenerative state from high to low speed. During normal commutation, total sum of all phase currents can be still maintained at the demanded value unless too large back EMF at some position appears. Figure 5-6(b) is a good example, which exhibits a little dip in the total sum of all phase currents. This should be attributed to the exccesive back EMF(larger than d.c. supply voltage) at some position, caused by high speed operation and large transient phase current.

CHAPTER 6

A VARIABLE STRUCTURE SPACE VECTOR CONTROLLED FLUX VECTOR SERVO DRIVE

6-1 INTRODUCTION

With recent advances in factory automation, robust speed control for variable speed drives is now indispensable in many general purpose adjustable speed applications. Such systems commonly employ dc or ac drives. The ac induction motor is robust in structure and very cost effective to manufacture and, with the advent of inverter control, is now replacing the conventional brushed dc motor throughout industry. The brushless d.c. motor, the permanent magnet synchronous motor and synchronous reluctance motor have excellent energy density properties with low rotor inertia and, when used with modern power inverters and advanced controllers, these drives exhibit excellent performance. The switched reluctance motor is simple and rugged in structure, has high energy density and low rotor inertia. Despite the potentially low cost of both the motor and the drive, the switched reluctance drive has not found wide acceptance in high performance industrial applications. Two reasons for this are the torque ripple and acoustic noise associated with this type of the drive.

Improved control schemes have been developed and proposed to tackle these problems [26–30]. Papers [26-28] describe controllers that are too complex to be implemented in a commercial drive. Paper [29] only discusses very small power application and [30] addresses low speed operation only. Moreover, [29,30] describe a three phase motor only and the motor needs special design to maintain a sinusoidal

phase inductance and its excited current must also be sinusoidal. The requirement for sinusoidal current in the motor phase windings is what restricts these schemes to low speed application because sinusoidal currents and sinusoidal inductances are difficult to maintain at high speed and under uncertain dynamic loads. Papers [40,41] describe high-performance switched reluctance drives, using a similar control scheme to [27], with simulated results [40] and practical implementation at powers up to 400 W [41]. In [41] the controller is still not particularly robust, only achieving a 7% speed error at rated load. It has been concluded therefore that a robust speed controller for a switched reluctance motor which simultaneously delivers low levels of torque ripple has still to be reported. This chapter addresses this need, describing how a robust speed controller has been developed and applied to a standard high power switched reluctance motor. This chapter brings together all the theory of sliding mode d.c. link power control and adds a modified variable structure speed control scheme so that a fast and robust speed response is achieved. The principle of the controller is illustrated for the case of a four phase switched reluctance motor though the equations are kept particularly general so that it could be applied to a switched reluctance motor with any number of phase windings.

6-2 SPACE VOLTAGE VECTOR MODULATION AND TOTAL PHASE POWER OF A SWITCHED RELUCTANCE MOTOR

A. Phase winding excitation and space vectors [36],[39],[42-44]

The switched reluctance motor produces motoring torque when current flows while the inductance of a phase winding is increasing. A power converter controls the

excitation of the phase windings in synchronism with the rotor rotation. The controller developed in this paper can be utilized with many possible power converters of which there are many variations in the literature. The most common power converter, the asymmetric half bridge converter shown in Fig. 6-1 will be used to describe the operation of the controller.

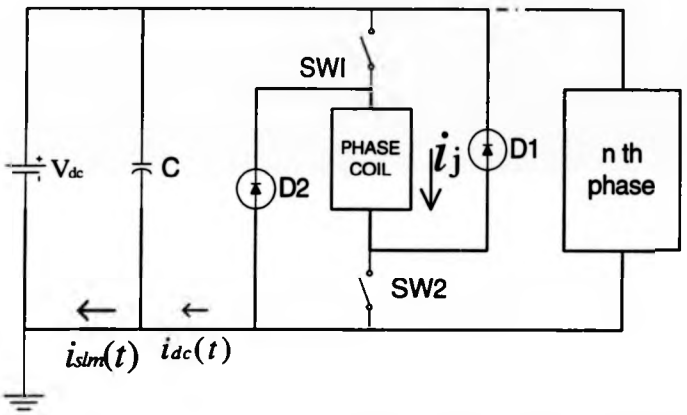

Fig. 6-1. The asymmetric half bridge power converter circuit for one phase of a switched reluctance motor.

The general voltage equation for a phase winding of a switched reluctance motor is given by

$$\upsilon = r\, i + \frac{d\,\lambda_s}{d\,t} \tag{6-1}$$

where υ is the voltage applied to a phase winding by the power converter and r is the resistance of the phase winding, i is the phase current, and λ_s is the stator flux linkage associated with the phase winding.

From equation (6-1), the stator flux linkage can be expressed as

$$\lambda_s = \int \upsilon\, dt - r \int i\, dt \tag{6-2}$$

If the switching frequency of each switch is fixed, and its corresponding switching period is denoted by T and the state of each switch is expressed by a switching function, then the voltage state across each phase winding can be written as

$$V_j = S_j * V_{dc} \qquad \text{for } j = 1, \cdots n \quad (6\text{-}3)$$

where j denotes a particular phase winding, n is the number of phase windings in the motor, S_j denotes the switching states of the power switches shown in Fig. 1 and V_{dc} denotes the voltage across the capacitor in the d.c. link, and

$S_j = 1$ when both switches Sw1 and Sw2 for the j th phase are turned on

$S_j = 0$ when only one switch (Sw1 or Sw2) for the j th phase is turned on and current is flowing through the phase winding , or when the j th pair of switches are turned off and no current flows in the j th phase winding.

$S_j = -1$ when the j th pair of switches are turned off and the current is still flowing through the phase winding via diodes D_1 and D_2 .

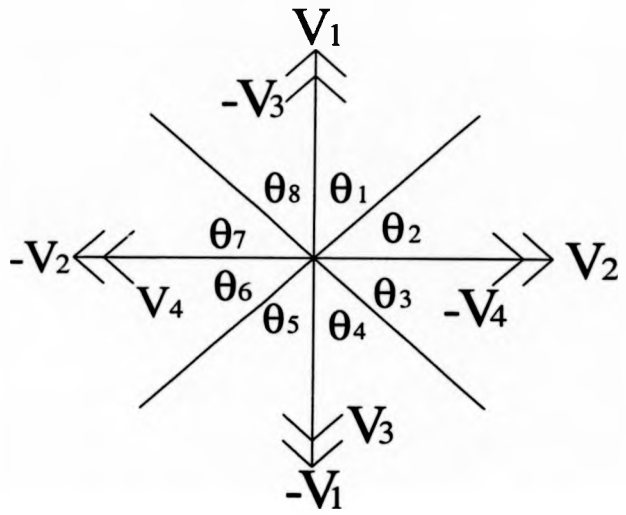

Fig.6-2(a). Available space voltage vectors and operating regions of a 4-phase switched reluctance motor.

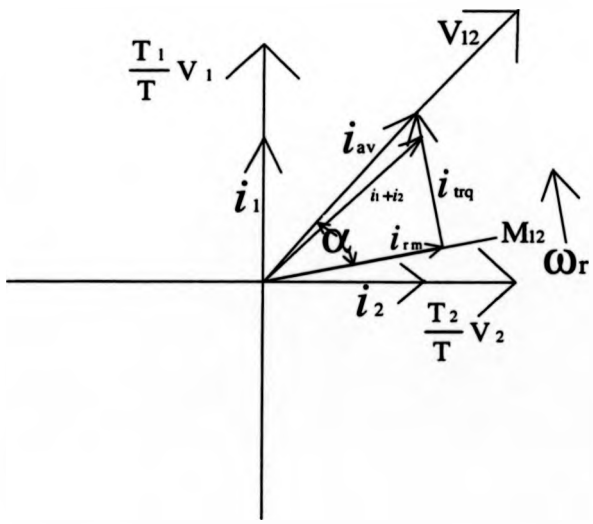

Fig. 6-2(b). Induced space current vectors and desired average current vector and decoupled current vectors operated in θ_1.

In a four phase switched reluctance motor, there are therefore, a total of nine space voltage vectors as shown in Fig.6-2(a). In motoring operation, the vectors V_j (j=1,2,3,4) represent a positive voltage across the respective phase winding (S_j = 1) during a rotor angle when the phase winding inductance is increasing and the vectors -V_j (j=1,2,3,4) satisfies S_j = -1. In regenerative operation. -V_j (j=1,2,3,4) denotes the voltage vectors applied within a region of decreasing phase winding inductance with respect to rotor position and satisfy S_j = 1. V_0 is the zero voltage vector which denotes all possible vectors V_j satisfying S_j = 0.

Table 6-1 Combined space voltage vectors for reverse rotation

Rotational State	Operating region (section)	Excited phases (Vectors)	S_4	S_3	S_2	S_1
Motoring	θ_3	(V_1+V_2)	0	0	1	1
Motoring	θ_2	(V_1+V_4)	1	0	0	1
Motoring	θ_1	(V_1+V_4)	1	0	0	1
Motoring	θ_8	(V_3+V_4)	1	1	0	0
Motoring	θ_7	(V_3+V_4)	1	1	0	0
Motoring	θ_6	(V_2+V_3)	0	1	1	0
Motoring	θ_5	(V_2+V_3)	0	1	1	0
Motoring	θ_4	(V_1+V_2)	0	0	1	1
Regeneration	θ_6	(V_1+V_4)	1	0	0	1
Regeneration	θ_5	(V_1+V_4)	1	0	0	1
Regeneration	θ_4	(V_3+V_4)	1	1	0	0
Regeneration	θ_3	(V_3+V_4)	1	1	0	0
Regeneration	θ_2	(V_2+V_3)	0	1	1	0
Regeneration	θ_1	(V_2+V_3)	0	1	1	0
Regeneration	θ_8	(V_1+V_2)	0	0	1	1
Regeneration	θ_7	(V_1+V_2)	0	0	1	1

In Fig.6-2(b) the winding of phase 1 is excited by V_j (j=1) for T_1 during switching time period T, while the winding of phase 2 is excited by V_j (j=2) for T_2 during the same switching time period T. Thus, corresponding current vectors in the excited

windings will flow and an average current vector i_{av} will be obtained. This current vector can be decoupled into two components: one is the magnetizing current i_{rm} which produces the rotor flux linkage aligned with rotor pole axis, another is the torque current i_{rq} providing the effective electromagnetic torque, which is orthogonal to the rotor pole axis, as shown in Fig. 6-2(b). If there are multiple phase windings which are simultaneously excited for T_k during T, the average decoupled current can be found in a similar way. This operation is repeated during each sector, which corresponds to each commutation region, until the next commutation appears. The whole rotational space is subdivided into 48 sectors based on the position code (hex) of the rotor encoder. In each sector, one or two voltage vectors can be selected and modulated by a high frequency digital carrier. The electrical cycle of each rotor pole occurs over eight sectors, with a complete revolution of the rotor taking 6 electrical cycles or 48 sectors. Table 6-1 is a practical example of the excitation strategy for a 4 phase switched reluctance motor in which two phases can be simultaneously excited. In Table 6-1, θ_1 to θ_8, denote the eight operating sectors comprising an electrical cycle, obtained from decoding a 4-bit position signal. The outputs, S_4 S_3 S_2 S_1, denote the switching state of four switches in power converter. This switching state must then be modulated in some way to control the current in each phase. In this controller, the same modulation time period T_k is applied to all excited phases simultaneously and this time period can be found by d.c link power feedback, which will be described in the next section, and its implementation will be illustrated in section 6-4.

B. Total stator phase flux linkage and phase power

As described in section A, if it is assumed that the power converter is operating with fixed switching frequency, f, (period, T) and is alternating between the state $S_j = 1$ (for time $T_k = T_{on}$) and $S_j = 0$ (for time T_{off})[or the state $S_j = -1$ (for time $T_k = T_{on} - T_{off}$)], where $T = T_{on} + T_{off}$, then equation (2) can be rewritten as

$$[\lambda_{s\,j}(t_k) - \lambda_{s\,j}(t_{k-1})] = V_j T_k - r T [i_j(t_k) + i_j(t_{k-1})]/2$$

$$= V_{dc} T_k - r T [i_j(t_k) + i_j(t_{k-1})]/2$$

$$\text{for } j = 1, \cdots, n \qquad (6\text{-}4)$$

where, $\lambda_{s\,j}(t_{k-1})$ and $i_j(t_{k-1})$ denote the initial stator flux linkage and the sampled current of the j th phase winding at the start of the k th switching cycle, while $\lambda_{s\,j}(t_k)$ and $i_j(t_k)$ denote the stator flux linkage and the sampled current of the same phase winding at the end of the k th switching cycle. If m phases of a n-phase switched reluctance motor are simultaneously excited and the average of the sum of all phase currents between t_{k-1} to t_k is denoted by $I_{av}(t_k)$, the scalar sum of the stator flux linkage is

$$\sum_{j=1}^{m} [\lambda_{s\,j}(t_k)] - \sum_{j=1}^{m} [\lambda_{s\,j}(t_{k-1})] = m V_{dc} T_k - r I_{av}(t_k) T \qquad (6\text{-}5)$$

assuming that phases j = 1,2 ... m (where $m \leq n/2$ is even; $m \leq (n+1)/2$ if n is odd) are the phases which are simultaneously excited.

If both sides of equations (6-5) are divided by the switching period T, an expression for the average total phase voltage applied to the motor from t_{k-1} to t_k is obtained

$$V_{av}(t_k) = m V_{dc} (T_k / T) - r I_{av}(t_k) \qquad (6\text{-}6)$$

Now both sides of equation (6-6) are multiplied by $I_{av}(t_k)$, the average value of the total power delivered to the motor phase windings is given by

$$P_{av}(t_k) = m\, I_{av}(t_k)\, V_{dc}\, (T_k/T) - r\, I_{av}^2(t_k)$$

$$= V_{dc}\, i_{dc}(t_k) - R\, i_{dc}^2(t_k) \qquad (6\text{-}7)$$

where $i_{dc}(t_k) = m\,(T_k/T)\, I_{av}(t_k)$ denotes the equivalent average current flowing into the converter from the d.c. link between t_{k-1} to t_k and R represents the total 'equivalent resistance' of the drive circuit and phase windings. From equation (6-7) , if R is known or can be neglected and V_{dc} is fixed, one can see that the d.c. link current can be controlled so that it can track a demanded current, then the average total phase power $P_{av}(t_k)$ will follow a demanded input power providing the instantaneous phase voltage in each phase winding is dynamically turned on and turned off based on T_k so that $I_{av}(t_k)=i_{dc}(t_k)/[m(T_k/T)]$ is satisfied. Therefore, using input power feedback, the switching of all phase currents can be carried out simultaneously according to equation (6-7) and the space voltage vectors with the appropriate positive or negative inductance slope. This control strategy therefore makes it unnecessary to have a current sensor to measure each phase winding current dramatically simplifying the controller design for a switched reluctance motor drive.

6-3 VARIABLE STRUCTURE CONTROL OF POWER AND SPEED

A. Approximate sliding mode power control using d.c. link current feedback [32],[39],[45-48],[53]

As described in chapter 5 and section 6-2, the control of the total phase power can be shifted to the d.c. link terminals and can be simplified as the control of the d.c. link current if the voltage of the input source is fixed. If the switching time period T in the equation (6-7) approaches zero theoretically, then $i_{dc}(t_k)$ will approach the

instantaneous sum of the phase currents $\sum_{j=1}^{m}(i_j)$ depending on the total stator flux rotational direction. Therefore there exist an 'equivalent inductance' and an 'equivalent resistance' satisfying equation (6-8) according to the equation (6-6).

$$\lim_{T\to 0} V_{av}(t_k) = \upsilon = L_{eq}(\theta_r)\frac{d\, i_{dc}(t_k)}{d\,t} + i_{dc}(t_k)\left(R + \omega_r \frac{d\, L_{eq}(\theta_r)}{d\,\theta_r}\right) \qquad (6\text{-}8)$$

where $L_{eq}(\theta_r)$ is the 'equivalent inductance' of a single coil which represents all simultaneously excited coils in the motor when the rotor is in a position θ_r , ω_r is the angular frequency of the rotor, and υ is the corresponding instantaneous total phase voltage. Thus the equation (6-8) can be rewritten as

$$\frac{d\, i_{dc}(t)}{d\,t} = [\upsilon - i_{dc}(t)\,\omega_r \frac{d\, L_{eq}(\theta_r)}{d\,\theta_r}] / L_{eq}(\theta_r) \qquad (6\text{-}9)$$

Therefore, to control the summation of all of the phase currents in order to track the reference current, sliding mode must be satisfied, i.e. $\lim_{\wp\to 0} \wp \frac{d\,\wp}{d\,t} < 0$. In this case one can select the following switching function in the phase plane.

$$\wp = i_{dc}(t) - I_c(t) \qquad (6\text{-}10)$$

where $I_c(t)$ is the reference current at the time instance t. To reduce current hattering, a soft sliding mode control law can be designed as follows:

$$\upsilon = +V_{dc} \quad \text{if } \wp \le -\epsilon \text{ and } \frac{d\wp}{d\,t} \le -\eta$$

$$\upsilon = -V_{dc} \quad \text{if } \wp \ge \epsilon \text{ and } \frac{d\wp}{d\,t} \ge \eta$$

$$\upsilon = -V_{dc}[k_p \wp + k_i \int \wp dt] \quad \text{if } -\epsilon \le \wp \le +\epsilon \qquad (6\text{-}11)$$

where η and ϵ are positive real constants which are used to determine the tolerable range of the equivalent d.c. link current, sliding along command reference current function, k_p and k_i are the proportional and integral constants, respectively.

To track the d.c. link current, the control law in the equation (6-11) needs to generate the appropriate T_{on} and T_{off} time signals in each independent phase winding to achieve control of d.c. link current, resulting in the appropriate total average phase voltage, as described by equation (6-6). This is not difficult to implement. It just needs a high frequency PWM current modulator based on the equation (6-7) to modulate the total sum of all phase currents, which is described in section 6-4. In the limit situation, i.e. exactly sliding along the switching function, the equivalent voltage can be found by taking the limit of the total average phase voltage $V_{av}(t_k)$ given by the equation (6-6) and (6-8). The equivalent voltage, obtained by substituting (10) into $d\wp/dt = 0$, is

$$\upsilon_{eq} = I_c(t)\omega_r \frac{d L_{eq}(\theta_r)}{d\theta_r} \tag{6-12}$$

$$|\upsilon_{eq}| < |V_{dc}| \tag{6-13}$$

Define a saturation function as follows

$$\begin{aligned} \text{sat}(\wp) &= -V_{dc} I_c(t)[k_p \wp + k_i \int \wp dt] \quad \text{if} \quad -\epsilon \le \wp \le +\epsilon \\ \text{sat}(\wp) &= -V_{dc} I_c(t) \,\text{sgn}(\wp) \quad \text{if} \quad |\wp| \ge \epsilon \end{aligned} \tag{6-14}$$

Therefore, in sliding condition, by equation (6-10) and (6-12), the equivalent total phase power becomes

$$P_{eq}(t) = I_c^2(t)\left(\omega_r \frac{d L_{eq}(\theta_r)}{d\theta_r}\right) = V_{dc} I_c(t) \tag{6-15}$$

but if the system is not in a sliding condition, then

$$P_{eq}(t) = V_{dc} I_c(t)[1 + \text{sat}(\wp)] \tag{6-16}$$

If both sides of the equation (6-15) are divided by angular speed ω_r, the average electromagnetic torque over the switching period T is then

$$\tau = (V_{dc} / \omega_r) I_c(t) \tag{6-17}$$

If $I_c(t) = K_t (\omega_r / V_{dc}) i_t(t)$, then electromagnetic torque can be further simplified to be

$$\tau = K_t \, i_t(t) \tag{6-18}$$

where K_t is a proportional torque constant and $i_t(t)$ is the equivalent d.c. link current providing electromagnetic torque.

B. Sliding mode speed control with feedforward and integral compensation [33],[49-52]

The electromagnetic dynamic model of a switched reluctance motor and loads can be expressed as follows :

$$\tau = J \frac{d\omega_r}{dt} + B_f \omega_r + \tau_l \tag{6-19}$$

where J is the inertia constant of the rotor and the load on the shaft, B_f is the viscous friction coefficient and τ_l is the load torque.

From equations (6-18) and (6-19), equ. (6-20) can be obtained

$$\frac{d\omega_r}{dt} = [K_t \, i_t(t) - \tau_l - B_f \omega_r] / J \tag{6-20}$$

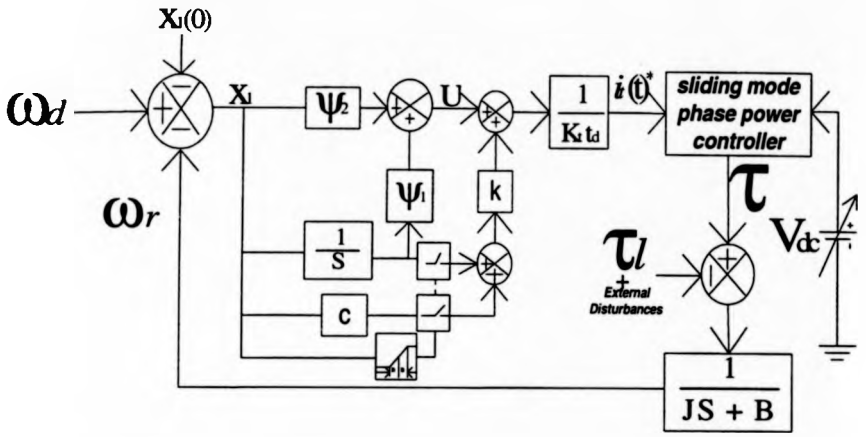

Fig. 6-3(a). Sliding mode speed and total phase power control with integral compensation.

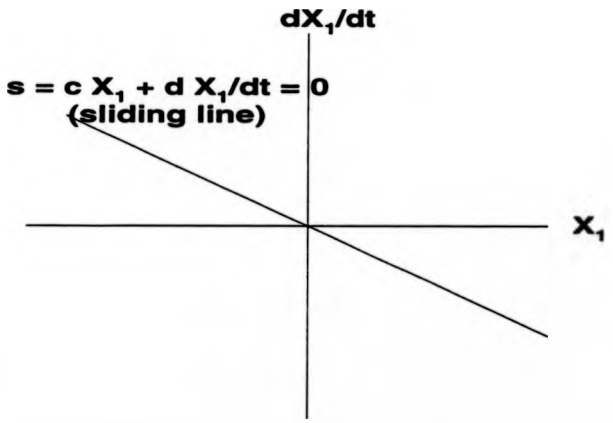

Fig.6-3(b). Sliding line and phase plane diagram.

Speed control can be implemented by a sliding mode variable structure controller but a discontinuous torque control signal would cause chattering of the speed response. In order to enable smooth torque control and reduce the chattering problem , i_1(t) must be smoothed according to equ. (6-18). An integrator can be inserted into

the feedforward path to achieve this requirement, as shown in Fig. 6-3(a). The phase variable state representation of Fig. 6-3(b) can be used to develop the required control scheme. It can be simplified as

$$\begin{bmatrix} \dot{x}_1 \\ \dot{x}_2 \end{bmatrix} = \begin{bmatrix} 0 & -1 \\ 0 & -a \end{bmatrix} \begin{bmatrix} x_1 \\ x_2 \end{bmatrix} + \begin{bmatrix} 0 \\ b \end{bmatrix} U \qquad (6\text{-}21)$$

where $x_1 = (\omega_d - \omega_r)$, ω_d is the demand rotor speed.; $x_2 = \dfrac{d\,\omega_r}{d\,t}$; $a = B_f/J$; $b = 1/(J\,t_d)$, t_d is a time delay constant ; ' $\bullet$ ' is a differential operator. U is a control signal which is used to control the speed error dynamics irrespective of the drive system parameter (a, b) variations. The sliding line in the phase plane diagram [Fig. 6-3(b)] can be described as follows:

$$S = c\,x_1 + \dot{x}_1 = 0 \qquad (6\text{-}22)$$

where, c is a time constant, which denotes the slope of the sliding line.

To satisfy the existence condition of sliding mode speed controller, the following must be satisfied

$$\lim_{s \to 0} s \frac{d\,S}{d\,t} \leq 0 \qquad (6\text{-}23)$$

The controller can be designed as follows:

$$U = \psi_1 x_1 + \psi_2 \dot{x}_1 \qquad (6\text{-}24)$$

where $\psi_1 = \begin{cases} \alpha_1 & \text{if } S\,x_1 > 0 \\ \beta_1 & \text{if } S\,x_1 < 0 \end{cases}$; $\psi_2 = \begin{cases} \alpha_2 & \text{if } S\,\dot{x}_1 > 0 \\ \beta_2 & \text{if } S\,\dot{x}_1 < 0 \end{cases}$

ψ_1 and ψ_2 are proportional and derivative gain constants, respectively. α_1, α_2, β_1, and β_2 are real constants. From the equations (6-23) and (6-24), the following existence condition must be satisfied

$$\begin{aligned} \beta_2 &< \min_{a,b} \left|\frac{c-a}{b}\right| \\ \textit{and} \quad & \max_{a,b} < \alpha_2 \\ \textit{and} \quad & \beta_1 < 0 < \alpha_1 \end{aligned} \tag{6-25}$$

Equations (6-24) and (6-25) are only suitable for a general sliding mode speed system. When higher loads or disturbances are applied to the drive system, the robustness is problematic. To improve speed robustness and accuracy, variable structure model following control scheme with feedforward of the sliding line is employed. In this controller, another proportional term, k S, when added to equ.(6-24) to roughly cancel large load disturbances or the command instant variation until the speed error approaches the boundary layer. When the speed error is within an allowable boundary layer, the conventional sliding mode control becomes dominant. In this case, the control signal is U rather than U plus k S, as shown in Fig. 6-3(a). Therefore the modified control signal with feedfoward of the sliding line becomes

$$U_m = \begin{cases} \psi_1 x_1 + \psi_2 \dot{x}_1 + k S & \text{if } |x_1| \geq B \\ \psi_1 x_1 + \psi_2 \dot{x}_1 & \text{if } |x_1| \leq B \end{cases} \tag{6-26}$$

where B is the allowable error bound of x_1 .

Since the linear control term k S is introduced into the controller, if there is a steady state speed error caused by external load disturbances or command speed variation, the controller will provide a proportional torque to force the real speed to move towards the command speed. Once the real speed approaches the command speed, the

speed error becomes smaller and the kS gain becomes smaller or its function even disappears. In this case, U_m will become U such that the controller becomes equivalent to a PI one. In such a case the real speed will virtually slide along the command speed. As a result, the proposed function, U_m, offers a better robustness compensation over the conventional sliding mode speed controller. From equations (6-18) and (6-26), the command current in the d.c. link is given by

$$i_t(t)^* = (1/K_t\, t_d)\,[\int U\,dt + k\int S\,dt\,]$$

$$= \begin{cases} (k/K_t\, t_d)\,[c\int x_1\,dt + x_1(t) - x_1(0)] & \text{if } |x_1| \geq B \\ (1/K_t\, t_d)\,\{\psi_1 \int x_1\,dt + \psi_2\,[x_1(t) - x_1(0)]\} & \text{if } |x_1| \leq B \end{cases} \qquad (6\text{-}27)$$

where $i_t(t)^*$ is command current in d.c. link, as shown in Fig.6-3(a).

6-4 IMPLEMENTATION OF THE CONTROLLER

The drive system consists of two main controllers; the speed controller and the total phase power controller. In the speed controller, it would be expected that an acceleration estimator is required [49] since the implementation of a robust speed controller needs acceleration information to judge if the sliding mode condition is satisfied and to determine whether to use U or U_m as the control signal. However, implementation of equation (6-27), an error bound detector, allows the controller to be simplified to a sliding mode PI controller plus another feedforward gain regulator, thus removing the needs for an acceleration estimator. By incorporating an analog multiplier AD 633 JN, command speed can be compared with the real speed, and the

resultant error signal passed a low pass filter to filter high frequency noise and any discontinuous chattering signals. If the speed error is larger than error bound B, then the output from another speed error integrator with gain c is added before the combined signal is multiplied by a programmable gain k according to equ. (6-27) (implemented in DAC 08 and 87c51) to get the d.c. link current signal. Conversely, if after filtering, the speed error is smaller than B, then it is amplified an integral gain ψ_1 and is summed with a further speed error signal with proportional gain ψ_2, as described in equation (6-27), to get the required current signal in the d.c. link.

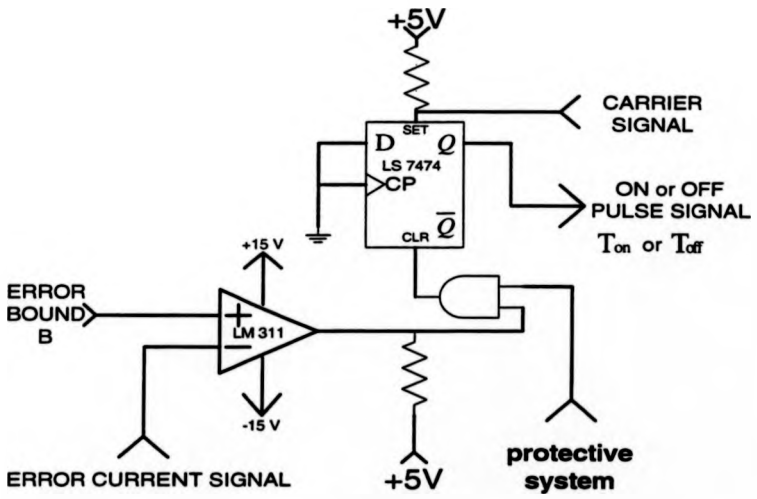

Fig. 6-4. Digital pulse width modulator for the sliding mode power controller.

In the inner loop, the control of sliding mode total phase power can be achieved by one current sensor HTP 100s, a comparator LM 311, a D-type flip-flop (74LS74) and a microcomputer (8751) as shown in Fig. 6-4. Timer T0 in 8751 generates the clock signal for the flip-flop (frequency is programmed to be approximately 20 kHz) and is

synchronously locked to the rotor position sensor. Measurement of d.c. link current to achieve sliding mode control of total phase power would be extremely problematic since the current in the d.c. link includes significant harmonic components which would reduce the quality of the controller. An acceptable alternative, to get a clear and continuous current signal without using indirect electronic filter, is to measure the sum of all instantaneous phase currents. Therefore, the real current signal $i_{dc}(t)$ in Fig. 6-1 is replaced by the current signal $i_{slm}(t)$. The power and hence torque controller is therefore controlling all phases simultaneously and thus removing the need for a current sensor for each phase. The command current is subtracted from the real current $i_{slm}(t)$ and the resultant error current is sent to an integrator (low pass filter) to smooth the error current and to reduce current ripple, and then it is compared (LM 311 comparator) with the reference error value, representing an allowable error current range. If the error current is larger than allowable band ϵ, then the rated or maximum d.c. link current signal (FFh) is used and the appropriate switches in the power converter are turned on. If the error current is smaller than ϵ, then the error current is amplified by a PI amplifier according to equation (6-14) and (6-16) to modulate the four IGBT modules in the power converter. Thus the approximate sliding mode total phase power can be obtained by multiplying the command d.c. current with a factor equivalent to the d.c. voltage level. This controller, whilst a digital pulse width modulator plays a very important role, it is very simple, as shown in Fig. 6-4. The circuit can be used to modulate real current or error current signal. The current ripple can also be controlled by simply programming the PWM switching frequency. If the error current signal is considered as a modulated signal, then it is compared with the command error bound ϵ by the comparator LM 311. The resultant output digital

signal is connected to the "CLR" of a flip-flop (74LS74). There is the option to introduce a further over-current protection signal on the "CLR" signal. Another input (set) of the flip-flop is connected to the output of a carrier generator. The resultant signal maintains at "HI" for T_{on} while it goes "LOW" for T_{off} ($T-T_{on}$) during each switching cycle depending on the real error current signal. Since the frequency of the carrier can be re-programmed in real time, approximately real time current controller can be achieved by this digital modulator. It also makes the sliding mode power controller very simple to implement.

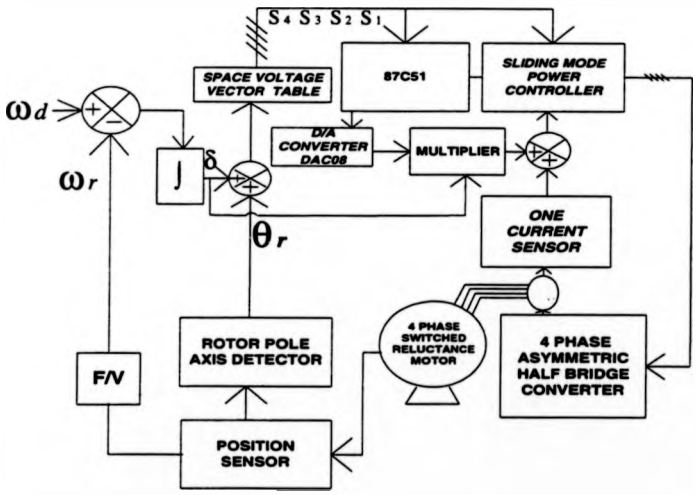

Fig. 6-5. Robust speed control of a 4 phase switched reluctance vector drive.

The complete block diagram of the drive system with the proposed controller is as shown in Fig. 6-5. The command rotor speed is compared with real rotor speed (using an analogue multiplier AD 633 JN) to get the control signal of sliding mode speed controller, the input to the sliding mode input power controller. In the sliding mode

power controller, the input signal is the command power and is converted to a current demand by a scalar factor representing the d.c. link voltage. From the position sensor the position code of the rotor pole axis is detected. This position code can be shifted (advanced) by an angle δ from the rotor pole position according to the phase angle δ, i.e. the integral of the difference between command rotor speed and real rotor speed. Using δ, the 87c51 can select suitable voltage vectors from space voltage switching table stored in the internal memory. This enables the appropriate switches in the power converter to provide the required torque as determined by the pulse width modulation scheme described above.

6-5 EXPERIMENTAL RESULTS

A 4 phase asymmetric half bridge converter (as in Fig. 6-1) was constructed for a 4kW 4 phase switched reluctance motor. In experiments, the load was a 7 kW, separately excited, d.c. generator. The system was installed with a torque and a speed transducer. The input d.c. voltage to the power converter was adjustable, up to a maximum value of + 225 V and the maximum peak phase current was limited at 60 A to protect the drive system. Fig. 6-6 (a and b) show the steady state response waveforms of the sliding mode d.c. link power controller. Fig. 6-6(a) shows the result obtained when the drive was operated at 500 r/min, producing an average torque output of 25 Nm. It can be seen that ideal sliding mode could not be achieved because the model was implemented by the 87c51 program with a finite switching frequency. The small amount of chattering was acceptable, particularly as it had minimal effect

on the torque or speed ripple and since the switching frequency was in ultrasonic range it does not contribute to acoustic noise. The phase current approximates to a half sinusoidal waveform and the ripple on the shaft torque corresponds to the phase excitation frequency. The shaft torque ripple was not insignificant and was caused by a combination of the high inertia of the load and the use of an input voltage of only 150 V. The torque ripple could be improved at higher powers and input voltages. Fig. 6-6(b) presents the steady state response of the drive operated at 1550 r/min. The speed ripple was negligible and the torque ripple was acceptable. It should be particularly noted that the ability of this controller to maintain low levels of torque ripple at higher speeds was particularly useful since this is where previous controllers have been limited.

Figure 6-7 shows a typical step speed response curve obtained using the sliding mode speed controller and the sliding mode input power controller. The high inertia of the load (approximately 1 kg m^2) required a shaft torque of nearly 90 Nm to accelerate the rotor from 200 r/min to 1980 r/min (the command speed) within 3 seconds. This rapid response was obtained by setting the gain (KS) to the largest possible value (FF_h) while the speed error was larger than 10 % but only 'PI-like' U gain was used when the error comes within 10 %. In this experiment, the load was unknown as the acceleration takes place and the response of the controller was in no way dependent on a pre-defined load model. The speed tracking was satisfactory and the torque ripple was low. Fig. 6-8 shows the effect of a change in load torque on the speed holding capability of the drive, with results shown for command speeds 178 r/min, 1000 r/min and 2500 r/min, and 1500 r/min, respectively. These results demonstrate the robustness of the drive under unpredicted load conditions. In Fig.6-

8(a) the drive was running at the command speed of 178 r/min when a load torque of approximately 35 Nm was applied by increasing the field current to the d.c. generator. The resulting deviation from the command speed was only 2.5 %. From Fig. 6-8(b) the speed was seen to dip by only 1.5 % from the command speed of 1000 r/min when the shaft torque was increased from no-load to 20 Nm. At 2500 r/min (Fig. 6-8(c)) a more substantial reduction in speed (about 5 %) is observed with a smaller load perturbation. This is expected in that this is well beyond the design speed of the phase windings such that the drive is very significantly voltage limited, thus reducing the electromagnetic torque available at the shaft to compensate for load disturbances. However, the final plot, Fig. 6-8(d), was obtained at the rated speed of the drive and with an increased d.c. link voltage of 225 V. In this case the speed error was reduced to approximately 1 %, despite a load disturbance of 45 Nm. This corresponds to 1.8 times the rated torque of the motor and was a very satisfactory result.

Virtually no speed chattering was seen in the experimental results. This should be attributed to the integral compensation action. The modified sliding mode speed controller, use a high gain saturation action KS plus U when the error was larger than 10 % but employed a proportional and integral gain U when the error was smaller than 10 %. The drive system was therefore forced to move towards and to approximately slide along the command reference speed switching surface. The higher the load or disturbance was the more power was applied to the system to accomplish the sliding condition.

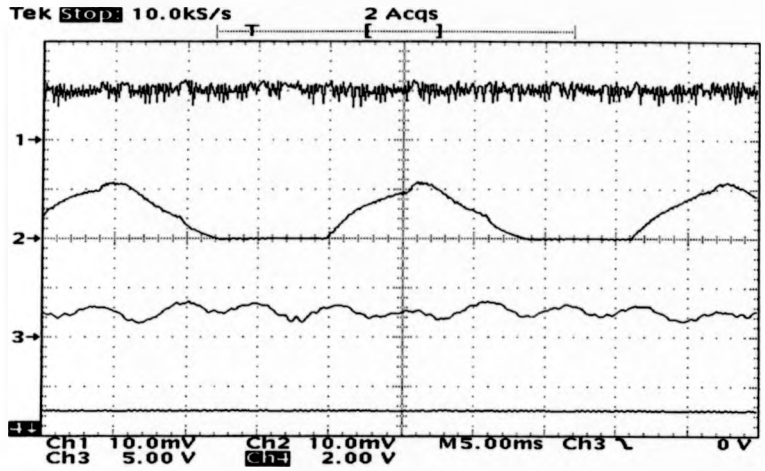

(a)

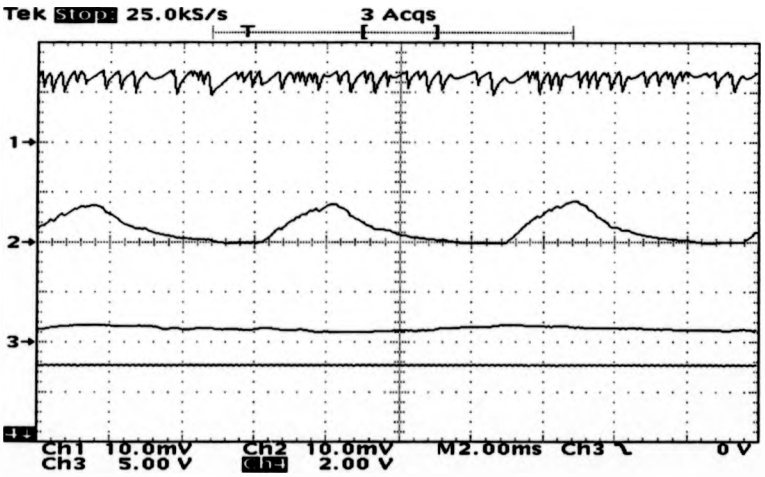

(b)

Fig. 6-6. Steady state response of d.c. link current, phase current, shaft torque, and rotor speed. (a) is operated at 500 r/min. Time: 5.00 ms/div. (b) is operated at 1550r/min. Time: 2.00 ms/div. Ch1 : d.c. link current, 10A/div; Ch2: phase-1 current, 20 A/div; Ch3: shaft torque, 50 Nm/div. Ch4: Shaft speed, 1000 r/min/div.

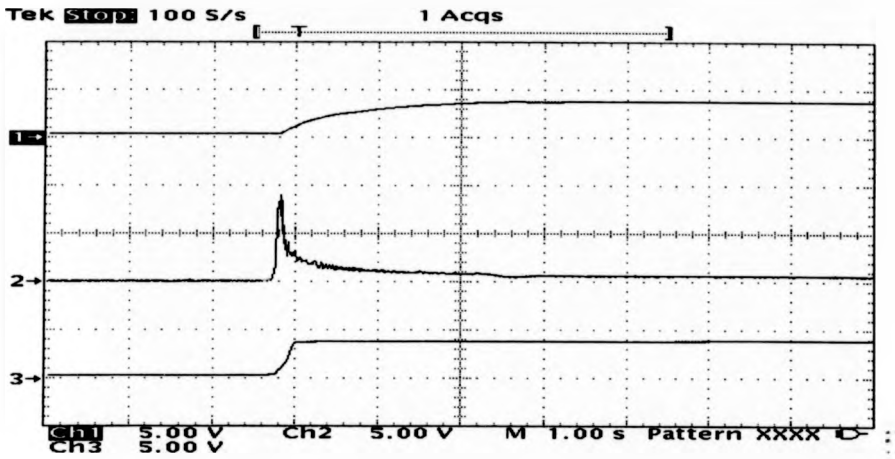

Fig. 6-7. Step speed response of a 4 phase switched reluctance vector drive under sliding mode speed controller.

Ch1: Rotor speed, 2500 r/min/div; Ch2: Shaft torque, 50 Nm/div; Ch3: command speed (1980/min), 2500 r/min/div. Time: 1.00 s/div.

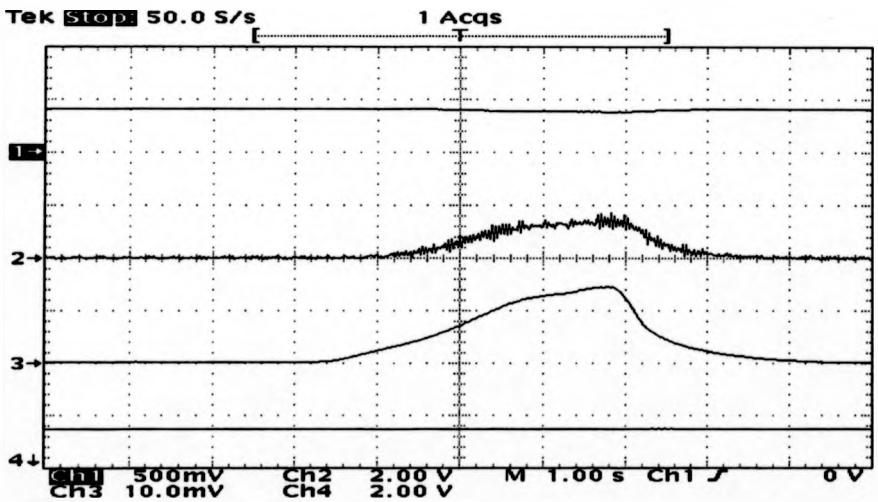

Fig. 6-8(a). Speed response operated under uncertain loads using a sliding mode speed controller. Command speed is 200 r/min.

Ch1: Rotor speed, 250 r/min/div; Ch2: Shaft torque, 50 Nm/div; Ch3: d.c. field excited current of a D.C. generator, 2A/div; Ch4: input d.c. voltage, 200 V/div. Time: 1.00 s/div.

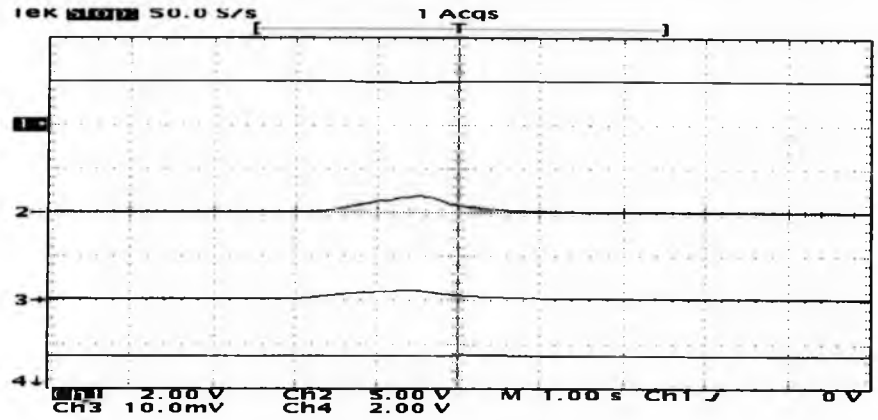

Fig.6-8(b). Speed response operated under uncertain loads using a sliding mode speed controller. Command speed is 1000 r/min.

Ch1: Rotor speed, 1000 r/min/div; Ch2: Shaft torque, 50 Nm/div; Ch3: d.c. field excited current of a D.C. generator, 5A/div. Ch4: input d.c. voltage, 200 V/div. Time: 1.00 s/div.

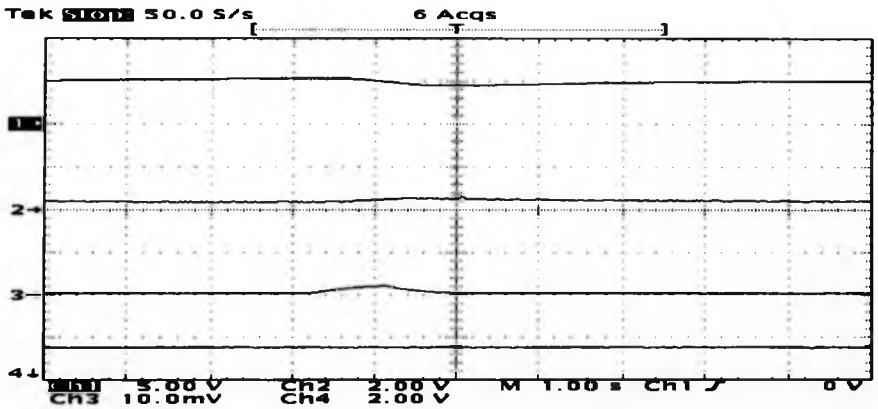

Fig. 6-8(c). Speed response operated under uncertain loads (a) using a sliding mode speed controller. Command speed is 2500 r/min.

Ch1: Rotor speed, 2500 r/min/div; Ch2: Shaft torque, 20 Nm/div; Ch3: d.c. field excited current of a D.C. generator, 5A/div. Ch4: input d.c. voltage, 200 V/div. Time: 1.00 s/div.

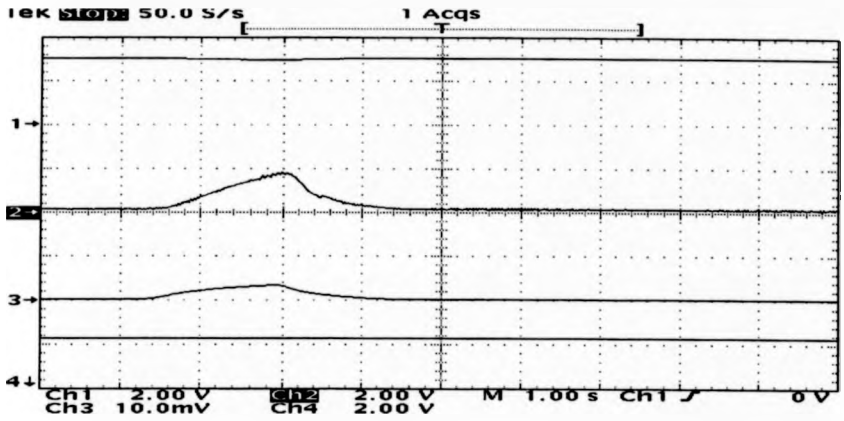

Fig.6-8(d). Speed response operated under uncertain loads using a sliding mode speed controller. Command speed is 1500 r/min.
Ch1: Rotor speed, 1000 r/min/div; Ch2: Shaft torque, 50 Nm/div; Ch3: d.c. field excited current of a D.C. generator, 5A/div; Ch4: input d.c. voltage, 200 V/div. Time: 1.00 s/div.

6-6 SPLIT-LINK CONVERTER BASED VARIABLE STRUCTURE SPACE VECTOR CONTROLLED SWITCHED RELUCTANCE FLUX VECTOR SERVO DRIVE

As described in previous section, variable structure space vector controlled switched reluctance drive has a very robust speed performance. Little speed variation on applications of large load disturbances is one of most important performance properties for a servo drive. Another more important performance property is a fast response. In the following section, split-link power converter replaced the existing power converter so that energy can be regenerated and bi-direction speed response could be significantly increased.

As described in chapter 5, split-link power converter can be used in the high-performance switched reluctance flux vector drive because total phase power can be controlled by the sliding mode d.c. link power controller and the phase shifting of space voltage vectors. However, to achieve speed servo performance, sliding mode speed controller with integral compensation and sliding slope feedforward must be added into the drive system.

6-6-1 Sliding Mode Speed Control With Feedforward and Integral Compensation [45-52]

Substituting (6-22) into (6-6), the motion dynamics of the motor drive system becomes

$$\frac{d\,\omega_r(t)}{d\,t} + c\,[\omega_r(t) - \omega_r^*(t)] + (\tau'/J_n) = \frac{V_{dc}\,[\,I_c(t) + i_F(t)\,]}{J_n\,\omega_r(t)} \qquad (6\text{-}28)$$

where c and J_n are positive real, denoting the prescribed sliding speed trajectory and nominal inertia constant, $\omega_r^*(t)$ is a demanded speed, τ' is an equivalent torque including all lumped uncertain load and disturbances, and parameter variation effects. $i_F(t)$ is an instantaneous dc link current used to eliminate τ', $I_c(t)$ is designed as follows:

$$I_c(t) = \begin{cases} \dfrac{J_n\,c\,\omega_r(t)\,[\omega_r(t) - \omega_r^*(t)]}{V_{dc}} & \omega_r(t) < \omega_r^*(t) \\ 0 & \omega_r(t) > \omega_r^*(t) \end{cases} \quad \text{and}$$

$$i_F(t) = \begin{cases} I_F(t) & \omega(t) < \omega^*(t) \\ 0 & \omega(t) > \omega^*(t) \end{cases} \qquad (6\text{-}29)$$

where $I_F(t)$ is the steady state dc link current corresponding to the steady state τ_F.

Generally, loads and disturbances have high and low frequency components, which are usually unknown and difficult to measure, so that robust control of speed becomes extremely difficult, especially under high power dynamic loads and disturbances. However, rotor speed is slow dynamic variable and input torque or transient dc link current are fast dynamic variables. This time-scale separation property can simplify system dynamics by singular perturbation analysis. During equilibrium steady state, the solution of (6-23) can be found by letting $J_n \cong 0$ [i.e. in the ideal case without inertia so that no speed variation occurs and no ac component in dc link current]. Thus (6-23) becomes

$$c\,[\omega_r(t) - \omega_r^*(t)] + (\tau'/J_n) = \frac{V_{dc}\,[\,I_c(t) + I_F(t)]}{J_n\,\omega_r(t)} \qquad (6\text{-}30)$$

where $I_F(t)$ is the steady state dc link current corresponding to τ_F.

Equation (6-25) means that if the dc link current includes only a dc component and satisfies equation (6-25), then transient acceleration will disappear and steady state acceleration can be included in τ'. When real speed approaches the demanded speed $\omega_r^*(t)$, the equivalent torque becomes

$$\tau' = \frac{V_{dc}\,I_F(t)}{\omega_r^*(t)} \qquad (6\text{-}31)$$

From (6-31) it can be seen that when real speed is as same as the demanded speed the steady state equivalent torque can be measured by the sliding mode feedforward dc link power and demanded speed. This simplifies the complexity of the system such that even there exist unknown loads, time-varying parameters variation or external disturbances the equivalent load torque can still be found by the steady state dc link current under a fixed dc link voltage. Thus (6-31) becomes a powerful steady state load torque observer.

From (6-28), (6-29) and (6-31), the following equation can be obtained.

$$\frac{d\,\omega_r(t)}{d\,t} = [-\frac{V_{dc}\,I_F(t)}{\omega_r^*(t)} + \frac{V_{dc}\,i_F(t)}{\omega_r(t)}]/J_n \qquad (6\text{-}32)$$

Now a switching surface is selected as follows:

$$S = c\,[\omega_r(t) - \omega_r^*(t)] + \frac{d\,\omega_r(t)}{d\,t} \qquad (6\text{-}33)$$

Define $x_1 = [\omega_r(t) - \omega_r^*(t)]$ and $x_2 = \frac{d\,\omega_r}{d\,t}$, then a sliding line equation S = 0 can prescribe the sliding trajectory of speed in phase plane, which is determined by c, as shown in Fig. 4(b).

Substituting(6-28) and (6-32) into (6-33) and taking $i_F(t) = I_F(t)$, the sliding line equation becomes

$$S = \begin{cases} -\frac{V_{dc}\,I_F(t)}{J_n\,\omega_r^*(t)} + \frac{V_{dc}}{J_n\,\omega_r(t)}\,[\,I_c(t) + I_F(t)\,] & \omega_r(t) < \omega_r^*(t) \\ -\frac{V_{dc}\,I_F(t)}{J_n\,\omega_r^*(t)} & \omega_r(t) > \omega_r^*(t) \end{cases} \qquad (6\text{-}34)$$

From (6-34) the following equation can be found

$$d\,S/\,dt = \begin{cases} -\frac{V_{dc}^{\,2}\,[\,I_c + I_F(t)][\omega_r^*(t) - \omega_r(t)]}{J_n\,\omega_r^{\,2}(t)\,\omega_r(t)\,\omega_r^*(t)} & \omega_r(t) < \omega_r^*(t) \\ 0 & \omega_r(t) > \omega_r^*(t) \end{cases} \qquad (6\text{-}35)$$

Substituting (6-33) and (6-34) into S dS/dt , the equation (6-31) holds.

$$S\,dS/dt \le 0 \qquad (6\text{-}36)$$

From (6-31), the speed controller given by (6-24) [or (6-29)] is shown to be stable and the sliding mode holds.

To reduce the hitting time from reaching mode to sliding mode, the equivalent torque in (6-26) can be added into drive system based on singular perturbation theory. From (6-24) - (6-26), and (6-29), a composite torque can be designed as follows:

$$\tau = \begin{cases} -\dfrac{V_{dc}\, I_F(t)}{J_n\, \omega_r^*(t)} + \dfrac{V_{dc}}{J_n\, \omega_r(t)} \left[I_c(t) + I_F(t) \right] & \omega_r(t) < \omega_r^*(t) \\ -\dfrac{V_{dc}\, I_F(t)}{J_n\, \omega_r^*(t)} & \omega_r(t) > \omega_r^*(t) \end{cases} \tag{6-32}$$

To increase speed robust performance, when speed is lower than demanded value, the feedforward dc link current in (6-32) can be increased by another proportional or integral component according to a allowable boundary value Bw of speed error. If the speed is higher than demanded speed the same torque scheme as shown in (6-32) is valid. Now the additional dc component is designed as follows:

$$\Delta I_F(t) = K\, I_m \qquad \text{if } (\omega_r(t) + B_w) < \omega_r^*(t) \tag{6-33}$$

$$\Delta I_F(t) = k_p \left[\omega_r^*(t) - \omega_r(t) \right] + k_I \int_0^T \left[\omega_r^*(t) - \omega_r(t) \right] dt$$

$$\text{if } 0 < \left[\omega_r^*(t) - \omega_r(t) \right] \le B_w \tag{6-34}$$

where, K, k_p, and k_I are positive real constant. The control scheme is shown in Fig. 4(a).

6-7 IMPLEMENTATION OF THE DRIVE

The implementation of 4-phase split-link converter based variable structure space vector controlled flux vector drive is no different from the drive described in the first part of this chapter. The only difference is the power converter used and the control of the flux linkage. In this section, as described in section 6-3, the implementation of a

robust speed controller does not need acceleration information because the system uses an equivalent load torque observer obtained dc link power and demanded speed. An error bound detector is used in the sliding mode speed controller so that the robust speed control can be achieved simply by optional P or PI type feedforward dc link current components. By incorporating an analog multiplier AD 633 JN, command speed is compared with real speed, the resultant error signal passes through a low pass filter to filter high frequency noise and discontinuous chattering signals. If the speed error is larger than error bound , P type $\Delta I_F(t)$ in (6-34) is added to $I_F(t)$ in (6-33), integral component $\Delta I_F(t)$ is added to $I_F(t)$ to eliminate steady state speed error. The steady state dc link current signal is kept invariant, as shown in (6-32). These signals are multiplied by a programmable gain K (or k_p plus k_I ; implemented in DAC 08 and 87c51) to get the required dc link current signal and torque signal.

In the inner loop, the control of sliding mode total phase power is achieved by one current sensor HTP 100s, a comparator LM 311, a D-type flip-flop (74LS74) and a microcomputer (8751) as shown in Fig. 6-4. The control of the phase currents and current modulation are the same as described for the previous drive.

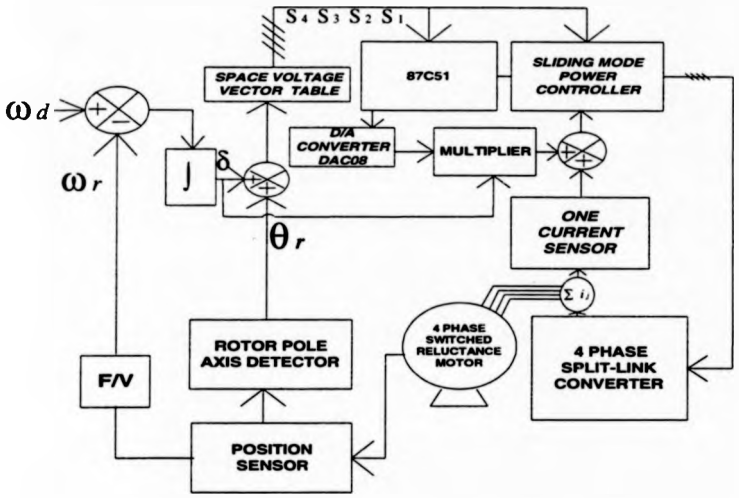

Fig. 6-9. Block diagram of sliding mode 4 phase switched reluctance flux vector drive.

The complete block diagram of the drive system is as shown in Fig. 6-9. The command rotor speed is compared with real rotor speed (using an analogue multiplier AD 633 JN) to get the control signal of sliding mode speed controller, the input to the sliding mode dc link power controller. In the sliding mode power controller, the input signal is the command power and is converted to a current demand by a scalar factor representing d.c. link voltage. From the position sensor the position code of the rotor pole axis is detected. This position code can be shifted (advanced) by an angle α from the rotor pole position according to the integral phase angle δ , i.e. the integral of the difference between command rotor speed and real rotor speed. Using δ, the 87c51 can select suitable voltage vectors from space voltage switching table stored in internal memory. This enables the appropriate switches in the split-link converter to provide the required torque as determined by the pulse width modulation described above.

6-8 EXPERIMENTAL RESULTS

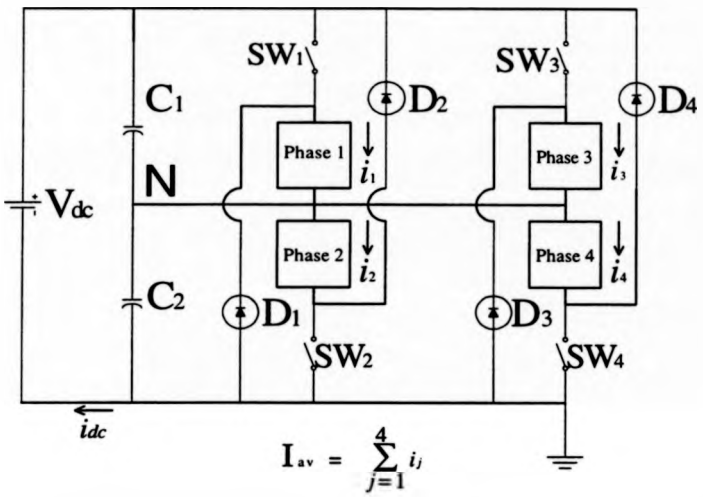

Fig. 6-10. 4 phase split-link converter for a switched reluctance motor.

A 4 phase split-link converter (as in Fig.6-10) was constructed for a 4kW 4 phase switched reluctance motor. In the experiments, the load was a 1kW, separately excited, d.c. generator. The input d.c. voltage to the power converter was adjustable, up to a maximum value of + 300 V and the maximum peak phase current was limited at 25 A to protect the drive system. As described in Chapter 5, the load phase power could be controlled to track the command value. Fig. 6-11(a) is the current and voltage waveform of phase-1 and phase-2 obtained when the motor was unning at 500 r/min. Fig. 6-11(b) is the waveforms of phase-3 and phase-4 obtained when the motor was running at the same operating point. Fig. 6-11(c) shows the waveforms of total sum of all phase currents when running at the same operating conditions. In Fig. 6-11(d), similar waveforms were obtained throughout period of regeneration. In Fig. 6-12, some similar results were obtained, running at 2380 r/min. Figure 6-13 are some

experimental results which demonstrate the control performance of total phase power, running at 500 r/min, 2380 r/min and at the other uncertain speed, respectively, when the motor was braked and then the motor was running from zero speed, 500 r/min, to 2380 r/min during a reverse rotational state. These experimental results show that total sum of all phase currents was an approximate constant no matter whether the speed was low, high or under regenerative conditions.

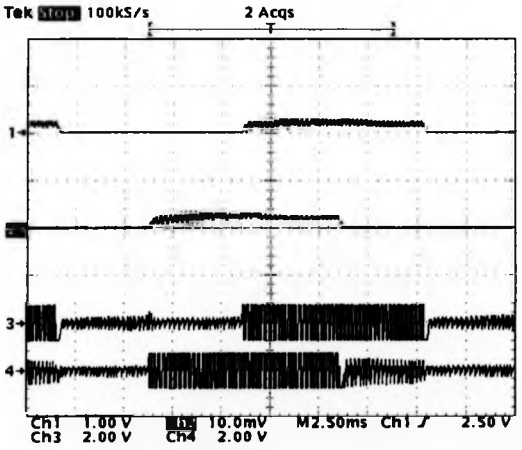

Fig. 6-11(a) Phase current and phase voltage waveforms during motoring state. Ch1: phase-1 current, 10 A/div; Ch2: phase-2 current, 10 A/div; Ch3: Phase-1 voltage, 400 V/div; Ch4: phase-2 voltage, 400 V/div. Time : 2.5 ms/div.

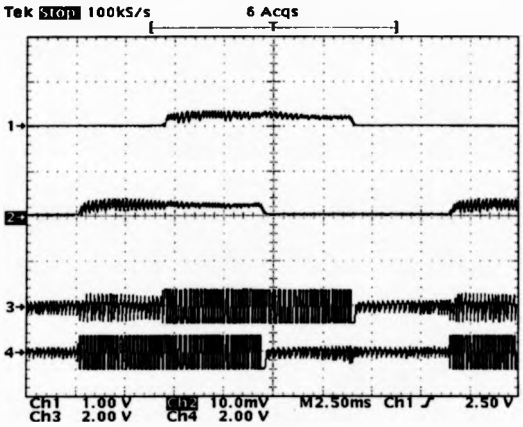

Fig. 6-11(b) Phase current and phase voltage waveforms during motoring state. Ch1: phase-3 current, 10 A/div; Ch2: phase-4 current, 10 A/div; Ch3: Phase-3 voltage, 400 V/div; Ch4: phase-4 voltage, 400 V/div. Time : 2.5ms/div.

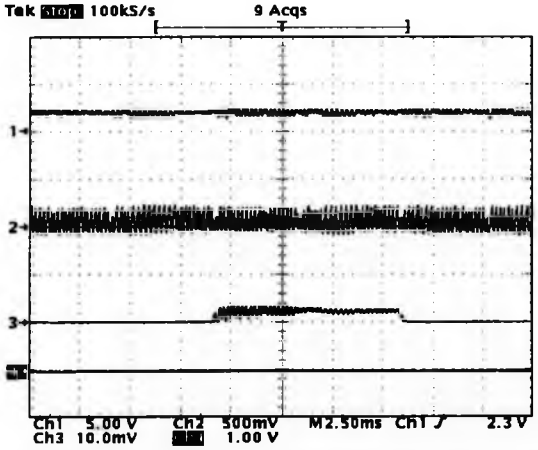

Fig. 6-11(c) Phase current and phase voltage waveforms during motoring state. Ch1: total som of all phase currents,12.5 A/div; Ch2: d.c. link current, 5 A/div; Ch3: phase-1 current, 10 A/div; Ch4: shaft speed, 500 r/min. Time: 2.5 ms/div.

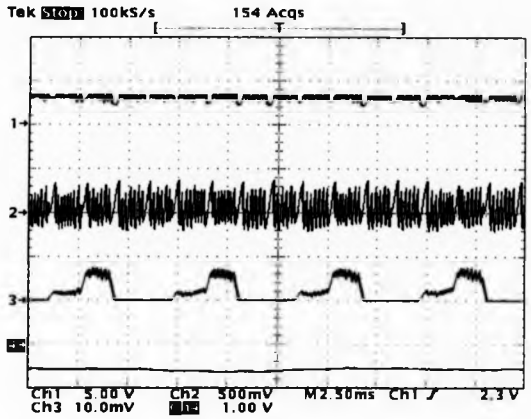

Fig. 6-11(d). Phase current and phase voltage waveforms during regenerative state. Ch1: total som of all phase currents,12.5 A/div; Ch2: d.c. link current, 5 A/div; Ch3:phase-1 current, 10 A/div; Ch4: shaft speed, 500 r/min. Time: 2.5 ms/div.

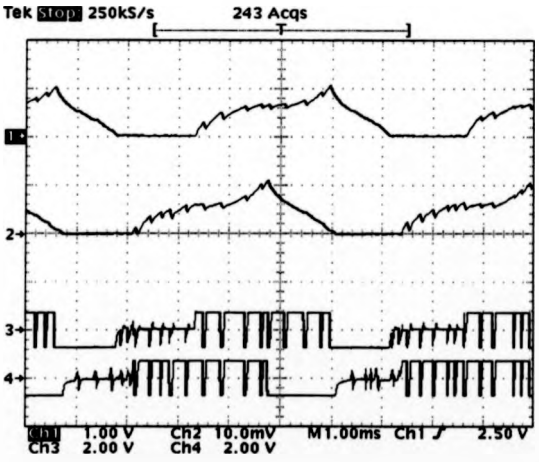

Fig. 6-12(a) Phase current and phase voltage waveforms during motoring state. Ch1: phase-1 current, 10 A/div; Ch2: phase-2 current, 10 A/div; Ch3: Phase-1 voltage, 400 V/div; Ch4: phase-2 voltage, 400 V/div. Time: 1 ms/div.

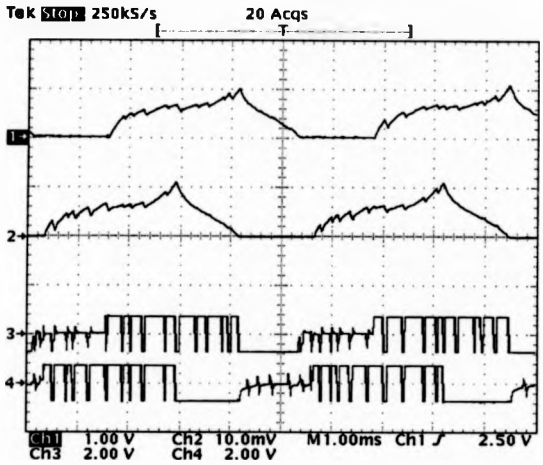

Fig. 6-12(b) Phase current and phase voltage waveforms during motoring state. Ch1: phase-3 current, 10 A/div; Ch2: phase-4 current, 10 A/div; Ch3: Phase-3 voltage, 400 V/div; Ch4: phase-4 voltage, 400 V/div. Time: 1ms/div.

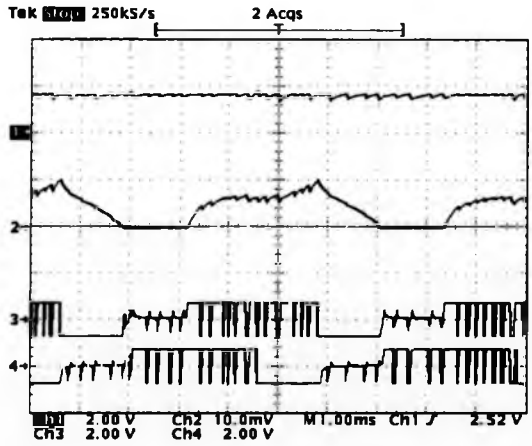

Fig. 6-12(c) Phase current and phase voltage waveforms during motoring state. Ch1: phase-1 current, 10 A/div; Ch2: phase-2 current, 10 A/div; Ch3: Phase-1 voltage, 400 V/div; Ch4: phase-2 voltage, 400 V/div. Time: 1ms/div.

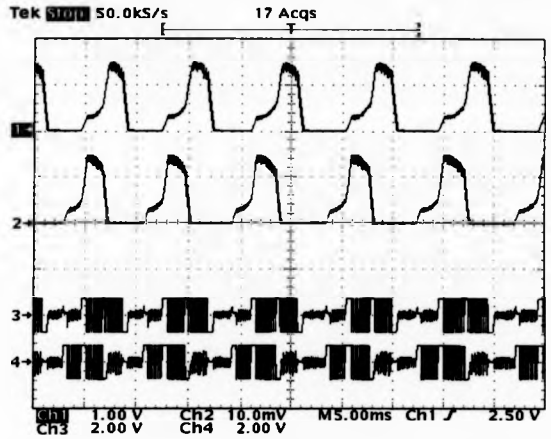

Fig. 6-12(d). Phase current and phase voltage waveforms during regenerative state.Ch1: phase-1 current, 10 A/div; Ch2: phase-2 current, 10 A/div; Ch3: Phase-1 voltage, 400 V/div; Ch4: phase-2 voltage, 400 V/div. Time: 5 ms/div.

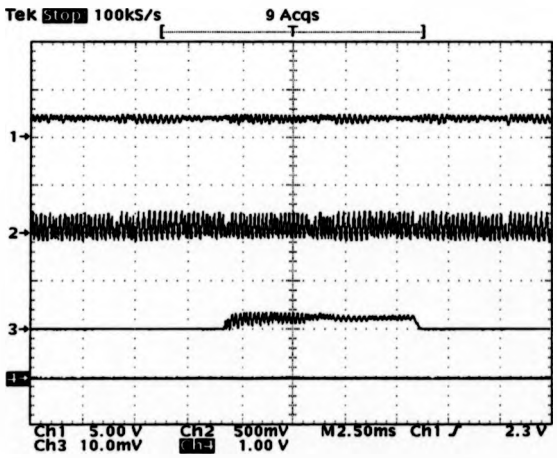

Fig.6-13(a). Current and phase voltage waveforms at 500 r/min. Ch1: total som of all phase currents,12.5 A/div; Ch2: d.c. link current, 5 A/div; Ch3:phase-1 current, 10 A/div; Ch4: shaft speed, 500 r/min. Time: 25 ms/div.

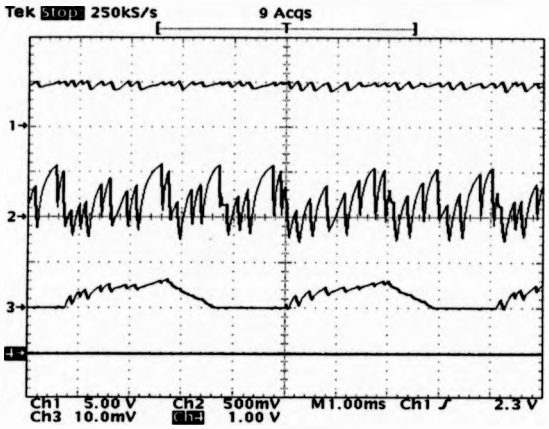

Fig. 6-13(b). Current and phase voltage waveforms at 2380 r/min.Ch1: total sum of all phase currents,12.5 A/div; Ch2: d.c. link current, 5 A/div; Ch3: phase-1 current, 10 A/div; Ch4: shaft speed, 2400 r/min. Time: 1 ms/div.

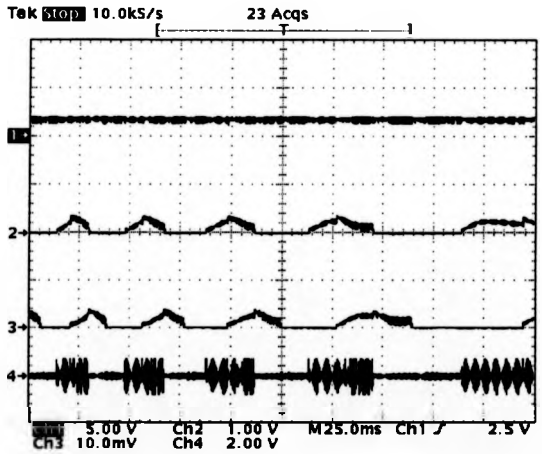

Fig. 6-13(c) Phase current and phase voltage waveforms during the transition from high speed to low speed state. Ch1: total sum of all phase currents,12.5 A/div; Ch2: phase-1 current, 10 A/div; Ch3:phase-2 current, 10 A/div; Ch4: phase-1 voltage 400 V/div. Time: 25 ms/div.

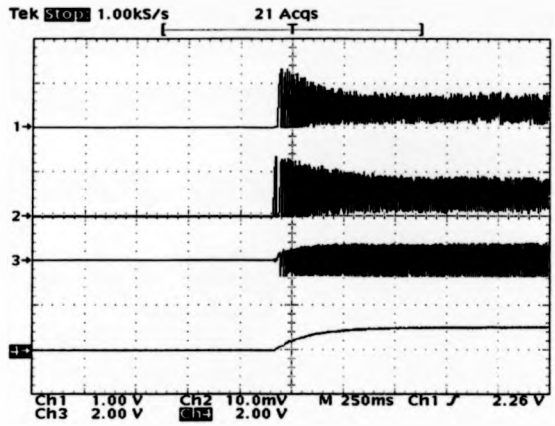

Fig. 6-14. Step shaft speed response from start to command speed (2860 r/min). Ch1: The total sum of all phase currents, 12.5 A/div; Ch2: d.c. link current, 5A/div; Ch3: Phase voltage, 400 V/div; Ch4: shaft speed, 5714 r/min/div. Time: 250 ms/div.

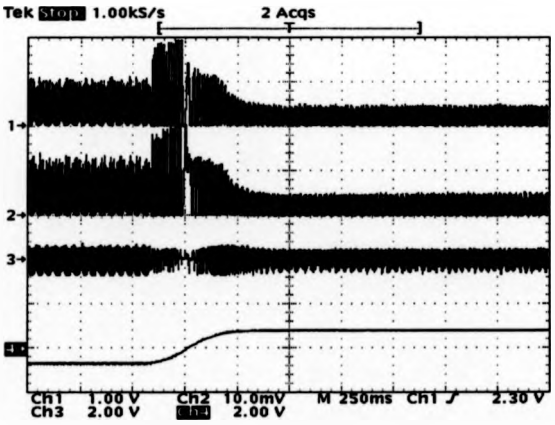

Fig. 6-15. Shaft speed response from reverse rotational state (2060 r/min) to forward rotational state (2285 r/min). Ch1: The total sum of all phase currents, 12.5 A/div; Ch2: d.c. link current, 5A/div; Ch3: Phase voltage, 400 V/div; Ch4: shaft speed, 5714 r/min/div. Time:250 ms/div.

In order to demonstrate the excellent speed servo performance, quicker step speed response and speed tracking experiments were performed and are showned in the Fig. 6-14 and Fig. 6-15. Figure 6-14 shows the result which is operated under 300 V and 4 A d.c. link source current. In this figure, channel one is total sum of four phase currents, channel two represents the waveform of d.c. link current, channel three represents the waveform of phase-1 voltage, and channel four represents the waveform of shaft speed, which tracked the demanded speed (2860 r/min) from start. It can be seen that the step speed response time was around 300 ms under overloading (rated power 500 W). Figure 6-15 is the experimental result which resulted operation is under 300 V and from 2060 r/min (command speed : 2000 r/min; revese rotation) to 2285 r/min (command speed: 2300 r/min; forward rotation). It can be seen that the response time was quick, about 400ms. These results that the drive with space vector and sliding mode speed controller was far away superior to the existing switched reluctance drive and an excellent speed servo perfornce has been achieved.

CHAPTER 7

CONCLUSION

7-1 CONCLUSION

The first commercially available switched reluctance motor was launched by TASC Drives in 1983. Even though the principle of operation of switched reluctance motor was established in the 1830's, it could not be implemented in practice until recently with to the progress of advanced power semiconductor devices. The new generation of power converter, based on IGBTs as power semiconductor switches and a digital application specific integrated circuit (ASIC) has overcome the reliability problem of the drive. Moreover, the computer aided design of the motor has made it possible to reduce the noise produced by the motor. Various applications of switched reluctance drives are under investigation at the moment. Smaller size switched reluctance motors have found applications in factory automation, positioning servos and variable speed drives. In medium and higher sizes, it has found application, such as centrifugal pumps and compressor drives. With its high efficiency throughout the operating range, its simple unipolar converter, the absence of rotor windings, it has considerable potential over inverter fed induction motor. In chapter 2, the basic characteristics and operating principle of the motor have been described. The simulation and experimental investigation of its characteristics and main operation wereinvestigated. The results have the characteristics shown in table 7-1.

Item	Similarities	The differences from other motors
1	The energy conversion theory used by the switched reluctance motor is not different from any other motor	Geometric structure and operating characteristics
2	Constant torque motoring mode operation is used below base speed and constant power operation is used above base speed	Chopping mode is used below base speed and phase advancing is used during high speed. Regenerative mode operation is also different
3	Flux weakening is necessary under high speed	Under high speed and high load the relative phase angle of the current with respect to the rotor pole must be advanced in the switched reluctance motor and single pulse mode can be used but other ac motor uses flux weakening only.
4	The kinetic energy in the motor can be removed during deceleration state	Energy can be returned to the d.c. link source by the power converter during regenerative operation but this is difficult for other a.c. motors

In chapter 3, a synchronous singly-excited control scheme was introduced to the switched reluctance motor control. By this technology, the conventional current chopper can be directly used but the operating phase angle of the excited phase current

must be limited within . This approach investigates the traditional switched reluctance drive to becoming a high performance vector drive; complex coordinate transformation is unnecessary and very simple in the implementation. However, for successful implementation the operating point should be limited below the base speed and only one phase winding should be excited at a time. Similarly, under high speed the phase angle of the phase current still needs to be advanced.

In chapter four, in order to overcome the disadvantage of the drive described in chapter 3, a space vector controlled 5-phase split-link converter is studied for the first time. The successful selection of space vectors achieved the fast acceleration and deceleration of the flux vector and satisfied the demanded total phase power. Under the fixed d.c. voltage this power control is equivalent to a feedforward control of the total phase current. Successful experimental results show that the odd-phase split-link converter can be used in the odd-phase switched reluctance drive system. This result has not previously been reported.

Chapter 5 has further shown the feasibility of the split-link converter in the control of the total phase power. A fast bi-direction speed response exhibits the potential of the split-link converter. In the last of the technical chapters, a robust speed controller- a sliding mode speed controller with d.c. link power feedforward was added to the variable structure space vector controlled split-link converter. Very fast and robust speed response pushes the drive toward becoming a high-performance servo drive. From author's experiments, it can be seen that the conventional variable structure control is not robust enough unless the space vector controller is added to the drivel system. The controller employs space vector modulation and sliding mode d.c. link power and speed controllers with sliding slope feedforward and integral

compensation. Conventional controllers make it difficult for a multiply-excited switched reluctance drive to be controlled with smooth average torque and robust speed performance without off-line characterization of the phase winding inductance profile and the load dynamics. Experimental results in chapter 5 and chapter 6 show that total phase power or equivalent d.c. link power can be used to successfully control a four phase switched reluctance motor drive system to obtain robust speed holding capability even under unknown highly dynamic loads. Experimental results show that space vectors can be selected from a suitable switching table and modulated according to load angle by the sliding mode speed controller. Steady state load torque can be monitored by d.c. link power and the demand speed so that speed response becomes faster and more robust, even under unknown highly dynamic loads. Results have shown that even under high load and disturbance, the speed error can be controlled below 1~3 %. It is expected that more robust speed holding could be achieved if the input d.c. voltage is increased up to 600 volt.

Most significantly, the implementation of this high performance controller needs only an 8 bit microcomputer, a few logic ICs and a single current sensor. There is no requirement for any power or voltage sensors. It can be concluded therefore that modified sliding mode controllers are effective in dealing with the highly nonlinear characteristics of the switched reluctance drive system. In this thesis, the controlled switched reluctance motor has been shown to exhibit excellent performance. This is not because the motor has been specially designed or specially chosen but because the power converter and its robust controller are employed. The conclusion is that any phase switched reluctance motor can become a high-performance servo drive if the drive proposed by the author is used.

7-2 AUTHOR'S CONTRIBUTION TO KNOWLEDGE AND TECHNOLOGY IN VARIABLE SPEED DRIVE

Conventionally, the switched reluctance motor has been considered as just a motor with low performance and low cost. However, it is well known that it is a high efficiency when properly designed and constructed This combined with the advanced control technology developed by the auther, the motor can become an excellent servo drive. In this thesis, the most significant of the author's contributions are the implementation of a high performance servo drive. Such results have not been previously reported in the literature. Other main contributions are listed as follows:

(1) The switched reluctance motor and the power converter used are not in any way limited to the number of phases (m) in the motor, providing the maximum number of which can be simultaneously excited does not exceed m/2.

(2) Approximate sliding mode total phase power can be maintained during each chopping cycle, even during regenerative or during a commutation period.

(3) Without previously knowledge of the characteristics of the motor and the load, a conventional switched reluctance motor can be used in a variable structure space vector controlled servo drive.

(4) Speed response is both fast and robust: maximum bi-direction response time is below 200 ms for 1kW motor and steady-state speed error is below 1 % under the rated load.

(5) Only one current sensor is required in the servo drive system.

(6) An 8-bit microprocessor is enough to implement the complete servo drive.

(7) An 4-bit position sensor is all that is required for the servo system. Potentially the sensor could be reduced to 1 bit.

(8) Split-link converter can be used to drive an odd-phase switched reluctance servo drive.

Item (1),(2),(3) and (8) have not been reported in the literatures for any existing switched reluctance drive. The other items are highly challenging and represent significant advances. Item 4 is particularly note worthy since the drive must be accurately controlled to avoid damage during a speed reversal These facts show that the switched reluctance drive now has great industrial potential and it is not just a low performance drive.

7-3 AREAS OF FURTHER WORK

Although significant progress in the control of switched reluctance drives has been achieved, the torque ripple under the multiple excitation is difficult to eliminate. The problem is attributed to having no profile information of the motor. Under single excitation or sliding mode condition, the thesis provides effective approach to torque ripple. However, for multiple excitation of the phases, the inductance profile with respect to the position and all phase currents are very important pieces of information. Even though the speed servo performance has been achieved, it is still difficult for the torque ripple to be removed. This is very challenging work for the future. Another more difficult topic would be a highly accurate, sensorless, servo drive system, achieving a low speed error. This should be possible because the switched reluctance

motor is basically a synchronous step motor. The used of soft commutation technology in the drive to replace hard chopping, to reduce the switching loss, and increase system efficiency should also investigated. These topics all need future research.

REFERENCES

[1] F. Harashima, H. Hashimoto, and S. Kondo, "Mosfet converter-fed position servo system with sliding mode control," IEEE Trans. Ind. Electron., vol. 32, no. 3, 1985.

[2] C. Namuduri and P.C. Sen, " Servo control system using a self-controlled synchronous motor with sliding mode controller," IEEE Trans. Ind. Applicat., vol. 23, no. 2, pp. 283-295, 1987.

[3] Hasimoto, H.,Yamamoto, H., Yanagisawa,S., and Harashima, F., "Brushless servo motor control using variable structure approach," IEEE Trans. on Industrial Applications,vol. 24, no. 2, pp. 160-170, 1988.

[4] E. Y.Y. Ho. and P.C. Sen, "Control dynamics of speed drive systems using sliding mode controllers with integral compensation," IEEE Trans. Ind. Applicat.,vol. 27, no. 5, pp. 883-892, 1991.

[5] Sabanovic, A., and Bilalovic, F., "Sliding mode control of AC drives," IEEE Trans. on Industrial Applications, vol. 25, pp. 70-75, 1989.

[6] G. S. Buja and M. I. Valla, " Control characteristics of the SRM drives- Part I: Operation in the linear region," IEEE. Trans, Ind.,Electro., vol. 38, no. 5, pp. 313-321, Oct. 1991.

[7] G. S. Buja and M. I. Valla, " Control characteristics of the SRM drives- Part II: Operation in the saturation region," IEEE. Trans, Ind.,Electro., vol. 41, no. 3, pp. 316-325, Oct. 1994.

[8] Akira Chiba,Tadashi Fukao, "An Analysis and An Operating Method of Switched Reluctance Motors Based on a Simple Inductance Representation," IEEE, IAS Annual Meeting pp. 419-426, 1995.

[9] P. P. Acarnley, Stepping Motors: A Guide to Modern Theory and Practice, IEE Control Engineering Series 19, (Peter Peregrinus, 1982)

[10] P. J. Lawrenson, J. M. Stephenson, P. T. Blenkinsop, J. Corda, and N. N. Fulton, "Variable speed switched reluctance motor," in Proc. IEEE, July 1980, pt. B, vol. 127, pp. 253-265.

[11] T. J. E. Miller, Switched reluctance motors and their control. Oxford, England: Clarendon, Oxford University Press, 1993.

[12] P. C. Krause, O. Wasynczuk, Electromechanical Motion Devices, McGraw Hill, 1989, pp. 34-36

[13] W. F. Ray and R. M. Davis, "Inverter drive for doubly salient reluctance motor: Its fundamental behavior, linear analysis and cost implications," Proc. Inst., Elec. Eng., Pt, B, Elec., power Appl., vol. 2, pp. 185-193, 1979.

[14] R. Krishnan, P. Materu, "Design of a single-switch-per-phase converter for switched reluctance motor drives" IEEE. Trans. IE., vol. 37, No. 6, pp. 469-476, Dec. 1990.

[15] J. T. Bass, M. Ehsani, T. J. E. Miller, and R. L. Steigerwald, "Development of a unipolar converter for variable reluctance motor drives," in Proc. IEEE Ind. Sec. Annu. Meeting, 1985, pp. 1062-1068.

[16] W. F. Ray ct., al, "Industrial switched reluctance drives - Concepts and performance," in Proc. Inst. Elec. Eng. Conf on Power Electronics. and Variable Speed Drives, 1984, pp. 357-360.

[17] W. F. Ray, P. J. Lawrenson, R. M. Davis, J. M. Stephenson, N. N. Fulton, and R. J. Blake, "High performance switched reluctance brushless drives," IEEE Trans. Ind. Applicat., vol. 22, no. 4 pp. 722-730, 1986.

[18] T. J. E. Miller, "Converter volt-ampere requirements of the switched reluctance motor drive. Conf. Record, IEEE. -IAS Annual Conference,Chicago, pp. 126-136, March 1981.

[19] M. Ehsani, J.T. Bass. T.J. E. Miller et al. "Davelopment of a unipolar conrerter Ibr variable rcluctance motor drives", IEEE Trans. Ind. Applicat., vol 23, no. 3 pp. 545-553, 1987.

[20] R. M. Davis, W. F. Ray and R. J. Blake, "Inverter drive for switched reluctance motor: circuits and component ratings", IEE Proc., Pt. b., Vol. 128, No. 2, pp. 126-136, March 1981.

[21] R. Krishnan, R. Arumugam and J. F. Lindsay, "Design procedure for switched reluctance motors", Conf. Record, IEEE-IAS Annual Meeting, Colorado, pp. 858-863, Oct. 1986.

[22] Pollock, B.W. Williams," A unipolar converter for a switched reluctance motor", Trans. IEEE. Ind. Appl. Soc., Vol. IA-26, No. 2, March 1990, pp. 222-228.

[23] Pollock and B.W. Williams, "Power converter circuits for the switched reluctance motor with the minimum number of switches", IEE Proc., Vol 137, Part B, No. 6, November 1990, pp. 373-384.

[24] R. Krishnan, P. Materu, " Analysis and design of a low-cost converter for switched reluctance motor drives" IEEE. Trans. IA-29, No. 2, pp. 320-326. Mar./Apr. 1993.

[25] J. Corda and J, M. Stephenson, "Analytical estimation of the minimum and maximum inductances of a double-salient motor", Proc. of Int. Conf. on Stepping Motors and Systems, Leeds, pp. 50-59, Sept. 1979.

[26] M. Ilic-Spong, T. J. E. Miller, S. R. MacMinn and J. S. Thorp, "Instantaneous torque control of electric motor drives," IEEE Trans. Power Electronics, vol. PE-2, no. 1, pp. 55-61, 1987.

[27] M. Ilic-Spong, R. Marino, S. Peresada and D. G. Taylor, "Feedback linearizing control of switched reluctance motors," IEEE Trans. Automat. Contr., vol. AC-32, no. 5, pp. 371-379,1987.

[28] R. S. Wallace and D. G. Taylor, "Balanced commutator for switched reluctance motors to reduce torque ripple," IEEE Trans. Power Electronics, vol. 7, no. 4, pp. 617-626, Oct. 1992.

[29] N. Matsui, N. Akao, and T. Wakino, "High-precision torque control of reluctance motors," IEEE Trans. Industry Applications, vol. 27, no. 5, pp. 902-907. Sept. 1991.

[30] T. H. Liu, Y. J. Chen, and M. T. Lin, "High Performance Field-Oriented Control For A Switched Reluctance Motor Drive ," IEEE. Power Electronics Specialist Conf. 95, pp. 180-185.

[31] A. M. Michaelides and C. Pollock, "Short Flux loops optimise the efficiency of a 5-phase switched reluctance motor" Conf. Proc. of IEEE IAS Annual Meeting, Oct. 1995, pp. 286-293.

[32] V. I. U.tkin, Sliding-mode and Their Application in Variable Structure System. Moscow: Mir Publishers, 1978.G. S.

[33] Buja, R. Menis, and M. I. Valla, "Variable structure control of an SRM drive" IEEE. Trans, IE-40, no. 1, pp. 56-63, Feb. 1993.

[34] R. Krishnan, J. F. Lindsay, and V. R. Stefannovic, "Design of angle-controlled current source inverter-fed induction motor drive," IEEE Trans. Industry Applications, vol. IA-19, No. 3. pp. 370-378 May/June 1983.

[35] E. Bassi, F. P. Benzi, S. Bolognani, and G. S. Buja, "Field orientation scheme for current-fed induction motor drives based on the torque angle closed-loop control," IEEE Trans. Industry Applications, vol.28, no. 5, pp.1038-1044, Sept./Oct. 1992.

[36] M. P. K. , M. A. Dzieniakowski, and W. S. , "Novel space vector based current controllers for PWM-Inverters" IEEE. Trans. Power Electronics, vol. 6, no. 1, pp. 158-165, Jan. 1991.

[37] I. Takahashi and T. Noguchi, "New quick response and high efficiency control strategy of an induction motor", IEEE Trans. Industry Applications, vol. 22, no. 5, pp. 820-827, Sep./Oct. 1986.

[38] S. D. Sudhoff and P. C. Krause, "Analysis of Steady-State Operation of a Multistack Variable-Reluctance Stepper Motor Using qdo Variables," IEEE Transactions on Energy Conversion, vol. 5, No. 3, September 1990, pp. 693-699.

[39] T. Tsuji, S. Naka, J. Sakakibara, "CSI Drive Induction Motor by Vector Approximation," IEEE Trans. Industry Applications, vol. 27, no. 4, pp. 715-719, July/Aug. 1991.

.[40] S. K. Panda and P. K. Dash, "Application of nonlinear control to switched reluctance motors: a feedback linearisation approach', Proc. IEE. part B, 143 , (5), pp. 371-379, 1996.

[41] Y. Haiquing , S. K. Panda, and L. Y. Chii, "Experimental Investigation of Feedback linearization Controller for Switched Reluctance Motor", IEEE Power Elec. Spec. Conf. Rec., 1996, pp. 1804- 1810.

[42] E. Bassi, F. P. Benzi, S. Bolognani, and G. S. Buja, "Field orientation scheme for current-fed induction motor drives based on the torque angle closed-loop control," IEEE Trans. Industry Applications, vol.28, no. 5, pp.1038-1044, Sept./Oct. 1992.

[43] I. Takahashi and T. Noguchi, "New quick response and high efficiency control strategy of an induction motor", IEEE Trans. Industry Applications, vol. 22, no. 5, pp. 820-827, Sep./Oct. 1986.

[44] Peter Vas, Vector control of a.c. machines, New York: Oxford University Press, 1990.

[45] V. I. U.tkin, "Variable structure system with sliding modes," IEEE Trans. Automat. Contr. vol. AC-22, no. 2, pp. 212-222, April 1977.

[46] L. Hsu and R. R. COSTA, "Variable structure model reference adaptive control using only input and output measurements - Part 1," 1989, Int. J. Control, vol. 49, no. 2, 399-416.

[47] V. I. Utkin, "Sliding-mode control design principles and Applications to electric drives," IEEE Trans. Ind. Electron., vol. 40, no. 1, pp. 23-36, 1993.

[48] G. Ambrosino, G. Celentano, F. Garofalo, "Variable Structure Model Reference Adaptive Control System," Int. J. Control, vol. 39, no. 6, pp. 1339-1349, 1884.

[49] E. Y.Y. Ho and P.C. Sen, "Control dynamics of speed drive systems using sliding mode controllers with integral compensation," IEEE Trans. Ind. Applicat., vol. 27, no., 5, pp. 883-892, 1991.

[50] E. Y.Y. Ho and P.C. Sen, " Microcontroller-based induction motor drive system using variable structure strategy with decoupling," IEEE Trans. Ind. Electron., vol. 37, no. 3, pp. 227-235, 1990.

[51] B.K. Bose, "Sliding mode control of induction motor," in IEEE/IAS Conf. Rec., 1985, pp. 479-486.

[52] G. John, A. R. Eastham, "Speed control of switched reluctance motor using sliding mode control strategy," Conf. Proc. of IEEE IAS Annual Meeting, pp. 263-270, Oct. 1995.

[53] J. F. Mognihan, S. Bolognani, R.C. Kavanagh, M.G. Egan, J.M.D. Murphy. "Single Current Control of AC Servo Drives Using only One Current Sensor in the DC-link" Proceed. of PEVD '94, pp. 458-464, 1994.

From the paper [38], the electromagnetic torque can be found. If there exist two phase currents whose current is sinusoidal, then the torque ripple can be effectively reduced. The figures shown in Fig. A1 ~ Fig. A10 are demonstrated their performance.

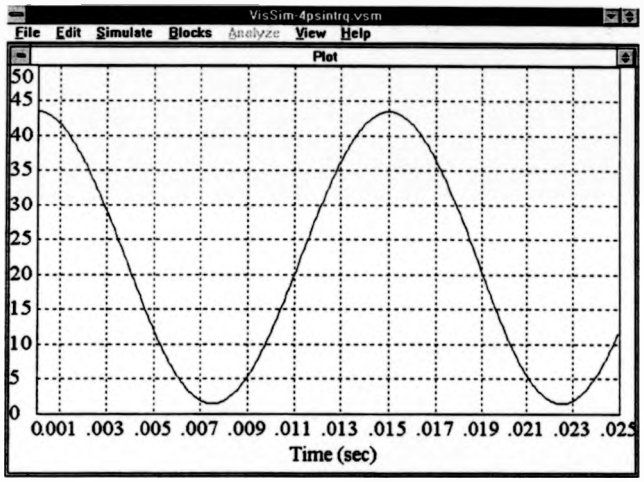

Fig. A1. The self-inductance in the phase-1 winding.

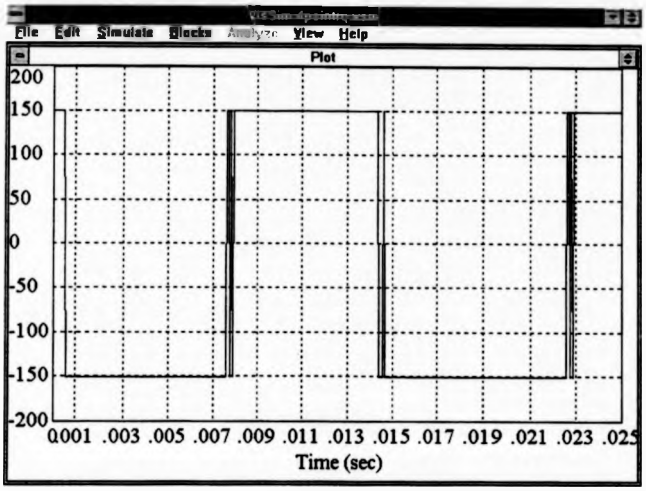

Fig. A2. The voltage in the phase-1.

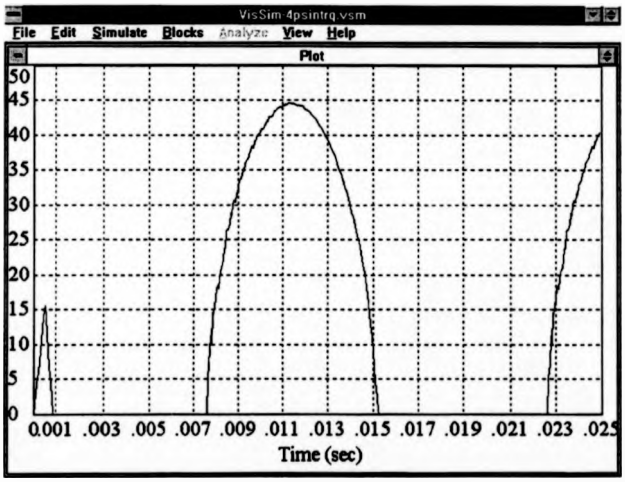

Fig. A3. The current in the phase-1.

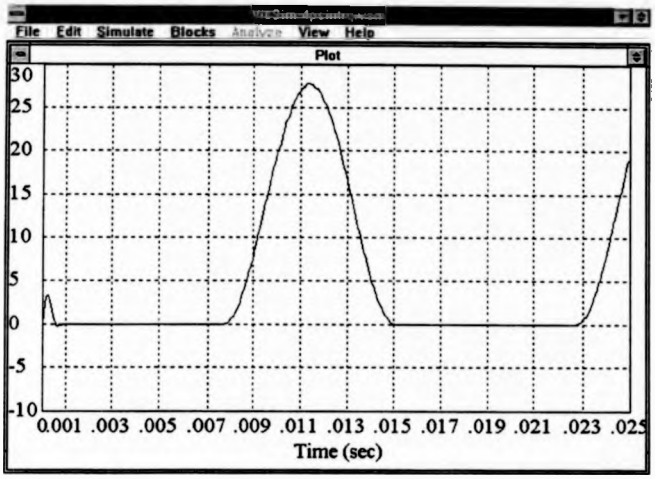

Fig. A4. The electromagnetic torque in the phase-1.

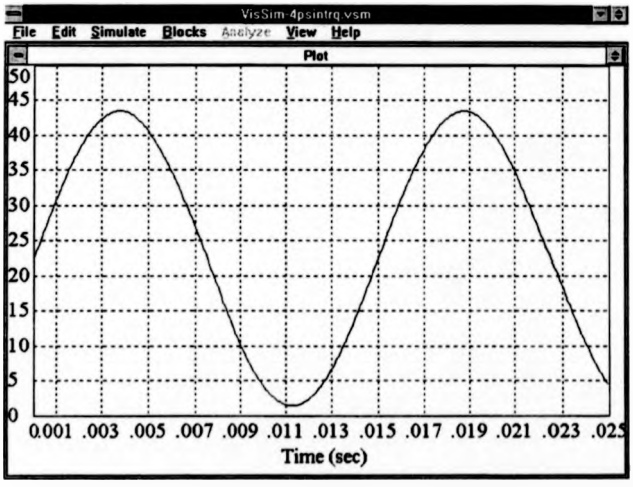

Fig. A5. The self-inductance in the phase-2 winding.

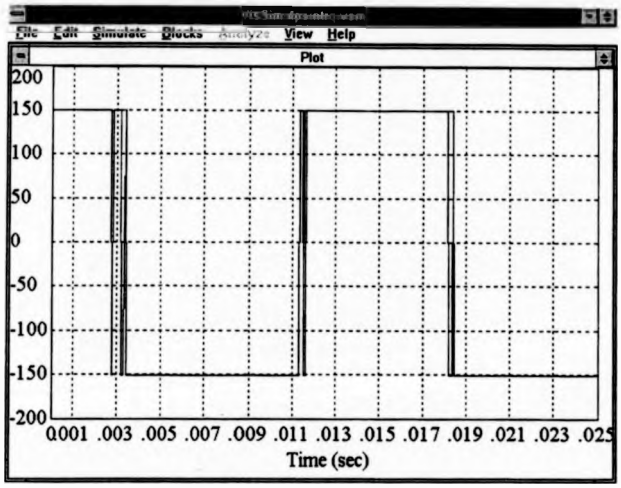

Fig. A6. The voltage in the phase-2.

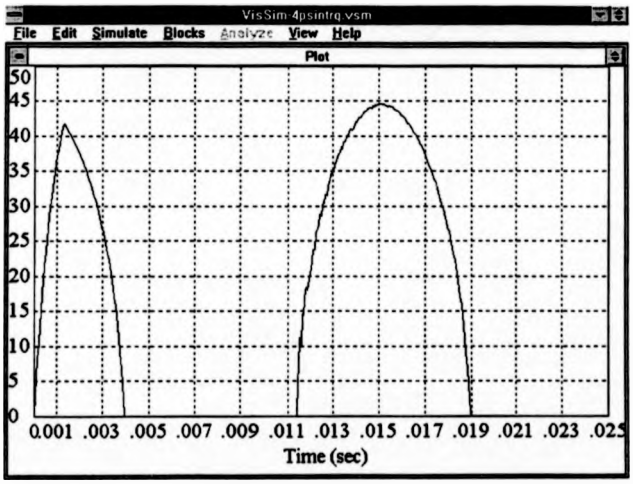

Fig. A7. The current in the phase-2.

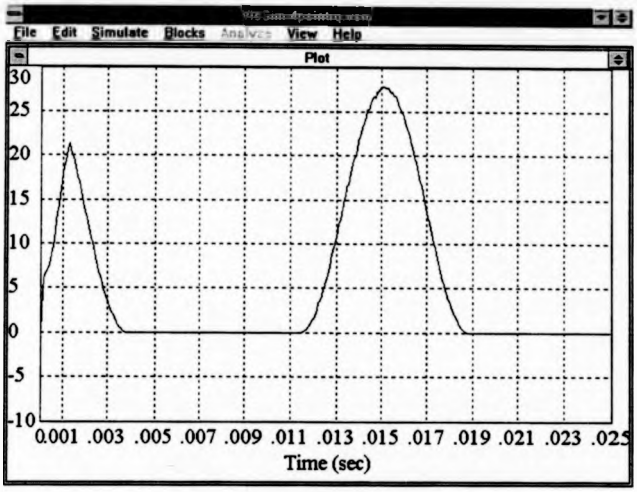

Fig. A8. The electromagnetic torque in the phase-2.

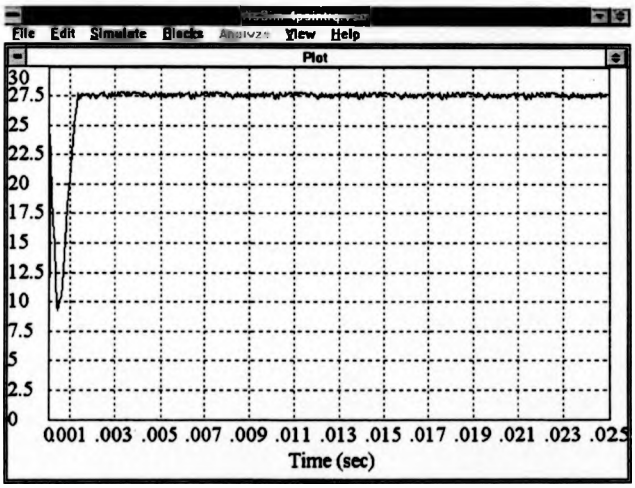

Fig. A 9 . Total electromagnetic torque with 4-phase.